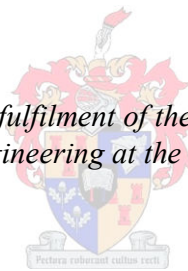


Assessment of seismic drift of structural walls designed according to SANS 10160 - Part 4

by
Rudolf Cornelis le Roux

*Thesis presented in partial fulfilment of the requirements for the degree
Master of Science in Engineering at the University of Stellenbosch*



Supervisor: Prof Jan Andries Wium
Faculty of Engineering
Department of Civil Engineering

December 2010

Declaration

By submitting this thesis/dissertation electronically, I declare that the entirety of the work contained therein is my own, original work, and that I have not previously in its entirety or in part submitted it for obtaining any qualification.

December 2010

Copyright © 2010 University of Stellenbosch

All rights reserved

Abstract

Reinforced concrete structures, designed according to proper capacity design guidelines, can deform inelastically without loss of strength. Therefore, such structures need not be designed for full elastic seismic demand, but could be designed for a reduced demand. In codified design procedures this reduced demand is obtained by dividing the full elastic seismic demand by a code-defined behaviour factor. There is however not any consensus in the international community regarding the appropriate value to be assigned to the behaviour factor. This is evident in the wide range of behaviour factor values specified by international design codes.

The purpose of this study is to assess the seismic drift of reinforced concrete structural walls in order to evaluate the current value of the behaviour factor prescribed by SANS 10160-4 (2009). This is done by comparing displacement demand to displacement capacity for a series of structural walls.

Displacement demand is calculated according to equivalency principles (equal displacement principle and equal energy principle) and verified by means of a series of inelastic time history analyses (ITHA). In the application of the equivalency rules the fundamental periods of the structural walls were based on cracked sectional stiffness from moment-curvature analyses.

Displacement capacity is defined by seismic design codes in terms of inter storey drift limits, with the purpose of preventing non-structural damage in building structures. In this study both the displacement demand and displacement capacity were converted to ductility to enable comparison.

The first step in seismic force-based design is the estimation of the fundamental period of the structure. The influence of this first crucial step is investigated in this study by considering two period estimation methods. Firstly, the fundamental period may be calculated from an equation provided by the design code which depends on the height of the building. This equation is known to overestimate acceleration demand, and underestimate displacement demand. The second period estimation method involves an iterative procedure where the stiffness of the structure is based on the cracked sectional stiffness obtained from moment-curvature analysis. This method provides a more realistic estimate of the fundamental period of structures, but due to its iterative nature it is not often applied in design practice.

It was found that, regardless of the design method, the current behaviour factor value prescribed in SANS 10160-4 (2010) is adequate to ensure that inter storey drift of structural walls would not exceed code-defined drift limits. Negligible difference between the equivalency principles and ITHA was observed.

Opsomming

Gewapende beton strukture wat ontwerp is volgens goeie kapasiteitsontwerp-riglyne kan plasties vervorm sonder verlies aan sterkte. Gevolglik hoef hierdie strukture nie vir die volle elastiese seismiese aanvraag ontwerp te word nie, maar kan vir 'n verminderde aanvraag ontwerp word. In gekodifiseerde ontwerpriglyne word so 'n verminderde aanvraag verkry deur die volle elastiese aanvraag te deel deur 'n kode-gedefinieerde gedragsfaktor. Wat egter duidelik blyk uit die wye reeks van gedragsfaktor waardes in internasionale ontwerp kodes, is dat daar geen konsensus bestaan in die internasionale gemeenskap met betrekking tot die geskikte waarde van die gedragsfaktor nie.

Die doel van hierdie studie is om seismiese verplasing van gewapende beton skuifmure te evalueer ten einde die waarde van die gedragsfaktor wat tans deur SANS 10160-4 (2009) voorgeskryf word te assessee. Dit word gedoen deur verplasingaanvraag te vergelyk met verplasingkapasiteit.

In hierdie studie word verplasingaanvraag bereken deur middel van gelykheidsbeginsels (gelyke verplasingbeginsel en gelyke energiebeginsel) en bevestig deur middel van nie-elastiese tydsgesiedenis analyses (NTGA). Die effek van versagting as gevolg van nie-elastiese gedrag word in aanmerking geneem in die toepassing van die gelykheidsbeginsels.

Verplasingkapasiteit word deur seismiese ontwerpkodes gedefinieer deur perke te stel op die relatiewe laterale beweging tussen verdiepings, met die doel om nie-strukturele skade te verhoed. Om verplasingaanvraag en -kapasiteit te vergelyk in hierdie studie, word beide omgeskakel na verplasingduktiliteit.

Die eerste stap in kraggebaseerde seismiese ontwerp is om die fundamentele periode te beraam. Die invloed van hierdie eerste kritiese stap word in hierdie studie aangespreek deur twee periodeberamingsmetodes te ondersoek. Eerstens kan die fundamentele periode bereken word deur 'n vergelyking wat 'n funksie is van die hoogte van die gebou. Dit is egter algemeen bekend dat hierdie vergelyking versnellingsaanvraag oorskakel en verplasingaanvraag onderskat. Die tweede metode behels 'n iteratiewe prosedure waar die styfheid van die struktuur gebaseer word op die gekraakte snit eienskappe, verkry vanaf 'n moment-krommingsanalise. 'n Beter beraming van die fundamentele periode word verkry deur hierdie metode, maar as gevolg van die iteratiewe aard van die metode word dit selde toegepas in ontwerppraktyk.

Die resultate van hierdie studie toon dat die huidige waarde van die gedragfaktor soos voorgeskryf in SANS 10160-4 (2010) geskik is om te verseker dat die relatiewe laterale beweging tussen verdiepings binne kode-gedefinieerde perke sal bly. Onbeduidende verskil is waargeneem tussen die resultate van gelykheidsbeginsels en NTGA.

Table of Contents

| | |
|--|----|
| 1. Introduction | 1 |
| 2. Literature review..... | 4 |
| 2.1 Definition of key principles | 4 |
| 2.1.1 Dynamic equation of motion | 4 |
| 2.1.2 Elastic earthquake spectra | 5 |
| 2.1.3 Peak ground acceleration (PGA) | 5 |
| 2.1.4 Elastic shear force | 6 |
| 2.1.5 Force reduction and ductility | 7 |
| 2.1.6 R- μ -T relationship..... | 9 |
| 2.1.7 Behaviour factor and design spectra | 10 |
| 2.2 Computational evaluation of the behaviour factor | 12 |
| 2.2.1 Calculation of the behaviour factor for timber structural walls | 12 |
| 2.2.2 Calculation of the behaviour factor through the capacity spectrum method | 13 |
| 2.2.3 Comparison between pushover analysis and incremental dynamic analysis (IDA) | 14 |
| 2.3 Assessment of the behaviour factor – the concept of ductility demand and capacity...17 | |
| 2.3.1 Ductility demand..... | 18 |
| 2.3.2 Ductility capacity..... | 18 |
| 3. Structural wall buildings..... | 23 |
| 3.1 Good conceptual design | 23 |
| 3.1.1 Adequate foundation | 23 |
| 3.1.2 Avoid discontinuities along the height of the building | 23 |
| 3.1.3 Do not offset structural walls..... | 23 |
| 3.1.4 Reinforced concrete slabs should act as rigid diaphragms | 24 |
| 3.1.5 Place at least two walls in two orthogonal directions..... | 24 |
| 3.1.6 Avoid asymmetric bracing..... | 24 |
| 3.1.7 Separate non-structural masonry walls by joints | 25 |
| 3.2 Generic structural wall | 25 |
| 4. Scope of the study..... | 29 |
| 4.1 Wall sectional shapes | 29 |
| 4.2 Ground types | 30 |
| 4.3 Wall aspect ratio | 30 |

| | | |
|-------|---|----|
| 4.4 | Period calculation method | 31 |
| 4.4.1 | Method 1 | 32 |
| 4.4.2 | Method 2 | 33 |
| 4.5 | Number of storeys..... | 35 |
| 5. | Methodology..... | 38 |
| 6. | Material properties..... | 42 |
| 6.1 | Material strengths | 42 |
| 6.2 | Stress-strain curves | 43 |
| 6.2.1 | Concrete..... | 43 |
| 6.2.2 | Reinforcing steel..... | 48 |
| 7. | Moment-curvature analysis | 51 |
| 7.1 | Section discretization | 51 |
| 7.2 | Calculation steps..... | 52 |
| 7.3 | Bilinear approximation to the moment-curvature curve | 53 |
| 7.4 | Moment-curvature results | 54 |
| 7.5 | Parameters which would not influence the outcome of this study..... | 57 |
| 8. | Design..... | 59 |
| 8.1 | Equivalent static lateral force | 59 |
| 8.2 | Bending moment demand | 61 |
| 8.3 | Capacity design | 63 |
| 8.4 | Bending moment capacity..... | 66 |
| 8.4.1 | Design equations..... | 66 |
| 8.4.2 | Design example..... | 69 |
| 8.5 | Longitudinal reinforcement content | 71 |
| 9. | Ductility capacity and demand..... | 72 |
| 9.1 | Force-displacement response of a SDOF wall from moment-curvature analysis | 72 |
| 9.2 | Force-displacement response of a MDOF wall from moment-curvature analysis | 76 |
| 9.2.1 | Conversion from MDOF to SDOF | 76 |
| 9.2.2 | Validity of linear curvature profile..... | 79 |
| 9.3 | Defining ductility capacity in terms of a code drift limit..... | 81 |
| 9.3.1 | Plastic hinge method | 81 |
| 9.3.2 | Approximate equation..... | 81 |

| | | |
|--------|--|-----|
| 9.4 | Calculating ductility demand from inelastic time history analysis (ITHA) results | 82 |
| 10. | Inelastic time history analysis..... | 84 |
| 10.1 | Degree of sophistication in element modelling | 84 |
| 10.2 | Beam properties..... | 84 |
| 10.2.1 | Elastic properties..... | 85 |
| 10.2.2 | Inelastic properties | 86 |
| 10.2.3 | Hysteresis rule..... | 86 |
| 10.3 | Representation of the plastic hinge in the finite element model..... | 88 |
| 10.4 | Time step integration parameters..... | 89 |
| 10.5 | Ground motions | 89 |
| 10.5.1 | Number of records..... | 89 |
| 10.5.2 | Selection of records..... | 90 |
| 10.6 | Damping | 92 |
| 10.7 | The validity of the equal displacement principle | 94 |
| 11. | Results | 97 |
| 11.1 | Design results (Figure 5.1 (3) of the methodology)..... | 97 |
| 11.2 | Analysis results (step 4 to 6 of the methodology) | 101 |
| 12. | Assessment of displacement prediction methods..... | 105 |
| 13. | Conclusion..... | 112 |
| 14. | Bibliography..... | 114 |

List of Figures

| | |
|---|----|
| Figure 2.1: Generation of elastic response spectra..... | 5 |
| Figure 2.2: Earthquake spectra of 1957 San Francisco earthquake | 6 |
| Figure 2.3: Force-displacement of elastoplastic SDOF system and its corresponding elastic SDOF system..... | 8 |
| Figure 2.4: Equal energy and equal displacement principles | 9 |
| Figure 2.5: Elastic pseudo acceleration spectra ($q = 1$) (SANS 10160-4, 2009, p. 12)..... | 11 |
| Figure 2.6: Proposed computational definition of the maximum value of the behaviour factor (Spathelf, 2008, p. 112)..... | 14 |
| Figure 2.7: Comparison between median IDA and pushover (Vamvatsikos & Cornell, 2002, p. 510)..... | 15 |
| Figure 2.8: Hardening behaviour in IDA (Vamvatsikos & Cornell, 2002, p. 498)..... | 15 |
| Figure 2.9: IDA versus pushover analysis as part of initial investigation | 16 |
| Figure 2.10: Definition of building performance levels according to FEMA 273 (ATC, 1997, p. 1-2)..... | 19 |
| Figure 3.1: Discontinuous structural walls | 23 |
| Figure 3.2: Bracing offsets..... | 24 |
| Figure 3.4: Separation of non-structural masonry walls (Elevation) | 25 |
| Figure 3.3: Asymmetric vs. symmetric bracing (Plan view)..... | 25 |
| Figure 3.5: Generic wall..... | 27 |
| Figure 3.6: Tributary area for axial load P | 28 |
| Figure 4.1: Wall sectional shapes (Dazio & Beyer, 2009, p.7-8) | 30 |
| Figure 4.2: Definition of wall dimensions | 31 |
| Figure 4.3: Overestimation of acceleration and underestimation of displacement..... | 33 |
| Figure 4.4: Effective cracked section stiffness from moment-curvature results | 34 |
| Figure 4.5: Design method 2 | 35 |
| Figure 4.6: Generic wall range..... | 36 |
| Figure 5.1: Methodology..... | 41 |
| Figure 6.1: Mander's stress-strain relationship for concrete..... | 43 |
| Figure 6.2: Confinement in a wall boundary element | 46 |
| Figure 6.3: Confined strength determination from lateral confining stresses for rectangular sections (Mander <i>et al.</i> , 1988, p. 1813) | 46 |
| Figure 6.4: Stress-strain relationship for reinforcing steel | 48 |
| Figure 6.5: Experimental stress-strain curves of reinforcing steel | 49 |
| Figure 7.1: Discretization of section..... | 52 |
| Figure 7.2: MATLAB moment-curvature program screenshot..... | 53 |

| | |
|--|-----|
| Figure 7.3: Bilinear approximation to moment curvature curve | 54 |
| Figure 7.4: Bilinear moment-curvature results | 55 |
| Figure 7.5: Dimensionless yield curvature as a function of axial load ratio..... | 56 |
| Figure 7.6: Influence of reinforcement content on strength and stiffness | 56 |
| Figure 7.7: Influence of axial load on strength and stiffness | 57 |
| Figure 8.1: Mass ratio as a function of the number of degrees of freedom..... | 60 |
| Figure 8.2: Tension shift..... | 62 |
| Figure 8.3: Bending moment demand and capacity..... | 63 |
| Figure 8.4: Height of plastic region (SANS 10160-4, 2009, p. 38)..... | 64 |
| Figure 8.5: Reinforcement layout of structural wall section (SANS 10160-4, 2009, p. 38)..... | 64 |
| Figure 8.6: Confinement in a wall boundary element..... | 65 |
| Figure 8.7: Critical wall thickness ductility relationship (Paulay & Priestley, 1992, p.403) | 66 |
| Figure 8.8: Equivalent stress block..... | 67 |
| Figure 8.9: Design example..... | 69 |
| Figure 9.1: Conversion from moment-curvature to force-displacement..... | 72 |
| Figure 9.2: Calculating the displacement profile from applied forces | 73 |
| Figure 9.3: Plastic hinge method | 74 |
| Figure 9.4: Equivalent SDOF wall..... | 77 |
| Figure 9.5: MDOF wall curvatures at yield | 80 |
| Figure 10.1: Typical finite element model of a structural wall | 85 |
| Figure 10.2: Moment-curvature properties..... | 86 |
| Figure 10.3: Modified Takeda Hysteresis rule (Priestey <i>et al.</i> , 2007, p. 202) | 87 |
| Figure 10.4: Plastic hinge spring | 88 |
| Figure 10.5: Artificial ground motion spectra..... | 92 |
| Figure 10.6: Raleigh damping..... | 93 |
| Figure 10.7: Average ratio of peak inelastic displacement to elastic displacement for modified Takeda hysteresis. (TS = tangent-stiffness proportional damping, IS = initial stiffness proportional damping, R = force reduction factor) (Priestley & Grant, 2005, p. 242) | 95 |
| Figure 10.8: Comparison of displacement ratios..... | 96 |
| Figure 11.1: Design results for ground type 1, design method 1 | 99 |
| Figure 11.2: Design results for ground type 1, design method 2 | 99 |
| Figure 11.3: Design results for ground type 4, design method 1 | 100 |
| Figure 11.4: Design results for ground type 4, design method 2 | 100 |
| Figure 11.5: Analysis results for ground type 1, design method 1 | 102 |
| Figure 11.6: Analysis results for ground type 1, design method 2..... | 103 |
| Figure 11.7: Analysis results for ground type 4, design method 1 | 103 |
| Figure 11.8: Analysis results for ground type 4, design method 2..... | 104 |

Figure 12.1: Equal displacement principle 105
Figure 12.2: Displacement prediction – methods 1 to 4 108
Figure 12.3: Displacement prediction – methods 3 to 5 110

List of Tables

| | |
|--|-----|
| Table 2.1: Values of the parameters which define the design pseudo acceleration spectrum (SANS 10160-4, 2009, p. 13) | 10 |
| Table 2.2: Description of seismic ground types (SANS 10160-4, 2009, p. 10) | 11 |
| Table 2.3: Rehabilitation objectives according to FEMA 273 (ATC, 1997, p. 2-5) | 20 |
| Table 4.1: Wall section lengths | 36 |
| Table 6.1: Material strengths | 43 |
| Table 6.2: Reinforcement experimental results | 49 |
| Table 10.1: Elastic beam properties | 85 |
| Table 10.2: Giberson beam properties | 86 |
| Table 10.3: Hysteresis rule properties | 87 |
| Table 10.4: Selected ground motions | 91 |
| Table 12.1: Displacement prediction methods considered | 107 |

Notation

Acronyms

| | |
|----------------|---|
| ATC | Applied Technology Council |
| BSO | Basic Safety Objective |
| DM | Damage Measure |
| DOF | Degree of freedom |
| FEMA | Federal Emergency Management Agency |
| IDA | Incremental dynamic analysis |
| IM | Intensity Measure |
| IS | Initial stiffness proportional damping |
| ITHA | Inelastic time history analysis |
| MDOF | Multi degree of freedom |
| PGA | Peak ground acceleration |
| $PGA_{u,code}$ | Peak ground acceleration prescribed by the design code |
| $PGA_{u,eff}$ | Peak ground acceleration at which failure criteria is reached |
| PEER | Pacific Earthquake Engineering Research Center |
| SDOF | Single degree of freedom |
| TS | Tangent stiffness proportional damping |

Symbols

Capital letters

| | |
|-------------|--|
| A | Gross cross sectional area of structural wall |
| A_1 | Elastic acceleration demand on the wall designed according to method 1 |
| A_2 | Elastic acceleration demand on the wall designed according to method 2 |
| A_r | Aspect ratio of structural wall |
| A_s | Shear area of structural wall cross section |
| $A_{s,ave}$ | An amount of longitudinal reinforcement complying with codified criteria, somewhere between the maximum and minimum allowable limits |
| A_{se} | Boundary element reinforcement area |
| A_{st} | Total reinforcement area |
| A_{sw} | Web reinforcement area per pair of bars |
| A_{sh1} | Cross sectional area of confining reinforcement in direction 1 of boundary element |

| | |
|-----------------|--|
| A_{sh2} | Cross sectional area of confining reinforcement in direction 2 of boundary element |
| E_c | Modulus of elasticity of the unconfined concrete |
| E_{cc} | Modulus of elasticity of the confined concrete |
| C_T | Factor used in the calculation of the fundamental period |
| EI_{eff} | Effective cracked sectional stiffness obtained from moment-curvature analysis |
| F | Externally applied dynamic force |
| F^* | Lateral force on equivalent SDOF system |
| G | Shear modulus of concrete |
| I_{eff} | Moment of inertia of cracked section |
| K_e | Confinement effectiveness coefficient |
| L_p | Plastic hinge length |
| L_{sp} | Strain penetration depth |
| M | Bending moment |
| M_n | Nominal yield moment obtained from moment-curvature analysis |
| M'_n | Nominal yield moment obtained from design equations |
| M'_y | First yield moment obtained from moment-curvature analysis |
| M_u | Ultimate moment obtained from moment-curvature analysis |
| N | Internal axial load |
| P | Vertical floor load transferred into the structural wall |
| R | Force reduction factor |
| R_1 | Force reduction factor of the wall designed according to method 1 |
| R_2 | Force reduction factor of the wall designed according to method 2 |
| S | Soil factor |
| S_d | Design pseudo acceleration |
| S_e | Elastic pseudo acceleration |
| T | Fundamental period of vibration |
| T_1 | Fundamental period of a structure according to Eq. 4.1 (SANS 10160-4, 2009) |
| $T_{1(real)}$ | Fundamental period at which the wall, designed according to method 1, responds |
| T_2 | Fundamental period at which the wall, designed according to method 2, responds |
| T_B and T_C | Periods defining the limits of the constant acceleration branch of the design pseudo acceleration spectrum |
| T_D | Period defining the beginning of the constant displacement range of the displacement spectrum |
| V_0 | Peak elastic base shear demand |
| V_b | Base shear force |

| | |
|------------|---|
| V_y | Base shear force corresponding to the yield moment of the elastoplastic SDOF system |
| W_x, W_i | Weight assigned to level x and i respectively |
| W013 | Structural wall with one storey and aspect ratio of three |
| W023 | Structural wall with two storeys and aspect ratio of three |
| W033 | Structural wall with three storeys and aspect ratio of three |
| W063 | Structural wall with six storeys and aspect ratio of three |
| W065 | Structural wall with six storeys and aspect ratio of five |
| W125 | Structural wall with twelve storeys and aspect ratio of five |
| W128 | Structural wall with twelve storeys and aspect ratio of eight |
| W188 | Structural wall with eighteen storeys and aspect ratio of eight |

Lower-case letters

| | |
|-----------------|--|
| a | Relative acceleration of a SDOF system |
| a_1 | Design pseudo acceleration according to design method 1 |
| a_2 | Design pseudo acceleration according to design method 2 |
| $a_{1(real)}^+$ | Pseudo acceleration capacity corresponding to M_n according to design method 1 |
| a_2^+ | Pseudo acceleration capacity corresponding to M_n according to design method 2 |
| a_g | Ground acceleration |
| a_t | Total or absolute acceleration of a SDOF system |
| b_c | Critical section width |
| b_w | Wall section width |
| c | Damping coefficient |
| d_{bl} | Diameter of the longitudinal reinforcement in the boundary elements of a wall |
| d_e | Displacement obtained from a static elastic analysis of a structure |
| d_r | Relative displacement between the top and bottom of a storey in a structure |
| d_s | Maximum inelastic response displacement |
| f | Post yield stiffness ratio of moment-curvature relationship |
| f_c | Concrete stress |
| f_{cd} | Design compressive cube strength |
| f'_{cc} | Mean cylinder strength of confined concrete |
| f'_{co} | Mean cylinder strength of unconfined concrete |
| f_{cu} | Concrete characteristic cube strength |
| f'_{i1} | Effective confining stress in direction 1 of boundary element |
| f'_{i2} | Effective confining stress in direction 2 of boundary element |
| f_y | Yield stress of reinforcement |

| | |
|------------|---|
| f_u | Ultimate stress of reinforcement |
| f_{yh} | Yield strength of the confining reinforcement |
| h^* | Effective height of equivalent SDOF system |
| h_1, h_2 | Dimensions of the boundary element |
| h_i, h_j | Height above the base to level i and j respectively |
| h_{pl} | Plastic region length |
| h_s | Storey height |
| h_w | Wall height, measured from the top of the foundation to top of the roof |
| h_x | Maximum horizontal spacing of the legs of the confining reinforcement |
| i | Storey number |
| k | Parameter used for the calculation of the plastic hinge length |
| k_0 | Initial stiffness of hysteresis rule |
| k^* | Lateral stiffness of a SDOF system |
| k_s | Plastic hinge spring stiffness |
| l_c | Boundary element length |
| l_w | Wall section length |
| m | Bending moment ratio |
| m_1 | Floor mass corresponding to design method 1 |
| m_2 | Floor mass corresponding to design method 2 |
| m^* | Effective first modal mass |
| m_1^* | Effective first modal mass of the wall designed according to method 1 |
| m_2^* | Effective first modal mass of the wall designed according to method 2 |
| m_{tot} | Total building mass or sum of floor masses |
| n | Total number of storeys |
| q | Behaviour factor |
| r | Post yield stiffness ratio of hysteresis rule |
| s | Horizontal spacing of web reinforcement |
| s_e | Reinforcement spacing in boundary element |
| s_h | Vertical spacing of the confining reinforcement |
| s_w | Reinforcement spacing in web region |
| t | Tension shift distance |
| u | Relative displacement of a SDOF system |
| u_m | Peak seismic displacement demand on the elastoplastic SDOF system |
| u_y | Yield displacement of the elastoplastic SDOF system |
| v | Relative velocity of a SDOF system |

| | |
|------------|--|
| $v_{s,30}$ | Average value of propagation of S-waves in the upper 30 meters of the soil profile at shear strains of 10^{-5} or less |
| x, x_n | Neutral axis depth |

Greek capitol letters

| | |
|---------------|---|
| Ω | Overstrength factor |
| Δ^* | Equivalent SDOF displacement |
| $\Delta\phi$ | Curvature increment used in moment-curvature analysis |
| Δ_{eq} | Equivalent SDOF displacement demand of a MDOF structural wall |
| Δ_i | Displacement of DOF i of a MDOF structural wall |
| Δ_p | Plastic displacement of a SDOF system |
| Δ_y | Yield displacement of a SDOF system |
| Δ_u | Ultimate displacement of SDOF system |

Greek lower-case letters

| | |
|---------------------|---|
| α | Unloading stiffness factor of the Modified Takeda Hysteresis Rule |
| α_e | Boundary element length ratio |
| α_x | Neutral axis depth ratio |
| β | Reloading stiffness factor of the Modified Takeda Hysteresis Rule |
| ε_c | Concrete strain |
| ε_{cc} | Strain at peak stress of confined concrete |
| ε_{ccu} | Ultimate strain confined concrete |
| ε_{co} | Strain at peak stress of unconfined concrete |
| ε_{cu} | Ultimate strain unconfined concrete |
| ε_{sh} | Strain at which strain hardening of reinforcement starts |
| ε_{sm} | Strain at peak reinforcement stress |
| ε_{sp} | Spalling strain of unconfined concrete |
| ε_{su} | Ultimate strain of reinforcement |
| ε_y | Yield strain of reinforcement |
| θ | Total rotation over the plastic hinge length |
| θ_b | Beam rotation over the plastic hinge length |
| θ_c | Code defined inter storey drift limit |
| θ_p | Plastic drift of a SDOF system |
| θ_s | Plastic hinge spring rotation |
| μ | Ductility |

| | |
|--------------------|---|
| μ_c | Ductility capacity |
| μ_d | Ductility demand |
| v | Reduction factor which takes into account the lower return period of the seismic action associated with the damage limitation requirement |
| ρ_1 | Volumetric ratio of confining material in direction 1 of boundary element |
| ρ_2 | Volumetric ratio of confining material in direction 2 of boundary element |
| ρ_s | Total volumetric ratio of confining material in both directions |
| ρ_e, ω_e | Boundary element reinforcement content ratios |
| ρ_t, ω_t | Total reinforcement content ratios |
| ρ_w, ω_w | Web reinforcement content ratios |
| ϕ | Curvature |
| ϕ'_y | First yield curvature obtained from moment-curvature analysis |
| ϕ_e | Reinforcement diameter in boundary element |
| ϕ_p | Plastic curvature |
| ϕ_y | Nominal yield curvature obtained from moment-curvature analysis |
| ϕ_u | Ultimate curvature obtained from moment-curvature analysis |
| ϕ_w | Reinforcement diameter in web region |
| ω | Circular natural frequency in rad/s |

1. Introduction

Buildings, in which structural walls resist most or all lateral loads, have in the past frequently been called *shear wall* buildings. This name may be misleading since it may imply that the structural wall's response may be dominated by shear action, whereas the desired response is ductile flexural action (Paulay & Priestley, 1992, p.362). Therefore, following the lead of Paulay & Priestley (1992, p.362), the term *structural wall* will be used in preference to *shear wall* in this study.

In the 1960's, with the development of inelastic time history analysis (ITHA), came the realization that well designed structures can deform inelastically without loss of strength (Priestley, Calvi & Kowalski, 2007, pp. 1-4). Engineers realized that structures need not be designed for the full elastic seismic demand, but could be designed for a reduced demand. This reduced demand is obtained by dividing the full elastic seismic demand by a code-defined behaviour factor. There does however not seem to be any consensus in the international community regarding the appropriate value to be assigned to the behaviour factor. This is evident in the wide range of behaviour factor values specified by international design codes (Priestley *et al.*, 2007, p. 13).

The purpose of this study is to assess the seismic drift of reinforced concrete structural walls to evaluate the current value of the behaviour factor, which according to SANS 10160-4 (2009) is equal to five. This study is a continuation of a study by Spathelf (2008) who computationally determined behaviour factor values for a series of structural walls.

The main influence of the behaviour factor becomes evident in seismic displacement demand. Therefore, in order to assess the current behaviour factor value, a comparison between seismic displacement demand and seismic displacement capacity is required. A series of structural walls will be assessed in this study. A first estimate of displacement demand of these walls will be obtained from the equal displacement and equal energy principles. The displacement demand will be verified by means of a series of ITHA on these walls. Displacement capacity is defined by seismic design codes in terms of inter storey drift limits to prevent non-structural damage in building structures. Thus, in essence, this study will assess if structural walls, designed with the current behaviour factor value, would suffer non-structural damage under the design earthquake. If it is found to be so, a lower behaviour factor value will be prescribed.

Additionally, this study will evaluate the way in which the fundamental period of a structure is estimated. Seismic design codes, including SANS 10160-4 (2009), provide a simple equation by which the fundamental period of a structure may be calculated. It is well known that this equation overestimates seismic design forces, and underestimates lateral displacement demand (Priestley *et al.*, 2007, p.11). The influence of this equation on both the design and displacement prediction will be assessed in this study. An alternative period calculation procedure, based on moment-curvature analysis, will also be assessed. This method provides a more realistic estimate of the fundamental period of structures, but due to its iterative nature it is not often applied in design practice.

This document is laid out as follows:

The literature review is presented in Chapter 2. It is divided into three sections. Firstly, some key principles are introduced. The second section deals with the methodology followed by Spathelf (2008) in the computational evaluation of the behaviour factor and the difference between static and dynamic analysis procedures. In Chapter 2.3 the concept of ductility demand and capacity, which forms the basis of the behaviour factor assessment, is discussed.

Chapter 3 deals with good conceptual design strategies that should be followed in the design of structural wall buildings, with the purpose of defining a generic structural wall which could be used throughout this study.

In Chapter 4 the scope of this study is discussed. Eight walls are defined which are used throughout this study.

Chapter 5 lays down the methodology by which the behaviour factor is assessed.

Chapter 6 introduces the assumptions regarding material properties used in the design and analysis of the structural walls.

In Chapter 7 the algorithm used for moment-curvature analysis of wall cross sections is introduced. The moment-curvature analysis results of the walls of this study are shown. Also, in light of the moment-curvature results, some parameters are identified which would not influence the outcome of this study.

Chapter 8 deals with the design requirements of structural walls. The structural walls defined in Chapter 4 are designed according to these requirements.

In order to compare displacement demand and capacity, both are converted to ductility. This is the purpose of Chapter 9, which deals with the derivation of ductility capacity from code drift limits, and the derivation of ductility demand from ITHA results.

Chapter 10 deals with all aspects regarding ITHA used in this study. As stated previously, ITHA will be used to validate the initial estimate of ductility demand obtained from the equal displacement and equal energy principles.

Finally, in Chapter 11 the ductility demand and capacity of the walls are compared. A conclusion regarding the current behaviour factor value is made.

Chapter 12 serves to introduce background information on current code displacement prediction methods. The results of different assumptions regarding stiffness and lateral force are compared.

Finally, in Chapter 13, conclusions are made and some suggestions are given for future research.

2. Literature review

This chapter is divided into three sections: Chapter 2.1 introduces some key principles. In 2.2 the study by Spathelf (2008) is discussed. Differences between static and dynamic analysis procedures are identified. This leads to 2.3 which deals with the basis of the behaviour factor assessment, namely ductility demand and capacity.

2.1 Definition of key principles

2.1.1 Dynamic equation of motion

In dynamic analysis, the first vibration mode is dominant in buildings when they are regular in plan and elevation, as discussed in Chapter 8.1. In other words, higher modes do not significantly influence the dynamic response or internal forces of the structure. The dynamic response of such a structure may be modelled using a single degree of freedom (SDOF) system.

The general dynamic equation of motion of a SDOF system is given by Eq. 2.1.

$$m^*a_t(t) + cv(t) + k^*u(t) = F(t) \quad \dots\dots\dots 2.1$$

(inertia force) (damping force) (shear force)

where

m^* is the mass of the system

$a_t(t)$ is the total, or absolute, acceleration of the mass m^*

c is the damping coefficient

$v(t)$ is the velocity of the mass m^* relative to the ground

k^* is the lateral stiffness of the system

$u(t)$ is the displacement of the mass m^* relative to the ground

$F(t)$ is an externally applied dynamic force (typically wind loads on a building)

In the case where the SDOF system is subjected to an earthquake ground motion, the externally applied dynamic force $F(t) = 0$, while the base of the system is subjected to ground acceleration $a_g(t)$. For this case the dynamic equation of motion may be derived by considering that the total acceleration of the mass $a_t(t)$ is the sum of the ground acceleration $a_g(t)$ and the acceleration relative to the ground $a(t)$.

$$a_t(t) = a_g(t) + a(t) \quad \dots\dots\dots 2.2$$

Substitution of Eq. 2.2 in Eq. 2.1 results in Eq. 2.3:

$$m^*a(t) + cv(t) + k^*u(t) = -m^*a_g(t) \quad \dots\dots\dots 2.3$$

Eq. 2.3 thus represents a SDOF system with an applied dynamic force $F(t) = -m^*a_g(t)$. Since the ground acceleration $a_g(t)$ varies arbitrarily with time, Eq. 2.3 can only be solved using a time-stepping method such as Newmark’s method (Chopra, 2007, p.165). The time-stepping analysis would deliver $a(t)$, $v(t)$, and $u(t)$. The absolute acceleration $a_t(t)$ is calculated from Eq. 2.2.

2.1.2 Elastic earthquake spectra

An elastic response spectrum represents the demand of an earthquake ground motion on an elastic SDOF system as a function of the natural period and viscous damping ratio of the system. The response spectrum may either be a displacement-, velocity-, or acceleration spectrum. The generation of an elastic response spectrum for a specific damping ratio is illustrated in Figure 2.1. For seismic design 5 % viscous damping is typically assumed.

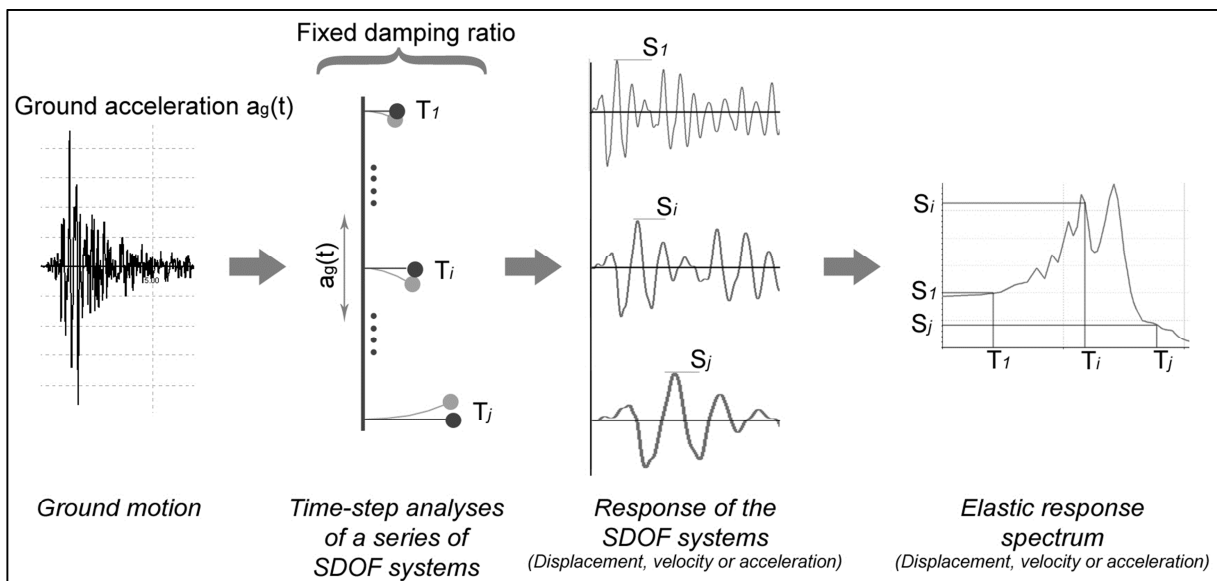


Figure 2.1: Generation of elastic response spectra

2.1.3 Peak ground acceleration (PGA)

Figure 2.2 shows one component of the acceleration time history as well as the corresponding 5 % damped displacement spectrum and 5 % damped acceleration spectrum of the 1957 San Francisco earthquake.

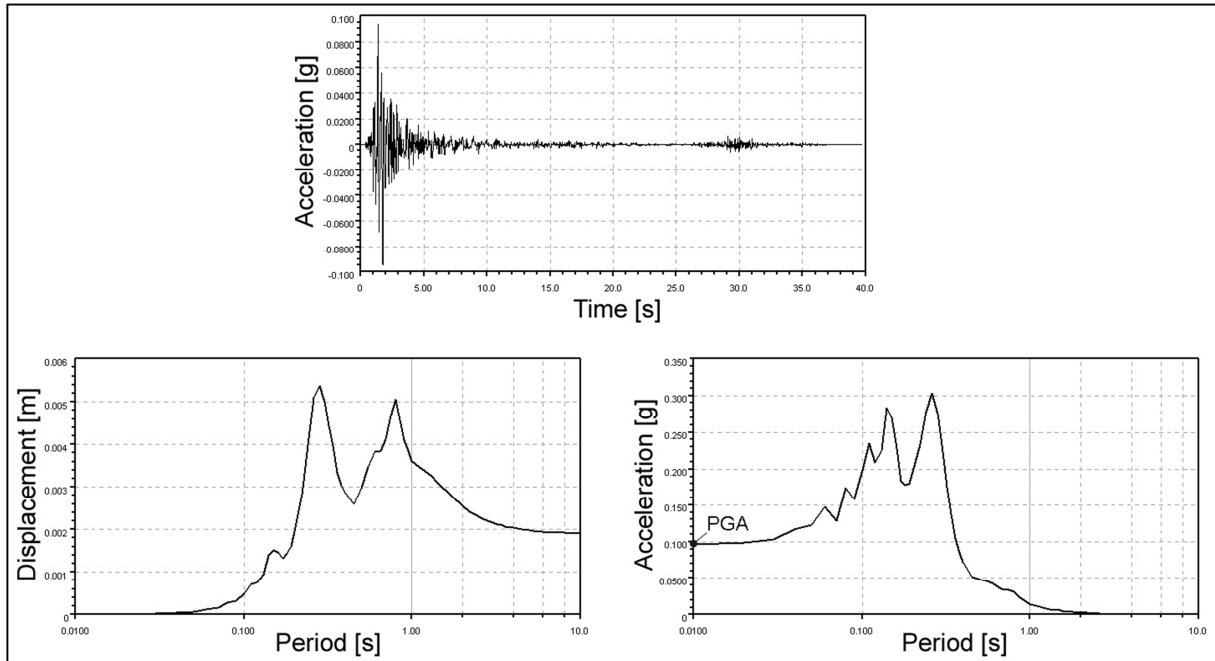


Figure 2.2: Earthquake spectra of 1957 San Francisco earthquake

An important property which can be read from the acceleration spectrum is the peak ground acceleration (PGA). The mass of a very stiff SDOF system ($Period \approx 0$) would essentially accelerate by the same amount as the ground. Thus the PGA can be read from the intersection of the acceleration spectrum with the vertical axis.

2.1.4 Elastic shear force

From Eq. 2.1 it can be seen that the internal shear force $V_b(t)$ of the SDOF system is obtained from the product of the stiffness and displacement of the system:

$$V_b(t) = k \cdot u(t) \tag{2.4}$$

If one were to design a SDOF system to resist the 1957 San Francisco earthquake for example, the period can be calculated from Eq. 2.5:

$$T = 2\pi \sqrt{\frac{m^*}{k^*}} \tag{2.5}$$

The peak displacement $u(T)$ can simply be read from the displacement spectrum, and the design base shear calculated according to Eq. 2.6:

$$V_b = k \cdot u(T) \tag{2.6}$$

In seismic design, this is however done differently. Seismic design codes provide only pseudo acceleration spectra ($S_e(T)$). The shear force on an elastic SDOF system is calculated as:

$$V_b = m^* S_e(T) \quad \dots\dots\dots 2.7$$

Pseudo acceleration is defined as

$$S_e = \omega^2 u \quad \dots\dots\dots 2.8$$

$$\text{where } \omega = \sqrt{\frac{k^*}{m^*}} \quad \dots\dots\dots 2.9$$

is the circular natural frequency in rad/s.

It should be noted that pseudo acceleration spectra are equal to acceleration spectra for systems with zero damping (Chopra, 2007, p. 244). This is evident from Eq. 2.3, which for systems with zero damping simplifies to:

$$m^* a(t) + k^* u(t) = -m^* a_g(t) \quad \dots\dots\dots 2.10$$

Substitute Eq. 2.2 and 2.9 in Eq. 2.10:

$$m^* a_t(t) + m^* \omega^2 u(t) = 0 \quad \dots\dots\dots 2.11$$

$$a_t(t) = -\omega^2 u(t) = -S_e(t) \quad \dots\dots\dots 2.12$$

Thus, the absolute value of acceleration and pseudo acceleration are equal for systems with zero damping.

The reason why seismic design codes currently base design forces on acceleration (Eq. 2.7) instead of displacement (Eq. 2.6) is found in the history of seismic design (Priestley *et al.*, 2007, p. 4). In the 1920's and 1930's it was observed that buildings which were designed to resist wind loads performed better under earthquake loads than those without wind load design. As a consequence, building codes specified a typical value of 10 % of the building weight as lateral design load. In the 1940's to 1960's the importance of dynamic characteristics of buildings became understood, leading to the development of period-dependant seismic loads (Priestley *et al.*, 2007, p. 4).

2.1.5 Force reduction and ductility

In the 1960's, with the development of ITHA, came the realization that well designed structures can deform inelastically without loss of strength (Priestley *et al.*, 2007, pp. 1-4).

Engineers realized that structures need not be designed for the full elastic seismic demand, but could be designed for a reduced demand. This led to the development of the force reduction factor. Relationships between ductility and the force reduction factor were subsequently developed (Priestley *et al.*, 2007, p. 4).

The following discussion of the concepts of force reduction and ductility is based on Chopra (2007, pp. 264-295). Figure 2.3 shows the force-displacement plot of an elastoplastic SDOF system and its corresponding elastic system.

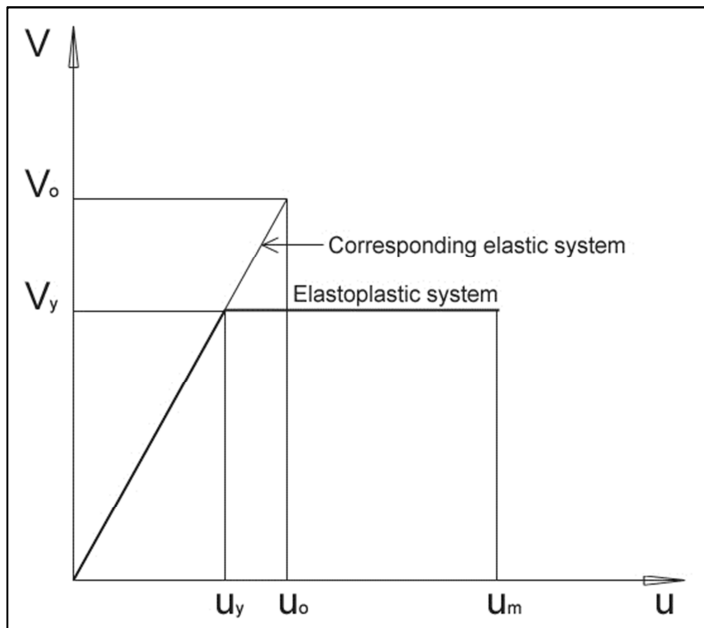


Figure 2.3: Force-displacement of elastoplastic SDOF system and its corresponding elastic SDOF system

The force reduction factor is defined as:

$$R = \frac{V_o}{V_y} \quad \dots\dots\dots 2.13$$

where V_o and u_o are the peak seismic base shear and displacement demand on the corresponding elastic system. V_y is the base shear force corresponding to the yield moment of the elastoplastic SDOF system.

Ductility is defined as:

$$\mu = \frac{u_m}{u_y} \quad \dots\dots\dots 2.14$$

where u_m is the peak seismic displacement demand on the elastoplastic SDOF system, and u_y is the yield displacement of the elastoplastic SDOF system.

2.1.6 R- μ -T relationship

The relationship between the force reduction factor and ductility is of interest. Two such relationships are called the *equal energy principle* and *equal displacement principle*. The equal energy principle has been observed to apply to short period systems, while the equal displacement principle applies to medium and long period systems (Chopra, 2007, p. 289). It should be noted that the validity of these principles has recently been questioned. This is discussed in Chapter 10.7. These principles are however sufficient to be used for initial estimation of displacements. The implications of these two principles are illustrated in Figure 2.4.

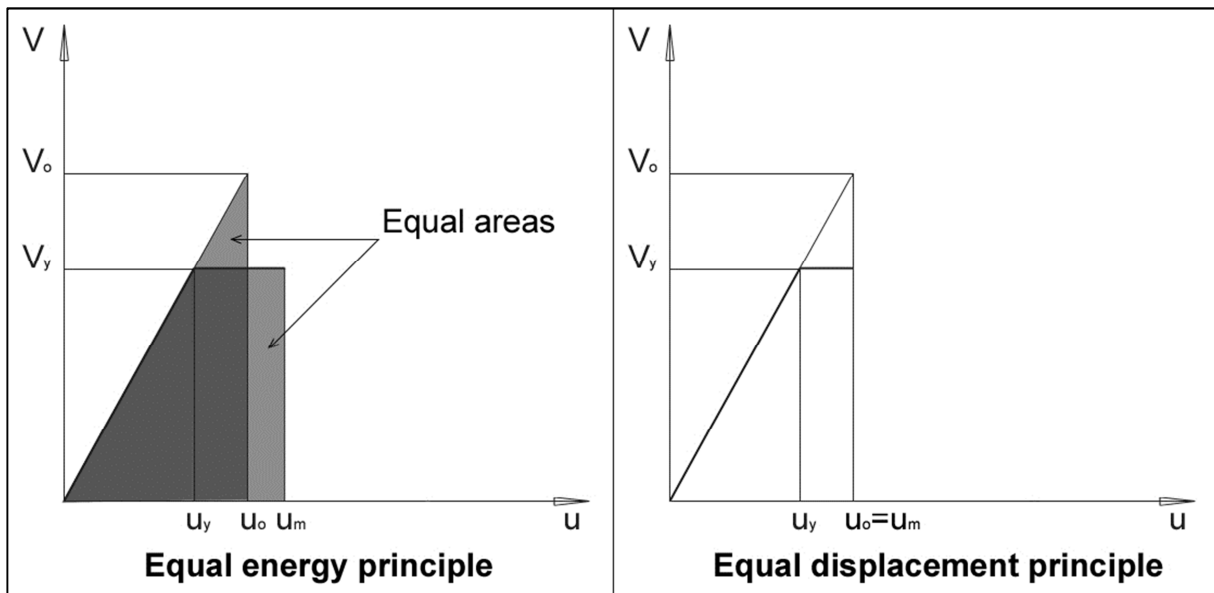


Figure 2.4: Equal energy and equal displacement principles

Mathematically these principles are expressed as (Chopra, 2007, p. 289):

$$R = \begin{cases} 1 & T < T_A \\ \sqrt{2\mu - 1} & T_B < T < T_{c'} \\ \mu & T > T_C \end{cases} \quad \begin{array}{l} \text{No force reduction allowed} \\ \text{Equal energy principle} \\ \text{Equal displacement principle} \end{array} \quad \dots\dots\dots 2.15$$

where T is the period of the system

$$T_A = 1/33 \text{ seconds}$$

T_B and T_C are defined in Table 2.1

$T_{c'}$ is obtained by the construction of acceleration, velocity, and displacement spectra on a four-way logarithmic graph paper (Chopra, 2007, pp. 118-119). $T_{c'}$

is only marginally smaller than T_C , and since Eq. 2.15 is used in this study only as an initial estimate of inelastic displacement demand, it was decided to choose $T_{c'} = T_C$.

2.1.7 Behaviour factor and design spectra

The behaviour factor (q) employed in seismic design codes acts in a similar fashion to the force reduction factor. Equations 2.16 to 2.19 define the design pseudo acceleration spectrum (SANS 10160-4, 2009, pp. 11-12). The elastic pseudo acceleration spectrum ($S_e(T)$ of Eq. 2.8) is obtained by setting $q = 1$.

$$0 \leq T \leq T_B: \quad S_d(T) = a_g \times S \left[\frac{2}{3} + \frac{T}{T_B} \left(\frac{2.5}{q} - \frac{2}{3} \right) \right] \quad \dots\dots\dots 2.16$$

$$T_B \leq T \leq T_C: \quad S_d(T) = a_g \times S \frac{2.5}{q} \quad \dots\dots\dots 2.17$$

$$T_C \leq T \leq T_D: \quad S_d(T) = \left\{ a_g \times S \frac{2.5}{q} \left[\frac{T_C}{T} \right] \right\} \text{ but } \geq \beta \times a_g \quad \dots\dots\dots 2.18$$

$$T_D \leq T: \quad S_d(T) = \left\{ a_g \times S \frac{2.5}{q} \left[\frac{T_C \times T_D}{T^2} \right] \right\} \text{ but } \geq \beta \times a_g \quad \dots\dots\dots 2.19$$

where a_g is the PGA,

S, T_B, T_C , and T_D are defined in Table 2.1,

T_B and T_C define the limits of the constant acceleration branch (see Figure 2.5),

T_D define the beginning of the constant displacement range of the spectrum (see Figure 2.5 and Figure 4.3), and

q is the behaviour factor.

β is a lower bound factor of the design spectra. A value of 0.2 is recommended.

Table 2.1: Values of the parameters which define the design pseudo acceleration spectrum (SANS 10160-4, 2009, p. 13)

| Ground type | S | T_B [s] | T_C [s] | T_D [s] |
|-------------|------|-----------|-----------|-----------|
| 1 | 1.00 | 0.15 | 0.4 | 2.0 |
| 2 | 1.20 | 0.15 | 0.5 | 2.0 |
| 3 | 1.15 | 0.20 | 0.6 | 2.0 |
| 4 | 1.35 | 0.20 | 0.8 | 2.0 |

Ground types 1 to 4 are defined in Table 2.2.

Table 2.2: Description of seismic ground types (SANS 10160-4, 2009, p. 10)

| Ground type | Description of stratigraphic profile |
|-------------|--|
| 1 | Rock or other rock-like geological formation, including at most 5 m of weaker material at the surface. |
| 2 | Deposits of very dense sand, gravel, or very stiff clay, at least several tens of m in thickness, characterised by a gradual increase of mechanical properties with depth. |
| 3 | Deep deposits of dense or medium dense sand, gravel or stiff clay with thickness from several tens to many hundreds of m |
| 4 | Deposits of loose-to-medium cohesion-less soil (with or without some soft cohesive layers), or of predominantly soft-to-firm cohesive soil |

The elastic pseudo acceleration spectrum, defined by equations 2.16 to 2.19 with $q = 1$, are plotted in Figure 2.5 for ground types 1 to 4.

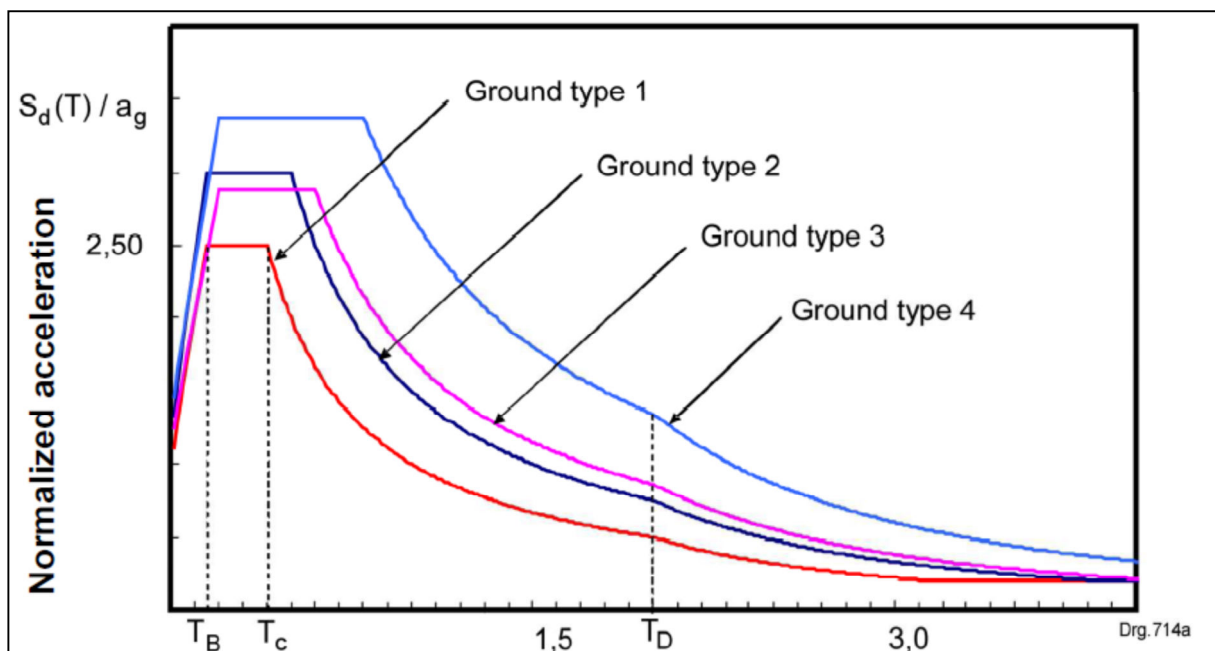


Figure 2.5: Elastic pseudo acceleration spectra ($q = 1$) (SANS 10160-4, 2009, p. 12)

Thus we see that the behaviour factor is similar to the force reduction factor, in that it reduces the elastic force demand. There are however two fundamental differences between the force reduction factor and the behaviour factor:

1. The yield strength of the structure (V_y) is normally higher than predicted during design. This is due to overstrength, which according to Dazio & Beyer (2009, p. 3-21) is caused by, among others, these three factors:

- a. Mean material strengths being higher than characteristic material strengths (see Chapter 6.1).

- b. Partial material and load factors. According to SANS 10160-1 (2009, p. 36) all partial factors for seismic design should be equal to unity (see Chapter 6.1). Thus, this factor does not contribute to overstrength in South Africa.
- c. Provided reinforcement is always more than needed reinforcement.

Thus, the behaviour factor could be related to the force reduction factor according to:

$$q = \Omega R \quad \dots\dots\dots 2.20$$

where

Ω is the overstrength factor.

2. In Figure 2.3 and Figure 2.4 it was assumed that the elastoplastic system has the same stiffness as the elastic system. However, if the strength of an elastic system is reduced, the resulting elastoplastic system would have a lower stiffness than the elastic system. This is due to the interdependency of strength and stiffness. According to Priestley *et al.* (2007, p. 9), “detailed analysis, and experimental evidence show ... that stiffness is essentially proportional to strength, and the yield curvature is essentially independent of strength, for a given section...”. One fundamental problem with force-based design is that the fundamental period, corresponding to an elastic system, is applied to a structure of which the strength (and stiffness) is reduced by the behaviour factor. This problem is addressed in Chapter 4.4. The influence of this problem on displacement prediction is assessed in Chapter 12.

2.2 Computational evaluation of the behaviour factor

2.2.1 Calculation of the behaviour factor for timber structural walls

This study is a continuation of a previous study by Spathelf (2008) who computationally determined values for the behaviour factor. Spathelf (2008) applied and adapted a method by Ceccotti (2008) which was developed for the calculation of behaviour factors for timber structural walls. Ceccotti’s method may be summarized in four steps (Ceccotti, 2008, pp. 157-158):

1. Design the structural wall for elastic seismic demand ($q = 1$) corresponding to a peak ground acceleration ($PGA_{u,code}$) prescribed by the code.
2. Define failure criteria. This may be based on material strain limits or inter storey drift limits.
3. Analyze a finite element model, which incorporates nonlinear hysteresis characteristics of the structure, according to an incremental dynamic analysis (IDA). An IDA is performed by subjecting the structural model to a set of ground motion records, each scaled to multiple levels of intensity, thus producing a set of curves of

intensity measure (IM) (e.g. PGA) versus damage measure (DM) (e.g. peak displacement) (Vamvatsikos & Cornell, 2002, p.491).

4. The PGA at which the failure criteria is reached, is defined as $PGA_{u,eff}$. The behavior factor is the ratio between $PGA_{u,eff}$ and $PGA_{u,code}$.

$$q = \frac{PGA_{u,eff}}{PGA_{u,code}} \quad \dots\dots\dots 2.21$$

2.2.2 Calculation of the behaviour factor through the capacity spectrum method

Spathelf (2008) used the same method, but instead of an IDA, he used the capacity spectrum method (Freeman, 2004). The main advantage of this method is that it is much less time consuming. A very brief summary of Spathelf's methodology is provided here. For more information please refer to (Spathelf, 2008).

1. The structural wall is designed for elastic seismic demand ($q = 1$). A static pushover analysis provides pushover curves which relate base shear force and MDOF displacement of the structure. The SDOF equivalent pushover curve can be calculated from the MDOF pushover curves. By dividing the base shear by the first modal mass, it is possible to draw a relationship between pseudo acceleration and displacement. This is the so called capacity spectrum.
2. Since a displacement response spectrum can be derived from the elastic pseudo acceleration spectrum, it is possible to plot pseudo acceleration versus displacement. This forms the demand spectrum.
3. The capacity spectrum can now be superimposed on the demand spectrum as shown in Figure 2.6. The elastic demand spectrum is scaled up to the point where it intersects the failure point on the capacity spectrum. PGA is defined as the intersection of the spectrum with the vertical axis, and thus the behaviour factor can easily be calculated according to Eq. 2.21.

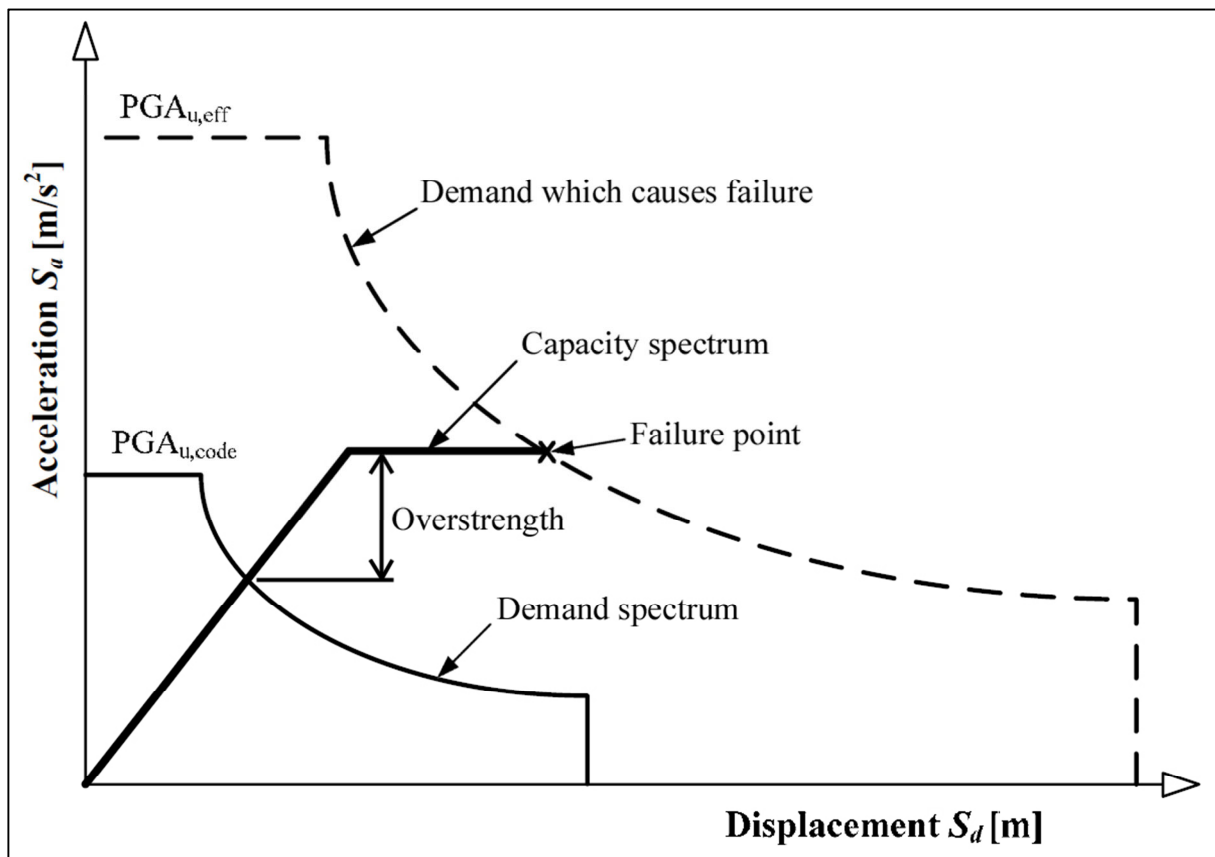


Figure 2.6: Proposed computational definition of the maximum value of the behaviour factor (Spathelf, 2008, p. 112)

Spathelf (2008) calculated the behaviour factor for a number of walls using the abovementioned method. If one however applies Ceccotti's method (Ceccotti, 2008) directly, i.e. by doing IDA, one finds that significantly higher levels of $PGA_{u,eff}$ are reached, resulting in much higher behaviour factor values. Possible reasons for this difference and the implication thereof are discussed below.

2.2.3 Comparison between pushover analysis and incremental dynamic analysis (IDA)

Vamvatsikos & Cornell (2002, p. 510) drew a comparison between pushover results and IDA results. This is shown in Figure 2.7 for a 20-storey steel moment resisting frame. The median IDA curve is obtained by calculating the median of the damage measure (DM) results for each level of intensity measure (IM). The equal displacement principle, which states that the peak displacement of an inelastic system is equal to the peak displacement of an equivalent elastic system, is also shown.

It may be seen that the median IDA curve rises much higher than the pushover curve. The reason for this is not provided, but Vamvatsikos & Cornell (2002) provide two reasons for the

hardening phenomenon which is often seen in IDA (see Figure 2.8). It may be that these same two reasons account for the difference between IDA and pushover results.

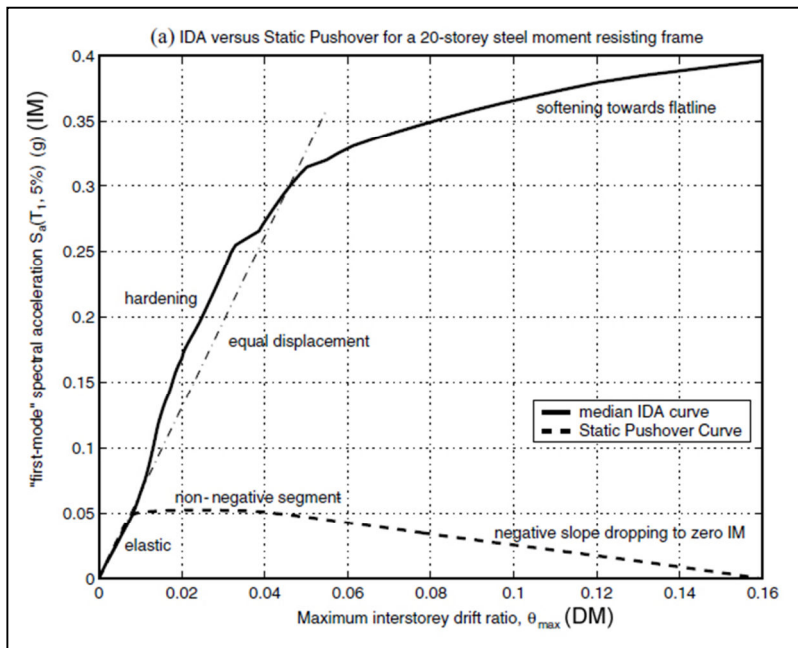


Figure 2.7: Comparison between median IDA and pushover (Vamvatsikos & Cornell, 2002, p. 510)

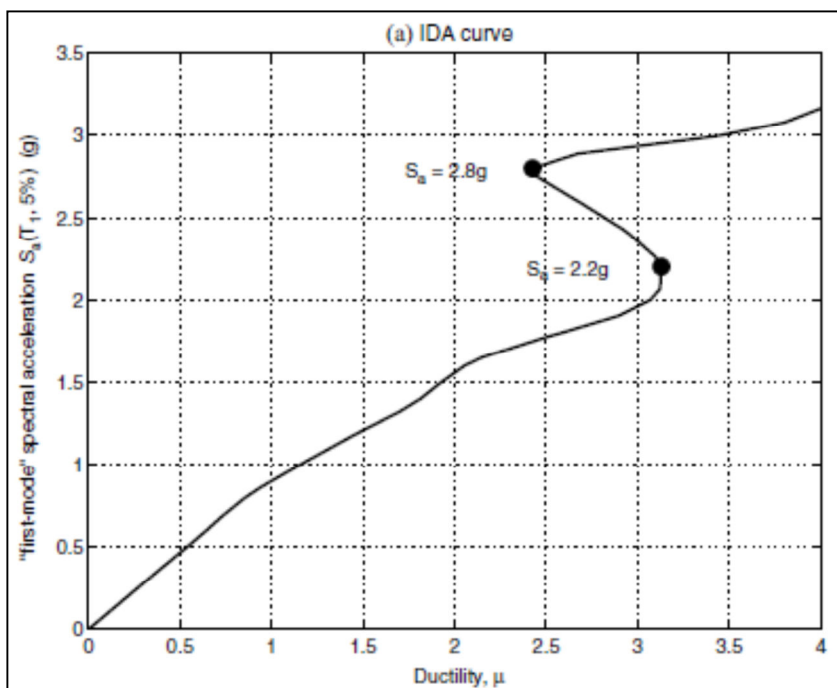


Figure 2.8: Hardening behaviour in IDA (Vamvatsikos & Cornell, 2002, p. 498)

Reason 1: "As the accelerogram is scaled up, weak response cycles in the early part of the response time-history become strong enough to inflict damage (yielding) thus altering the

properties of the structure for the subsequent, stronger cycles” (Vamvatsikos & Cornell, 2002, p. 499). This applies to multi-storey buildings where a lower storey that yields, acts as a fuse for higher storeys.

Reason 2: Hardening behaviour is not only observed for MDOF systems. SDOF oscillators have also been observed to exhibit hardening behaviour, which could perhaps be attributed to “period-elongation” (Vamvatsikos & Cornell, 2002, p. 499). An increase in fundamental period (called period-elongation) occurs when a structure softens due to yielding of its members. This increase in period leads to a reduction in acceleration demand and an increase in displacement demand (Freeman, 2004, p. 5).

As part of the initial investigation for this study a similar comparison between pushover analysis and IDA was done for a reinforced concrete structural wall. Seismostruct (Seismosoft, 2010) was used for the analysis. Failure was defined as the point where the confined concrete reaches a compressive strain of 0.015. Twenty ground motions, obtained from Dhakal, Mander & Mashiko (2006), were used for the IDA of which eight caused the structure to fail below a PGA of 10 m/s^2 . A viscous damping ratio of 5 percent was assumed throughout. The results are shown in Figure 2.9.

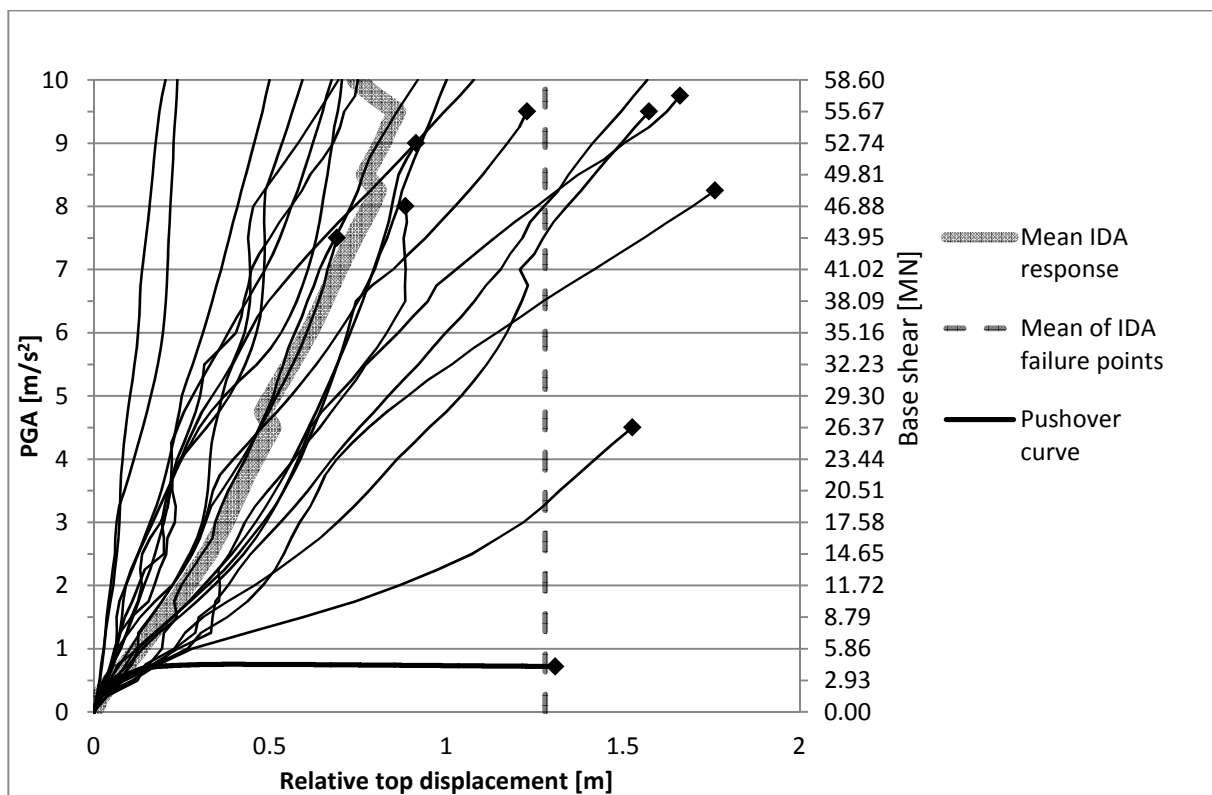


Figure 2.9: IDA versus pushover analysis as part of initial investigation

It is interesting to observe from Figure 2.9 that the mean of the eight IDA failure point displacements correspond very well with the failure displacement predicted by the pushover analysis. The PGA at which the IDA failures occur is however much larger than the PGA corresponding to the pushover analysis failure. Vamvatsikos & Cornell (2002, p. 509) had made a similar observation.

Whatever the reasons for the difference between IDA and pushover analysis might be, it is clear from Figure 2.9 that the pushover analysis predicts the absolute worst case response of a structure. This explains why IDA predicts higher behaviour factor values than pushover analysis. The discussion below explains why the high behaviour factor values predicted by IDA could not be trusted.

This author does not agree with the application of Ceccotti's method (Ceccotti, 2008) to reinforced concrete structural walls. The fundamental problem lies with starting the procedure with a behaviour factor of 1 and then obtaining as result a much higher behaviour factor (of 5 for example). A structure designed with a behaviour factor of 1 would have a much lower fundamental period than a structure designed with a behaviour factor of 5, and thus the dynamic response of the two structures would be completely different. In fact, the structure designed with a behaviour factor of 5 would displace more than the structure designed with a behaviour factor of 1. If one were to repeat Ceccotti's method, this time starting with a behaviour factor of 5, the result of the method should be a lower behaviour factor value (of 3 for example). It would thus seem that Ceccotti's procedure would have to be repeated numerous times, each time starting with the behaviour factor determined in the previous run of the procedure. This iteration process would have to be repeated until the difference between the start and end behaviour factor values are below an acceptable limit.

Since this iterative procedure would include IDA on a set of walls (see Chapter 4), it would be an almost insurmountable task. Instead of calculating a unique value for the behaviour factor, it would make more sense to rather only assess the current value of the behaviour factor.

2.3 Assessment of the behaviour factor – the concept of ductility demand and capacity

The behaviour factor represents the measure of overstrength and displacement ductility. Therefore, the assessment of the current behaviour factor value could best be accomplished by comparing displacement demand and displacement capacity. Displacement demand may

be calculated by using the equal displacement and equal energy principles ($R-\mu-T$ relationship of Eq. 2.15) or through ITHA, while displacement capacity is defined by code inter storey drift limits. Both the displacement demand and displacement capacity may be expressed in terms of ductility (defined in 2.1.5) for comparison purposes.

2.3.1 Ductility demand

It will be shown in Chapter 12 that the displacement calculation method prescribed by seismic design codes such as SANS 10160-4 (2009) is based on the equal displacement principle. However, the validity of the equal displacement principle has recently been questioned. The equal displacement principle was derived from the average results of sets of ITHA. Priestley *et al.* (2007, pp. 26-29) question the assumptions regarding the damping model assumed in these analyses. This is discussed in more detail in Chapter 10.7. Therefore, in this study ductility demand will be calculated according to the equal displacement or equal energy principles (depending on the fundamental period), and then verified by means of ITHA. This concept is addressed in step 4 of the methodology (Chapter 5).

2.3.2 Ductility capacity

In order to identify the applicable drift limits upon which ductility capacity should be based, an understanding of the seismic design strategies of current seismic codes is required. It will be shown that performance-based design forms the design strategy of both EN 1998-1 (2004) and SANS 10160-4 (2009).

FEMA 273 (ATC, 1997) is a guideline for the seismic rehabilitation of buildings. However, it serves to illustrate the following two key characteristics of any performance-based design guideline:

1. Building performance levels are made up of structural and non-structural performance levels. This is shown in Figure 2.10.
2. Building performance levels are matched with seismic hazard levels to define “limit states” or “safety objectives”. This is shown in Table 2.3. One such safety objective, called the basic safety objective (BSO), is satisfied when a structure complies with the “Life safety” performance level under a BSE-1 earthquake, and the “Collapse prevention” performance level under a BSE-2 earthquake (see Table 2.3).

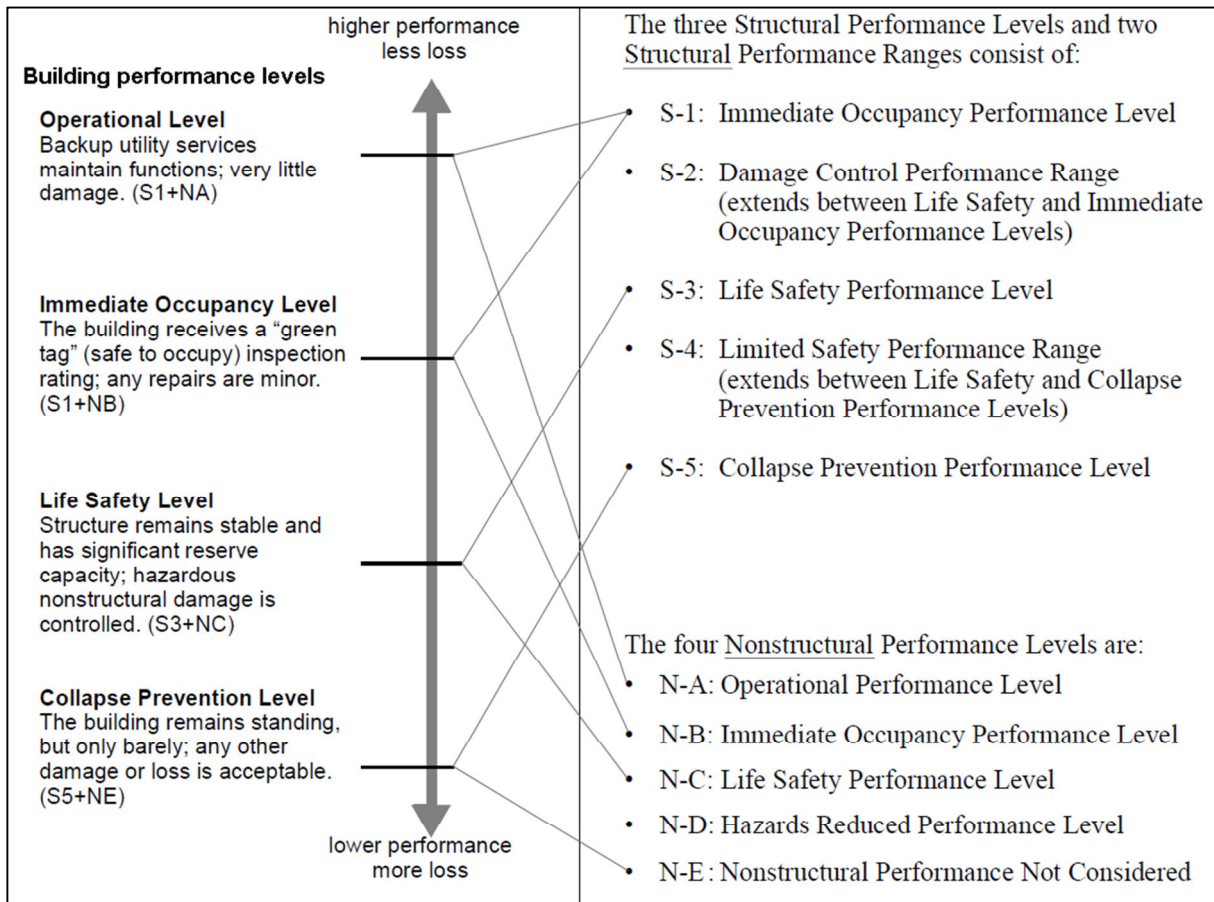


Figure 2.10: Definition of building performance levels according to FEMA 273 (ATC, 1997, p. 1-2)

Table 2.3: Rehabilitation objectives according to FEMA 273 (ATC, 1997, p. 2-5)

| | | Building Performance Levels | | | |
|-------------------------|----------------------|-------------------------------------|---|-------------------------------------|---|
| | | Operational Performance Level (1-A) | Immediate Occupancy Performance Level (1-B) | Life Safety Performance Level (3-C) | Collapse Prevention Performance Level (5-E) |
| Earthquake Hazard Level | 50%/50 year | a | b | c | d |
| | 20%/50 year | e | f | g | h |
| | BSE-1 (~10%/50 year) | i | j | k | l |
| | BSE-2 (~2%/50 year) | m | n | o | p |

k + p = BSO

EN 1998-1 (2004) and SANS 10160-4 (2009) are based on the same principle. EN 1998-1 (2004) defines two performance requirements (equivalent to building performance levels in FEMA 273), namely the “damage limitation requirement” and the “no-collapse requirement”. SANS 10160-4 (2009) does not explicitly define any performance level, but implicitly conforms to the *no-collapse requirement* of EN 1998-1 (2004).

The desired structural performance for the *no-collapse requirement* of EN 1998-1 is described in EN 1998-1 (2004) as: “the structure shall be designed and constructed to withstand the design seismic action ... without local or global collapse, thus retaining its structural integrity and a residual load bearing capacity after the seismic events”.

Priestley *et al.* (2007, p. 71) describes the desired structural performance at this limit state as follows:

At this limit state, a certain amount of repairable damage is acceptable, but the cost should be significantly less than the cost of replacement. Damage to concrete buildings and bridges may include spalling of cover concrete requiring injection grouting to avoid later corrosion. Fracture of transverse or longitudinal reinforcement, or buckling of longitudinal reinforcement should not occur, and the core concrete in plastic hinge regions should not need replacement. (Priestley et al., 2007, p. 71)

As stated in the extract from EN 1998-1 (2004) above, the structural performance is deemed to be satisfied if the structural system is designed in the ultimate limit state for the design seismic action. For this limit state the design seismic action is defined, in both EN 1998-1 (2004) and SANS 10160-4 (2009), by an earthquake with a return period of 475 years. The design spectrum is defined by Eqs. 2.16 to 2.19. Design to satisfy this limit state is discussed in Chapter 8.

Non-structural performance criteria however also need to be assessed at this limit state. Priestley et al. (2007, p. 71) states that “it is difficult to avoid excessive damage when the drift levels exceed about 0.025, and hence it is common for building design codes to specify drift limits of 0.02 to 0.025”.

The following drift limits are specified by EN 1998-1 (2004):

- *For buildings having non-structural elements of brittle materials attached to the structure:*

$$d_r v \leq 0.005 h_s \quad \dots\dots\dots 2.22$$

- *For buildings having ductile non-structural elements:*

$$d_r v \leq 0.0075 h_s \quad \dots\dots\dots 2.23$$

- *For buildings having non-structural elements fixed in a way so as not to interfere with structural deformations, or without non-structural elements:*

$$d_r v \leq 0.01 h_s \quad \dots\dots\dots 2.24$$

where d_r is the relative displacement between the top and bottom of a storey in the structure

h_s is the storey height

ν is a reduction factor which is equal to between 0.4 and 0.5, depending on the importance class of the structure.

SANS 10160-4 (2009, p. 27) imposes the following drift limits:

$$d_r \leq 0.025h_s \quad \text{if } T < 0.7 \text{ s} \quad \dots\dots\dots 2.25$$

$$d_r \leq 0.02h_s \quad \text{if } T > 0.7 \text{ s} \quad \dots\dots\dots 2.26$$

where T is the fundamental period of the structure, defined in Eq. 4.1

It will be shown in Chapter 3 that separating non-structural infill panels from the structural system forms part of good conceptual design practice. Thus, Eq. 2.24 would apply. It may be seen that for a ν value of 0.5, Eq. 2.24 yields a drift limit of 0.02, which corresponds to the SANS drift limit for fundamental periods longer than 0.7 seconds. Thus, in this study ductility capacity is based on the period-dependent drift limits of Eqs. 2.25 and 2.26. The calculation of the ductility capacity as a function of drift limits is described in Chapter 9.3.

This chapter has served to introduce key principles and defines the purpose of this study, which is to assess the current value of the behaviour factor by comparing displacement demand and capacity. It was argued that the calculation of an exact behaviour factor value is not feasible. In Chapter 3 a generic structural wall is defined by considering good conceptual design guidelines.

3. Structural wall buildings

In order to perform a comprehensive study which is manageable within the time frame of a Master's thesis it becomes necessary to consider an individual structural wall which would be representative of all structural walls designed according to SANS 10160-4 (2009). It is possible, for analysis purposes, to isolate such a generic structural wall from a building as long as the conceptual design of the building is sound.

3.1 Good conceptual design

SANS 10160-4 (2009) and other sources such as (Bachmann, 2003) provide guidelines for conceptual design of structural wall buildings. The following description of conceptual design guidelines, relevant to structural walls and this study are based on Bachmann (2003).

3.1.1 Adequate foundation

The structural walls are anchored in sufficiently rigid foundations, such as raft foundations, which would transmit loads from the superstructure without allowing the walls to rock.

3.1.2 Avoid discontinuities along the height of the building

Discontinuities in the stiffness of the structural walls along the height of the building should be avoided. All walls should extend over the full height of the structure. It is preferable that the wall cross section remains constant over the height of the wall. Discontinuities in stiffness cause irregular dynamic behaviour and disrupt the flow of forces through the structural system. An increase in stiffness and strength from the bottom up, such as in the left of Figure 3.1, is less favourable than a decrease in stiffness, such as in the right of Figure 3.1. In both cases, however, the calculation of forces, design, and detailing should be done very carefully.

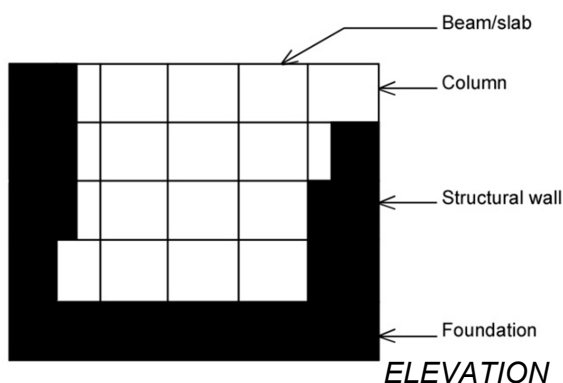


Figure 3.1: Discontinuous structural walls

3.1.3 Do not offset structural walls

Bracing offsets should be absolutely avoided (see Figure 3.2). This includes both in plane bracing offsets (top of the plan figure) or out of plane offsets (bottom of the plan figure).

Internal forces and displacement of beams and columns are greatly increased. The seismic resistance of such a structure is usually also noticeably reduced.

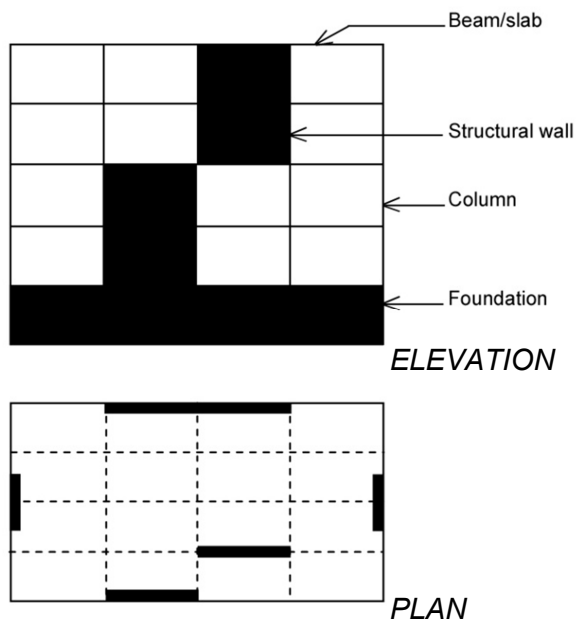


Figure 3.2: Bracing offsets

3.1.4 Reinforced concrete slabs should act as rigid diaphragms

Floor slabs should be connected to all vertical structural elements and ensure that all lateral loads are distributed to the structural walls. Slabs made of prefabricated elements are not adequate unless they are covered with reinforced concrete of sufficient thickness. “Monolithic reinforced concrete slabs with eventual additional boundary reinforcement bars are much better suited to act as diaphragms” (Bachmann, 2003).

3.1.5 Place at least two walls in two orthogonal directions

Place at least two structural walls in each of two orthogonal directions as close as possible to the perimeter of the building. This assures adequate lateral resistance in both directions as well as torsional stability.

3.1.6 Avoid asymmetric bracing

Asymmetric bracing should be avoided. Each floor plan in Figure 3.3 has a centre of mass ‘M’ through which inertia forces act. The point marked ‘S’ represents the centre of stiffness. Where the centre of mass and the centre of stiffness do not coincide, twisting motion about the centre of stiffness occurs. This has the most adverse effect on the columns furthest away from the centre of stiffness which often fail rapidly.

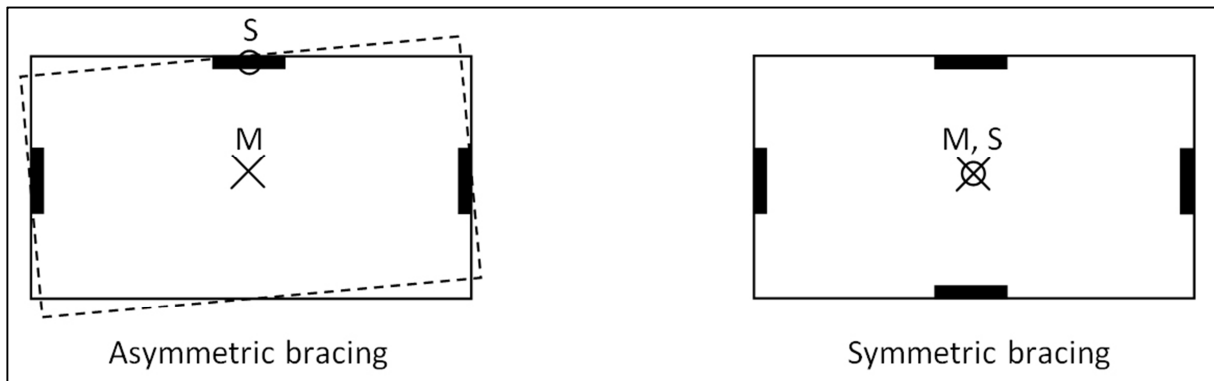


Figure 3.3: Asymmetric vs. symmetric bracing (Plan view)

3.1.7 Separate non-structural masonry walls by joints

In order to prevent damage to brittle masonry infill panels, which could cause serious injury or fatalities, it is necessary to provide joints between masonry walls and reinforced concrete members (see Figure 3.4). Such joints should consist of a very soft soundproof material, such as soft rubber. Styrofoam or cork would be too stiff. Often it would also be necessary to secure the masonry walls against out of plane action, e.g. by support angles.

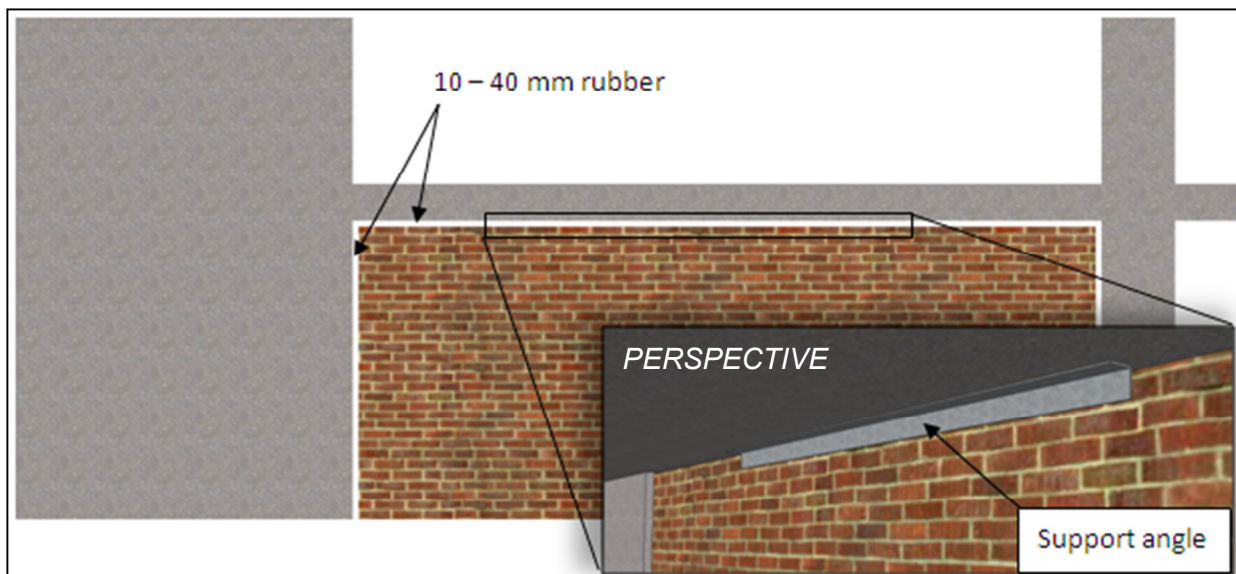


Figure 3.4: Separation of non-structural masonry walls (Elevation)

3.2 Generic structural wall

Based on the above mentioned conceptual design guidelines (3.1.1 – 3.1.7) it is possible, for analysis purposes, to isolate a structural wall from a structural wall building in the following way (see Figure 3.5):

1. The wall is assumed to be built on a rigid foundation allowing no rotation or movement of the base of the wall.

2. The cross section of the wall remains constant over the full height of the wall. The wall extends to the roof of the building.
3. No offsets occur over the height of the wall.
4. Reinforced concrete slabs act as rigid diaphragms. It is thus possible to consider floor masses as lumped masses at each storey (Figure 3.5(d)).
5. At least two structural walls are placed in each of two orthogonal directions on the perimeter of the building. If more than two walls are placed in a direction, the additional walls may be internal, i.e. not near the perimeter of the building.
6. Bracing is perfectly symmetric:
 - a. Due to twisting motion, structural walls which form part of an asymmetric building would experience a greater force demand than walls that form part of a symmetric building. SANS 10160-4 (2009, p. 26) does however make provision for such walls. In addition, SANS 10160-4 (2009, p. 26) makes provision for accidental eccentricities. Both of these provisions increase the force capacity of such walls. Since both force demand and force capacity of asymmetric walls would increase, it was assumed for this study that all bracing is perfectly symmetric. Additional loads due to torsional effects are thus ignored.
 - b. The earthquake is assumed to act in one of the orthogonal directions. SANS 10160-4 (2009, p. 18) specifies that the design seismic load in each direction should be increased by adding 30 % of the seismic load of the other orthogonal direction. This is to take into account the event in which the earthquake acts in a non-orthogonal direction. The same argument as in 6(a) holds true: both the force demand and force capacity would increase. For this reason, this provision is ignored in this study.
 - c. At least two walls on opposite sides of the building work in parallel to resist the seismic load. The responses of the walls are equal and thus only one of the two walls needs to be analyzed (Figure 3.5(b)).
7. It is assumed that the structural wall resists the total lateral seismic load. The contribution from the reinforced concrete frame is assumed to be negligible (Paulay & Priestley, 1992, p.363) (Dazio & Beyer, 2009, p.5-25). Non-structural masonry walls do not contribute to the lateral resistance since they are separated by means of isolation joints as discussed in 3.1.7.

It is thus possible to define a structural wall as a cantilever beam with lumped masses at the storey heights (see Figure 3.5(d)). An axial load P , representing the vertical floor loads transferred into the wall, is applied at each storey. Both the axial load and the lumped mass

depend on the value of the distributed floor load. The axial load depends on the column spacing, while the lumped mass associated with each wall depends on the distance between parallel walls. In Chapter 5 it will be shown that the magnitude of the lumped mass, and thus the hypothetical wall spacing used in the analyses, is influenced by the period calculation method used in design.

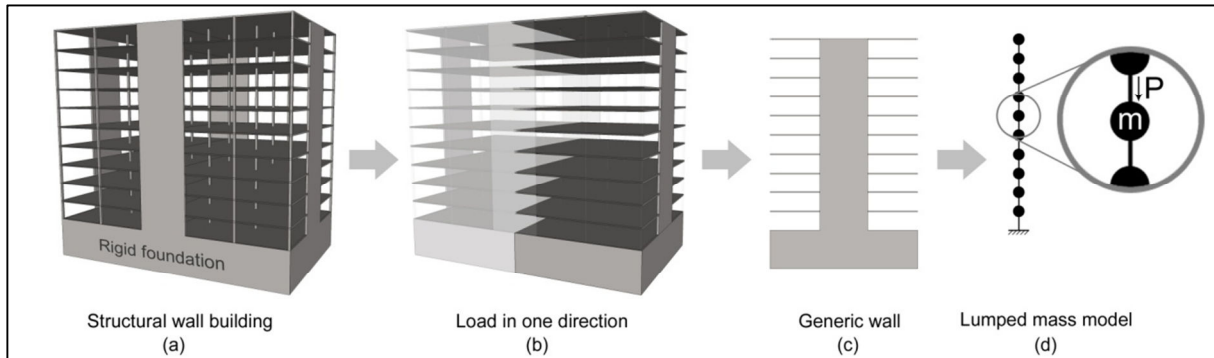


Figure 3.5: Generic wall

It will be shown in Chapter 7.5 that the value of the axial load does not affect the outcome of this study, and could thus be chosen arbitrarily. However, to estimate a realistic value for the axial load, the following calculations were carried out using SANS 10160-2 (2009):

- A slab thickness of 250 mm results in a self-weight of 6 kPa. A self-weight distributed load of 5 kPa is added which is representative of all non-structural components and equipment, which could include screed, infill wall panels, and services. An imposed load of 5 kPa is assumed, which corresponds to the maximum distributed floor load according to SANS 10160-2 (2009, p. 11).
- The combination factor for variable actions in occupancy class category A to D and G is 0.3 (SANS 10160-1, 2009, p. 29).
- The value of the permanent distributed floor load is thus:

$$w = G + 0.3Q = (6 + 5) + 0.3(5) = 12.5 \text{ kPa}$$
- Assuming a column spacing of 6 m and a wall section length of 6 m, the tributary area for vertical load is 72 m² (See Figure 3.6).
- The generic wall may be either internal or on the perimeter of the building. To adopt a reasonable axial load value to represent both cases, the value of the axial load contribution from each floor is calculated as $P = 0.75wA = 0.75(12.5)(72) = 675 \text{ kN}$. This value of P was used for all walls throughout this study.

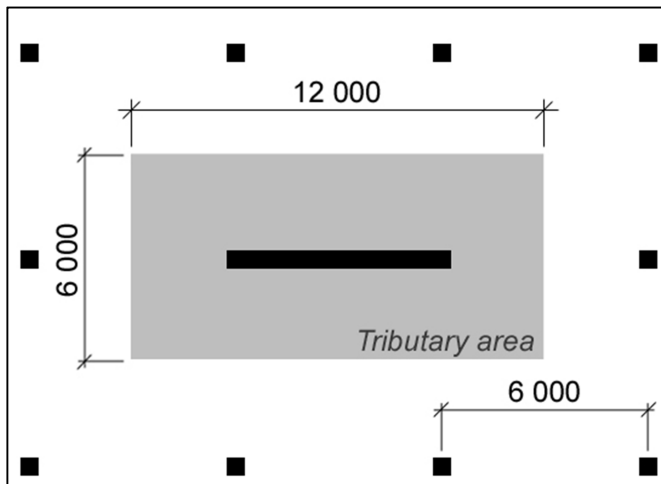


Figure 3.6: Tributary area for axial load P

The value of the lumped mass will be calculated individually for each wall. This will be discussed in Chapter 5.

Thus we have seen how, for analysis purposes, a structural wall can be isolated from a structural wall building. In this chapter the structural wall was of rectangular cross sectional shape and no particular dimensions. The next chapter will look at parameters which define the characteristics of structural walls and would influence the outcome of this study.

4. Scope of the study

The purpose of this chapter is to identify parameters which would influence the outcome of this study. A suitable selection of these parameters is made to arrive at a set of structural walls which would define the scope of this study. The following parameters are identified:

- Wall section shapes
- Ground types
- Wall aspect ratio
- Period calculation method
- Number of storeys

Other parameters which are identified, but not treated in this chapter are the following:

- The reinforcement content of the wall section
- The axial load on the section
- The width of the wall section (b_w)
- Material strengths

The influence of these parameters on the outcome of this study can only be fully understood in the light of moment-curvature analysis results. Thus, these parameters are only discussed in Chapter 7.5.

4.1 Wall sectional shapes

Figure 4.1 shows some of the most commonly used sectional shapes of structural walls (Dazio & Beyer, 2009, p.7-8). The rectangular section is by far the simplest section to design. Walls with boundary elements such as shown in Figure 4.1(b) are subject to high shear stresses (Dazio & Beyer, 2009, p.7-8). Unsymmetrical walls, such as a T or L sections require very careful design, since their strength and stiffness differ depending on the loading direction (Priestley *et al.*, 2007, p.314).

It would thus be very difficult, if at all possible, to create a generic wall of any of the sectional shapes in Figure 4.1 (b) to (d). The rectangular cross section is the simplest form, and a component of any of the other more complex forms. For this reason, and since Bachmann (2003, p.26) states that “reinforced concrete structural walls of rectangular cross-section constitute the most suitable bracing system against seismic actions”, only walls with rectangular cross-section is considered in this study.

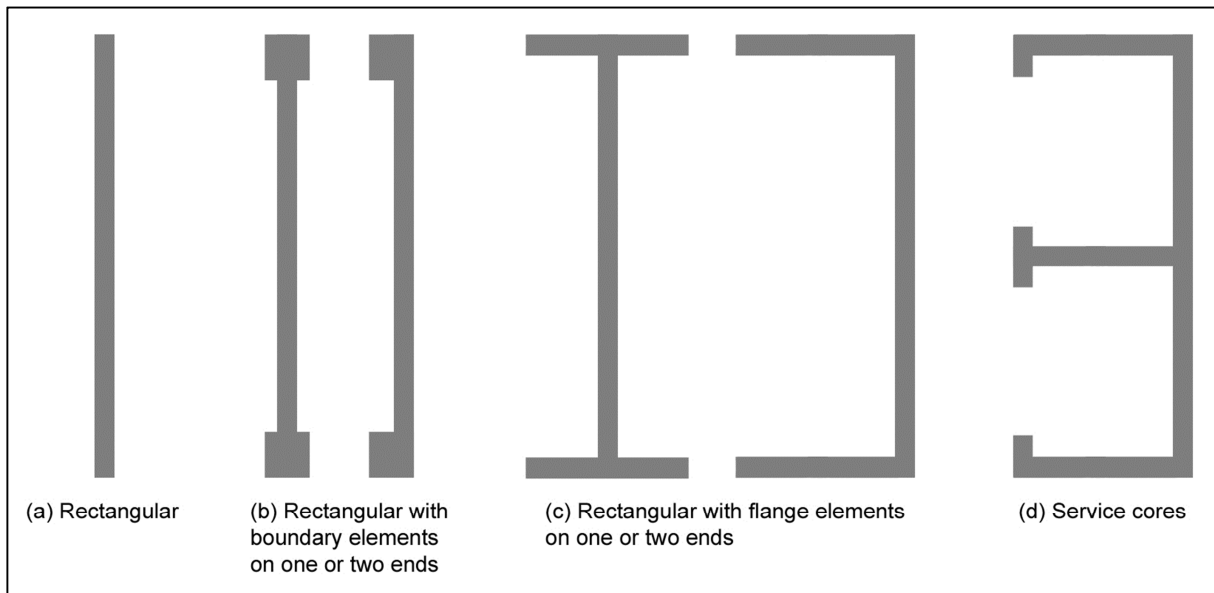


Figure 4.1: Wall sectional shapes (Dazio & Beyer, 2009, p.7-8)

4.2 Ground types

In Chapter 2.1.7 the pseudo acceleration design spectra were defined for ground types 1 to 4 (see Figure 2.5). It can be seen that Ground Types 1 and 4 define the envelope of all acceleration demand. Thus only these two ground types are considered in this study.

4.3 Wall aspect ratio

The aspect ratio of the wall, defined as the height of the wall h_w divided by the length of the wall section l_w (see Figure 4.2), is another variable to be considered.

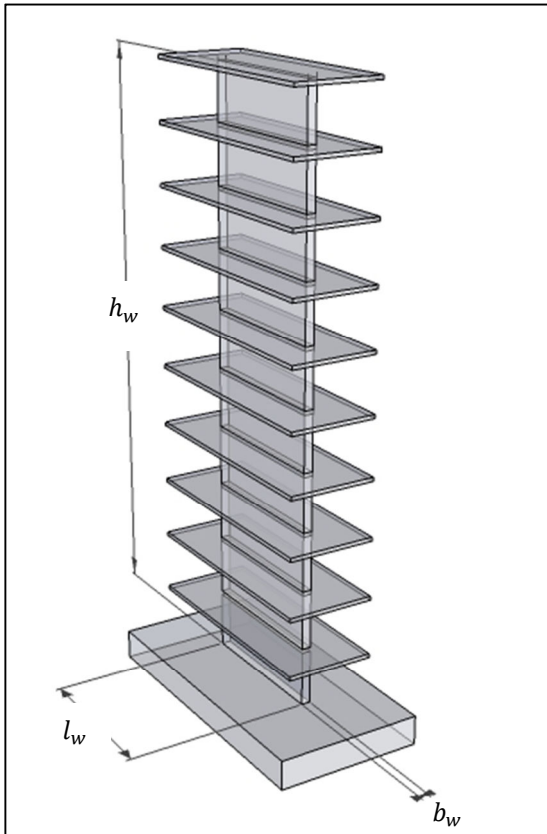


Figure 4.2: Definition of wall dimensions

The aspect ratio determines the extent to which a wall responds in flexure or shear. A wall with an aspect ratio of less than three responds predominantly in shear (Paulay & Priestley, 1992, p.371). As already stated, a structural wall should preferably respond in ductile flexural action.

The aspect ratio should also not be too large. Priestley *et al.* (2007, p.326) have shown that the elastic seismic force should not be reduced at all (behaviour factor ≤ 1) for walls with an aspect ratio of more than approximately 9. This is discussed in Chapter 9.3.2.

For the two abovementioned reasons it was decided to consider walls with aspect ratios of 3, 5 and 8. Bachmann (2003, p. 26) states, as part of conceptual design guidelines, that wall aspect ratios should preferably be between 3 and 5. The aspect ratio of 8 is considered to assess the impact of such a high aspect ratio on the ductility capacity.

4.4 Period calculation method

The walls in this study are designed according to the two period calculation methods discussed below.

4.4.1 Method 1

According to SANS 10160-4 (2009, p. 24) the fundamental period of a structure may be calculated using Eq. 4.1:

$$T_1 = C_T h_w^{\frac{3}{4}} \quad \dots\dots\dots 4.1$$

where:

T_1 is the fundamental period of the structure according to SANS 10160-4 (2009)

$$C_T = \frac{0.075}{\sqrt{A_c}} \text{ for structural walls} \quad \dots\dots\dots 4.2$$

where A_c is, among other, a function of the number of structural walls in the direction under consideration. Since a generic wall will be used in this study, the number of walls is unknown. Few walls would imply a large period, which is covered by Method 2 described below. A short period implied by a large number of walls would lead to a significant underestimation of displacement (see Chapter 12). Thus it was decided to use $C_T = 0.05$, which corresponds to roughly eight walls and is recommended by the code for use on “all other buildings” (SANS 10160-4, 2009, p. 24).

h_w is the height of the building, in meters, from the top of the foundation or rigid basement (see Figure 4.2).

Eq. 4.1 has been shown to correspond well to measured building periods (Priestley *et al.*, 2007, p.11). These measurements were however taken at very low levels of vibration (normally resulting from wind vibration), where nonstructural participation is high and concrete sections are uncracked (Priestley *et al.*, 2007, p.11). Under seismic excitation, however, sections are allowed to crack and thus structures respond at much higher fundamental periods. It has often been argued that using a too low period is conservative, since the acceleration demand is then overestimated (see Figure 4.3(a)) (Priestley *et al.*, 2007, p.11). This is however not true, since an underestimation in period results in an underestimation of displacements as shown in Figure 4.3(b) (Dazio & Beyer, 2009, p.5-15). More information on this topic is provided in Chapter 12.

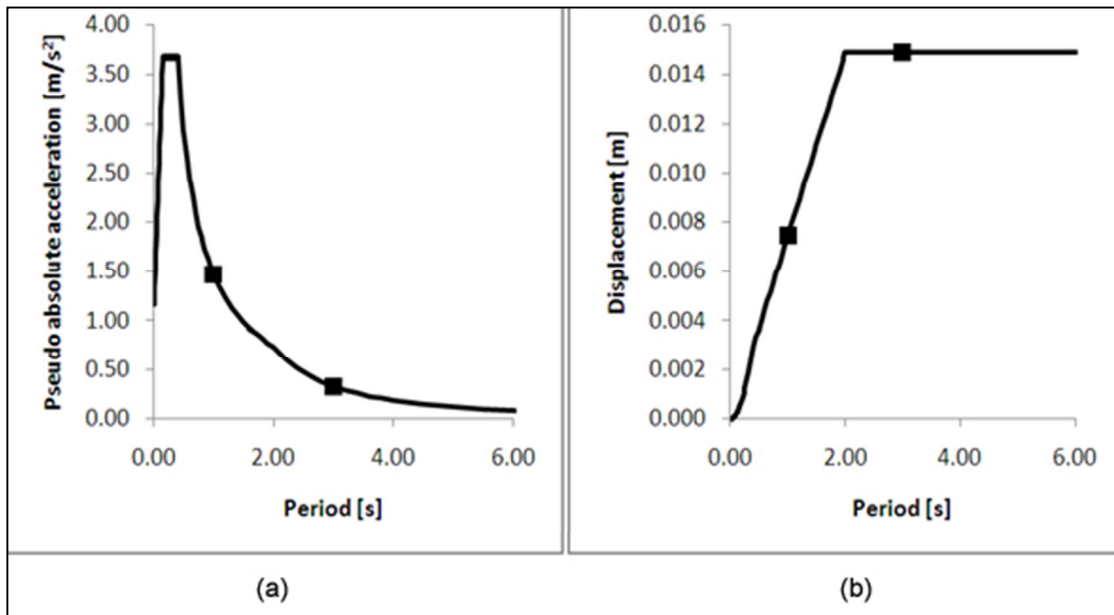


Figure 4.3: Overestimation of acceleration and underestimation of displacement

Because Eq. 4.1 underestimates the fundamental period, Dazio & Beyer (2009, p.5-16) state that it “should never be used”. Eigenvalue analyses based on the stiffness derived from the cracked section should rather be used (Dazio & Beyer, 2009, pp.5-16 – 5-18) (Priestley *et al.*, 2007, p.11).

4.4.2 Method 2

The stiffness of a cracked reinforced concrete section can be obtained from a moment-curvature analysis of the section. This is done by drawing a bilinear approximation to the moment-curvature curve as shown in Figure 4.4. This is described in Chapter 7.

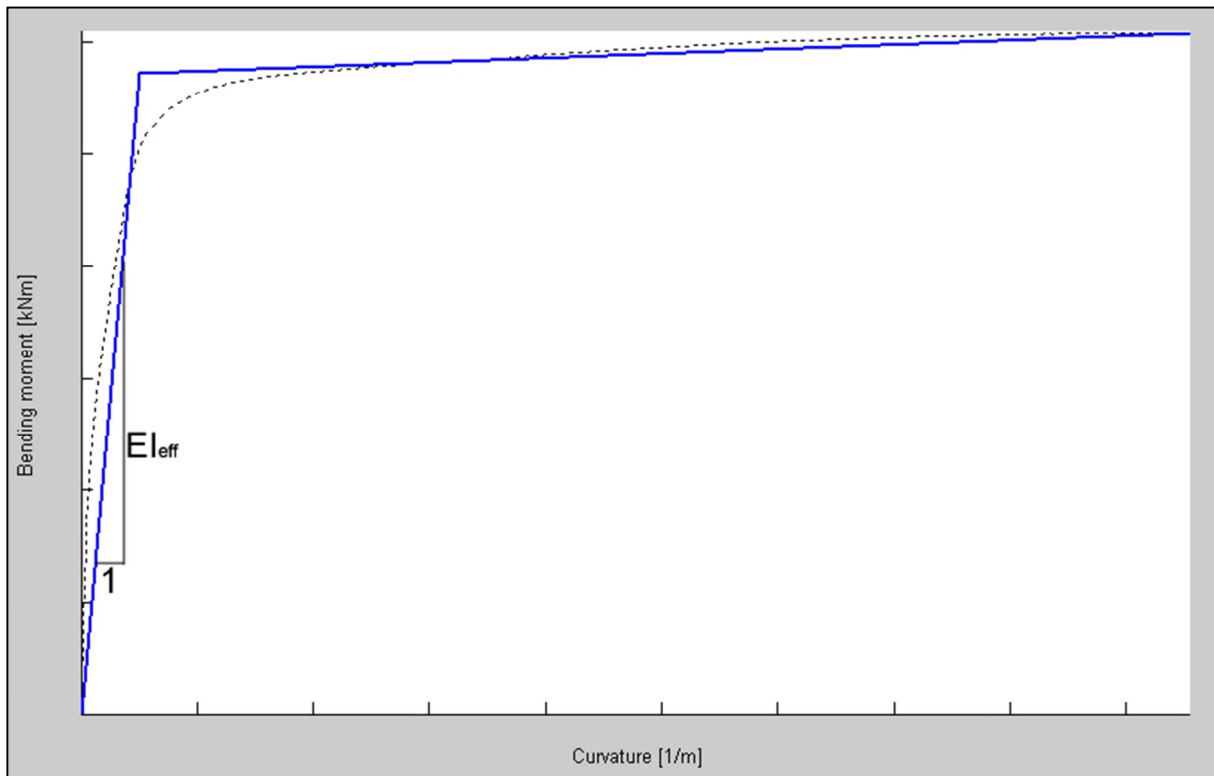


Figure 4.4: Effective cracked section stiffness from moment-curvature results

The fundamental period is obtained from an eigenvalue analysis, assuming the same sectional stiffness, EI_{eff} , over the height of the wall. The design of a wall, using this method, is unfortunately iterative, since the moment curvature analysis cannot be done unless the reinforcement content and layout of the section is known, and the demand on the section depends on the stiffness of the section. The iterative method depicted in Figure 4.5 should thus be followed.

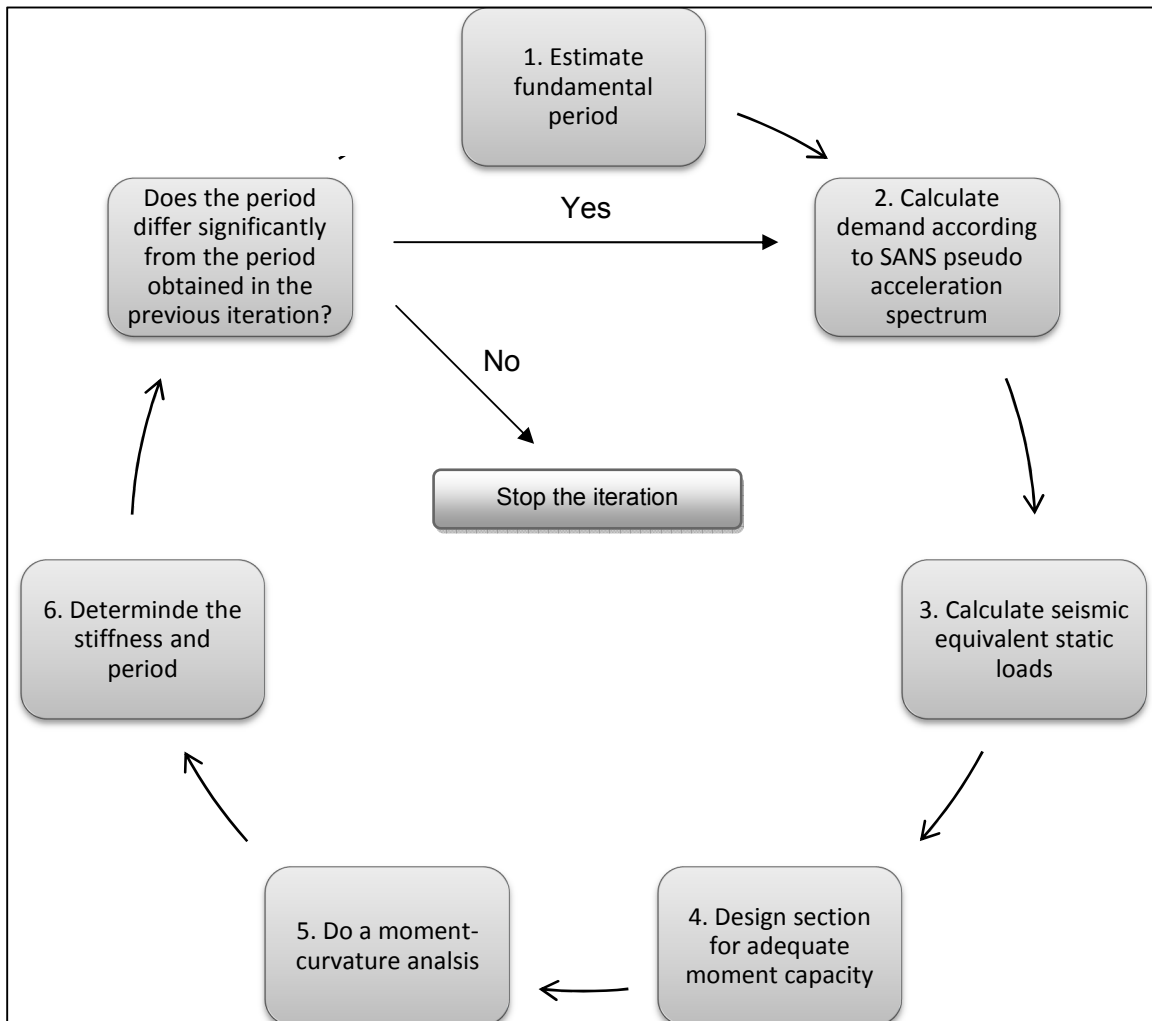


Figure 4.5: Design method 2

4.5 Number of storeys

This study will focus on the series of walls shown in Figure 4.6. The storey height was chosen as 3.23 m. Eq. 4.1 is only applicable for buildings up to a height of 40 m. It was initially decided to study walls with heights of approximately 20, 40, and 60 m. The 60 m wall is designed according to Method 2 only. The shorter walls were later added to the study to obtain structures with short fundamental periods.

The reason that the aspect ratio increases with height is that the wall section lengths needed to remain within reasonable limits. The wall section lengths are shown in Table 4.1. It may be seen that only the shaded cells contain reasonable section lengths.

Table 4.1: Wall section lengths

| Length of wall section (l_w) [m] | | | | |
|--------------------------------------|------------|--------------|--------|-------|
| Number of storeys | Height [m] | Aspect ratio | | |
| | | 3 | 5 | 8 |
| 1 | 3.230 | 1.080 | 0.640 | 0.400 |
| 2 | 6.460 | 2.160 | 1.300 | 0.800 |
| 3 | 9.690 | 3.240 | 1.940 | 1.220 |
| 6 | 19.380 | 6.460 | 3.880 | 2.420 |
| 12 | 38.760 | 12.920 | 7.760 | 4.840 |
| 18 | 58.140 | 19.380 | 11.620 | 7.260 |

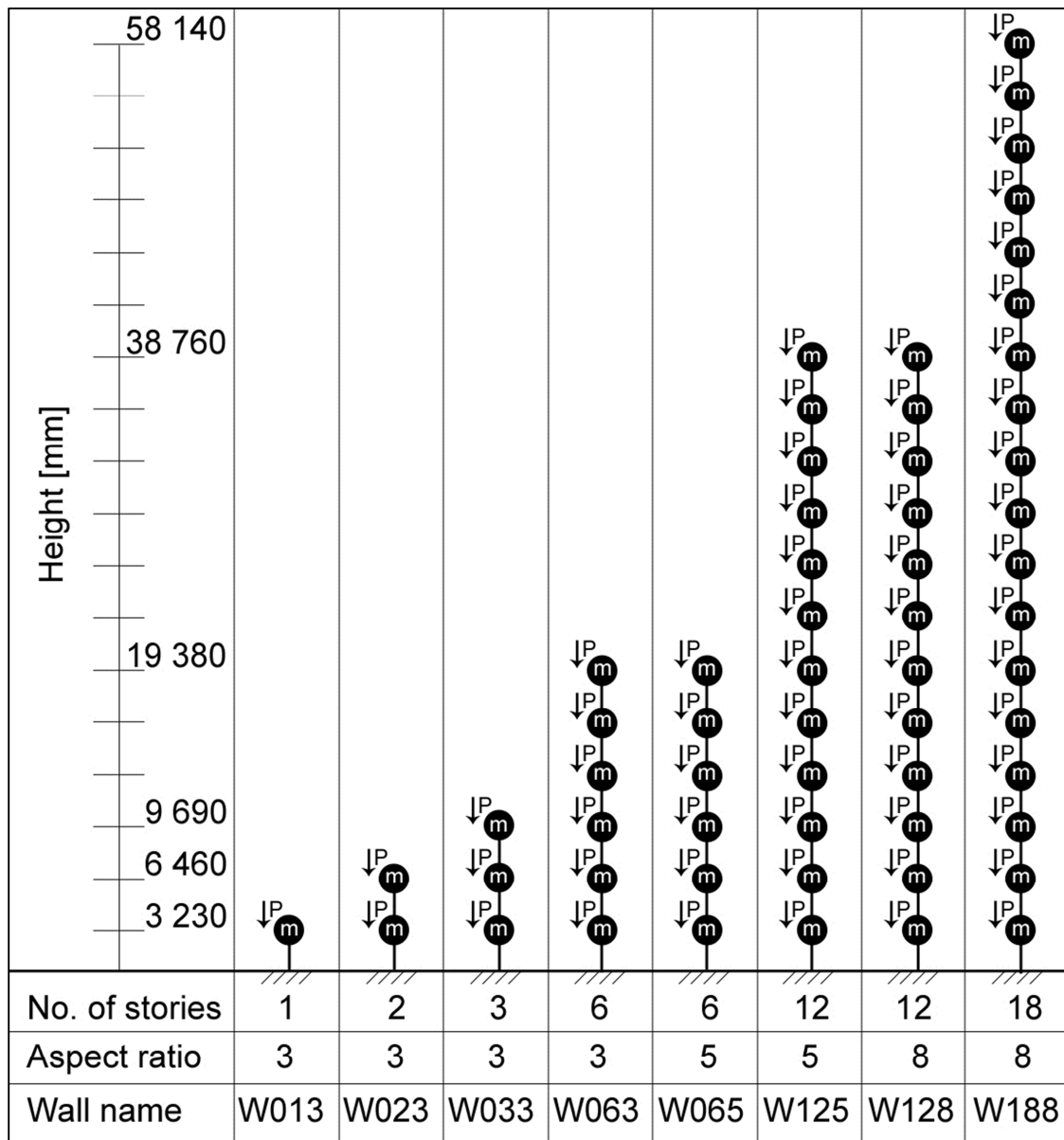


Figure 4.6: Generic wall range

For easy reference the walls were labelled as indicated in Figure 4.6. The first two digits of the name is the number of storeys, while the last digit is the aspect ratio of the wall.

Thus, the scope of this study is composed of the eight walls shown in Figure 4.6. These walls will be designed according to both period calculation methods discussed earlier. Ground types 1 and 4 of SANS 10160-4 (2009) will be used to define the range of seismic ground types. The methodology according to which seismic drift will be assessed for these eight walls is discussed in the next chapter.

5. Methodology

As stated in the introduction, the purpose of this study is to assess the seismic drift of reinforced concrete structural walls designed according to SANS 10160-4 (2009). This is done by comparing ductility demand to ductility capacity, where the ductility capacity corresponds to code drift limits. For the definition of ductility refer to Chapter 2.1.5.

The key parameter which, during design, influences the ductility demand is the behaviour factor (refer to Chapter 2.1.7). The purpose of this investigation therefore, is to assess if the use of the current value of the behaviour factor, as provided in SANS 101060-4 (2009, p. 22), results in the design of walls of which the seismic drift would be within acceptable limits. If not, revision of the behaviour factor might be necessary.

The methodology used in this study is illustrated in Figure 5.1 and is listed in steps 1 through 6 below. These steps are applied to each of the eight walls defined in the scope of this study for both ground types 1 and 4 (refer to Chapter 4). Thus, the steps are applied a total of 16 times. Steps 1 to 3 describe the design of the walls, while steps 4 to 6 describe the assessment of the walls.

Two period calculation methods were introduced in Chapter 4.4. The difference between these two methods will be evaluated by using both these period calculation methods in the design of the walls.

Different period calculation methods would produce different force demands. In practice, the mass of a structure is fixed, and thus different force demands would be reflected in the longitudinal reinforcement content of the structural wall, or the wall cross-section dimensions. For this study however, the cross-sectional dimensions are fixed (for purpose of comparison), and thus it was decided to use an “inverse” design method, where the capacity of the cross-section is fixed at the start (step 1) and the associated floor masses are obtained as the final result of the design (step 3).

1. From Figure 4.6 the height of the wall and the aspect ratio is known. Thus the length of the wall section l_w can be calculated. The width of the wall section b_w is chosen such that wall instability due to out-of-plane buckling in the plastic hinge region does not occur (see Chapter 8.3).

An amount of reinforcement must be provided to comply with codified criteria, somewhere between the maximum and minimum allowable limits. It will be shown in Chapter 7.5 that the amount of reinforcement chosen in this step does not affect the outcome of the study.

2. The axial load at the base of the wall is known, and thus the **moment capacity** can be determined using either the design equations (see Chapter 8.4.1) or a moment curvature analysis (see Chapter 7). The moment capacity calculated using the design equations (M'_n) corresponds to characteristic material strengths, while the nominal yield moment (M_n) obtained from moment-curvature analysis corresponds to mean material strengths (see Chapter 6).
3. The purpose of this step is to **calculate the floor masses** m_1 and m_2 corresponding to the two period calculation methods described in Chapter 4.4.

3.1. Method 1

3.1.1 The fundamental period (T_1) is calculated using Eq. 4.1.

3.1.2 The design pseudo acceleration (a_1) is obtained from the design spectrum.

3.1.3 The floor mass m_1 should be of such a magnitude that the resulting base moment is slightly less than the nominal yield moment (M'_n) obtained from the design equations. This is to take the additional strength due to reinforcement choice into consideration (see the discussion on overstrength in Chapter 2.1.7).

3.1.4 A better estimate of the fundamental period at which the wall would respond ($T_{1(real)}$) is obtained by means of an eigenvalue analysis based on the cracked sectional stiffness obtained from the moment-curvature analysis.

3.2. Method 2

3.2.1 This step starts by assuming a value for T_2 . A good estimate is $T_{1(real)}$, obtained in the previous step.

3.2.2 The design acceleration demand (a_2) is obtained from the design spectrum.

3.2.3 Similar to 3.1.3 above, the floor mass m_2 can be obtained.

3.2.4 A new estimate of T_2 is calculated using an eigenvalue analysis. Iteration, such as shown in Figure 4.5, is required until the value of m_2 does not change significantly between two iterations.

4. The purpose of this step is to estimate the **ductility demand according to the equal displacement and equal energy principles** (see Chapter 2.1.6). For this purpose the MDOF wall is converted into an equivalent SDOF wall.
 - 4.1. Firstly, the properties of the equivalent SDOF system need to be calculated. This includes the equivalent SDOF height h^* and the effective first modal masses m_1^* and

- m_2^* . The equivalent height is obtained from Eq. 9.23, while the effective first modal masses may be obtained from finite element modal analyses.
- 4.2. The shear (V_n) corresponding to nominal yield moment can be calculated from the nominal yield moment (M_n) obtained from moment-curvature analysis.
 - 4.3. For both methods the acceleration ($a_{1(real)}^+$, a_2^+) corresponding to the yield shear can be calculated.
 - 4.4. The elastic acceleration demand (A_1 and A_2) can be calculated from the elastic pseudo acceleration spectrum.
 - 4.5. The force reduction factors (R_1 and R_2) are calculated as the ratio between elastic demand (A_1 and A_2) and yield capacity ($a_{1(real)}^+$ and a_2^+). Refer to Chapter 2.1.5 for the definition of the force reduction factor.
 - 4.6. The ductility demand can now be calculated as a function of the force reduction factor according to the R- μ -T relationship presented in Eq. 2.15.
 5. The **ductility capacity based on code drift limits** can be determined as set out in Chapter 9.3.1 and 9.3.2.
 6. Compare the ductility demand and capacity.
 - 6.1. If the demand is greater than the capacity, choose a lower behaviour factor and repeat from step 3.
 - 6.2. If the demand is less than the capacity, the ductility demand needs to be **verified by means of ITHA**. ITHA is discussed in Chapter 10. The calculation of ductility demand from ITHA results is discussed in Chapter 9.4. If the ductility demand is found to be less than the ductility capacity the current behaviour factor is adequate. The current behaviour factor value ($q = 5$) is higher than most behaviour factor values in other codes. Refer to Priestley *et al.* (2007, p. 13) for a comparison between international seismic codes. Hence, it is not the intention of the code committee to suggest the use of an even higher value.

6. Material properties

In this chapter the material properties of the concrete and steel used in this study are discussed. Material strengths are discussed in 6.1, while material stress-strain models, used in moment-curvature analyses, are discussed in 6.2.

6.1 Material strengths

SANS 10160-1 (2009, p. 36) states that if sufficient ductility for structural resistance can be provided the partial material factors should be taken as 1.0. Paulay & Priestley (1992, p.362) state that if special detailing measures are adopted, reliable ductile response can be achieved for reinforced concrete structural walls. This is confirmed by Dazio, Beyer & Bachmann (2009). Such special detailing measures are included in SANS 10160-4 (2009) and are explained in more detail in Chapter 8.3. Thus, since sufficient ductility can be provided by designing walls in accordance with SANS 10160-4 (2009), characteristic material strengths should be used for design.

For this study all concrete has a characteristic cylinder strength of 25 MPa and a characteristic cube strength of 30 MPa. The design equations, derived in Chapter 8.4.1 which are used for the design of the walls, are based on concrete cube strength. The moment-curvature analysis, however, uses the concrete cylinder strength. The characteristic yield strength of steel was taken as 450 MPa.

In order to predict the most likely strength and stiffness of a wall cross section it is necessary to use the mean material strengths. Therefore, mean material strengths are used for moment-curvature analysis (refer to Chapter 7). Characteristic strengths are used only in the design of the walls (refer to Chapter 8).

For steel the mean yield strength is obtained by multiplying the characteristic yield strength by 1.1 (Mirza & MacGregor, 1979). For concrete the mean compressive strength is obtained by adding 8 MPa and 9 MPa to the characteristic compressive cylinder and cube strengths respectively (SIA 262, 2004, p.25). The 9 MPa increment in cube strength corresponds to a standard deviation of 5.5 MPa which corresponds to an average degree of quality control according to the Cement and Concrete Institute (1998). The material strengths are summarized in Table 6.1.

Table 6.1: Material strengths

| | Concrete | | Reinforcement yield strength |
|-------------------------------|----------|----------|------------------------------|
| | Cube | Cylinder | |
| Characteristic strength [MPa] | 30 | 25 | 450 |
| Design strength [MPa] | 30 | 25 | 450 |
| Mean strength [MPa] | 39 | 33 | 495 |

6.2 Stress-strain curves

6.2.1 Concrete

Mander’s stress-strain relationship is used for unconfined and confined concrete (Mander, Priestley & Park, 1988, pp.1807-1808). Both stress-strain curves are shown in Figure 6.1.

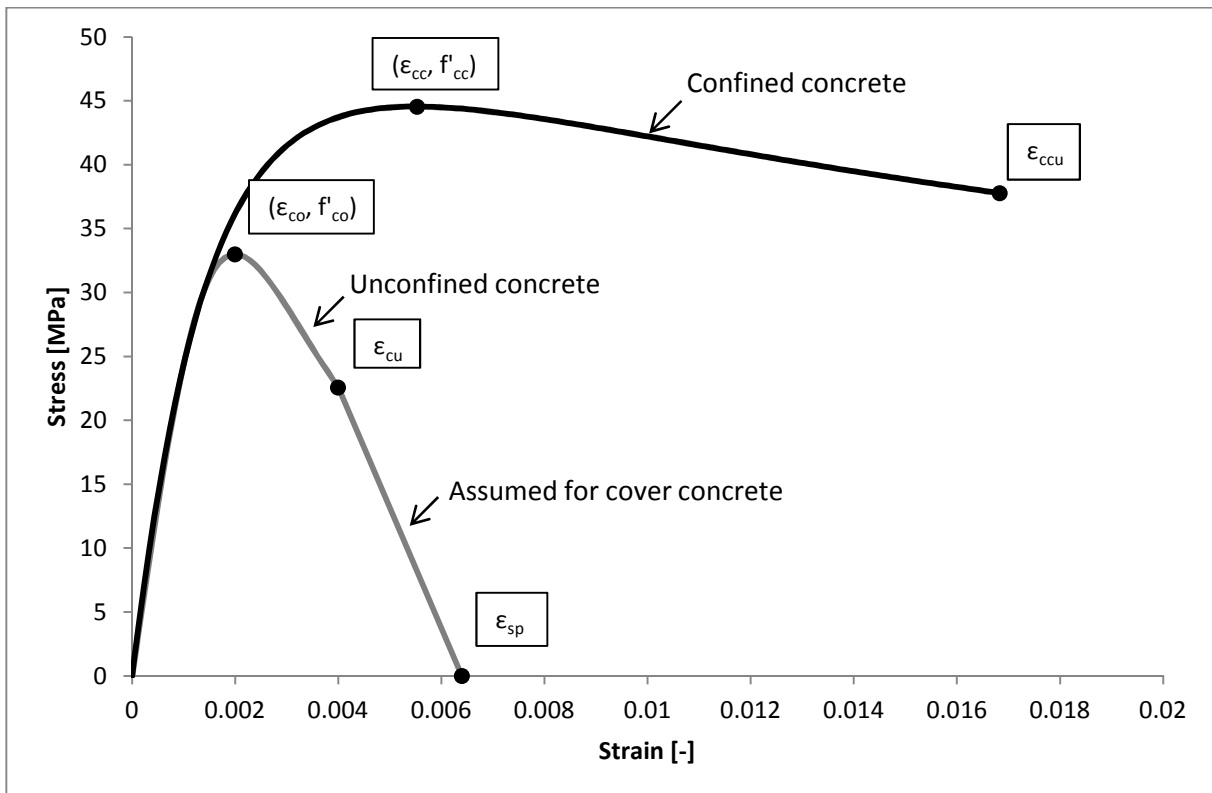


Figure 6.1: Mander’s stress-strain relationship for concrete

6.2.1.1 Unconfined concrete

The stress-strain relationship for unconfined concrete is defined by Eq. 6.1:

$$f_c = \frac{f'_{co} x^r}{r-1+x^r} \tag{6.1}$$

where

f_c is the concrete stress,
 f'_{co} is the cylinder strength, and

$$x = \frac{\varepsilon_c}{\varepsilon_{co}} \quad \dots\dots\dots 6.2$$

where

ε_c is the concrete strain,
 $\varepsilon_{co} = 0.002$ is the strain at peak stress, and

$$r = \frac{E_c}{E_c - E_{sec}} \quad \dots\dots\dots 6.3$$

where

$E_c = 4700\sqrt{f'_{co}}$ is the modulus of elasticity of the unconfined concrete (Paulay & Priestley, 1992, p.96), and

$$E_{sec} = \frac{f'_{co}}{\varepsilon_{co}} \quad \dots\dots\dots 6.4$$

The value for the ultimate strain ε_{cu} according to SABS 0100-1 (2000) is 0.0035. However, this value is based on experiments where concrete is subjected to uniform compression or constant moment. Critical regions of concrete members under seismic loading are usually subjected to significant moment gradients. Experiments on such elements have shown that crushing of concrete occurs only at strains well in excess of 0.003 and sometimes as high as 0.006 to 0.008 (Paulay & Priestley, 1992, p.98). Paulay & Priestley (1992, p.98) recommend a conservative value of 0.004 be used for ε_{cu} .

In order to model the spalling of cover concrete realistically the stress is assumed to decrease linearly with strain from the ultimate strain ε_{cu} to the spalling strain ε_{sp} . The value of the spalling strain was assumed to be 0.0064 in accordance with the default values of the moment-curvature analysis program CUMBIA (Montejo & Kowalsky, 2007).

6.2.1.2 Confined concrete

The strength and ultimate strain of ordinary concrete may be significantly increased by using confining transverse reinforcement. This is typically done in the boundary regions of structural wall cross sections. This is discussed in Chapter 8.3.

The stress-strain equations used for confined concrete are exactly the same as that of unconfined concrete. However, the peak stress, strain at peak stress, and ultimate strain have higher values. The confined concrete strength is directly related to the effective confining stress that can be developed at the yield of confining reinforcement, which is given by

$$f'_{l1} = K_e \rho_1 f_{yh} \quad \dots\dots\dots 6.5$$

$$f'_{l2} = K_e \rho_2 f_{yh} \quad \dots\dots\dots 6.6$$

where

K_e is a confinement effectiveness coefficient, which according to Paulay & Priestley (1992, p.102) is typically 0.6 for rectangular wall sections,

$f_{yh} = 450 \text{ MPa}$ is the yield strength of the confining reinforcement, and

ρ_1 and ρ_2 are the volumetric ratios of confining material, defined in Eqs. 6.7 and 6.8 and Figure 6.2.

$$\rho_1 = \frac{A_{sh1}}{h_1 s_h} \quad \dots\dots\dots 6.7$$

$$\rho_2 = \frac{A_{sh2}}{h_2 s_h} \quad \dots\dots\dots 6.8$$

where s_h is the vertical spacing of the confining reinforcement.

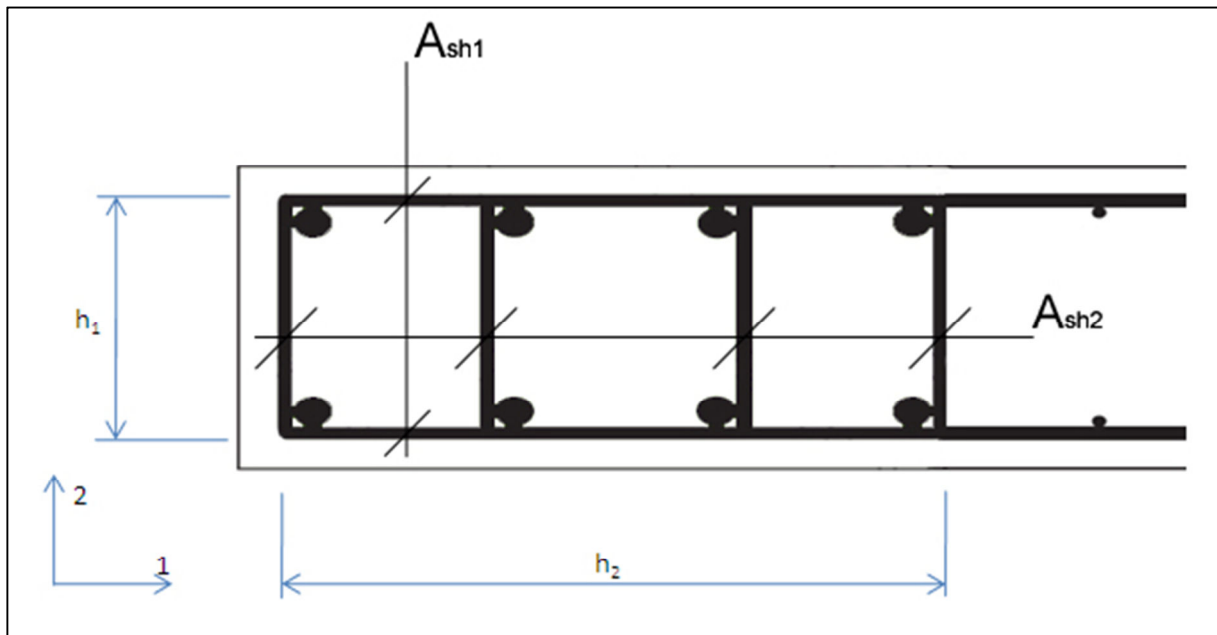


Figure 6.2: Confinement in a wall boundary element

With the confining stresses known the confined concrete strength can be read from Figure 6.3. Note that the labels f'_{l1} and f'_{l2} in Figure 6.3 are the smallest and largest confining stresses respectively and therefore do not necessarily coincide with those in Eqs. 6.5 and 6.6.

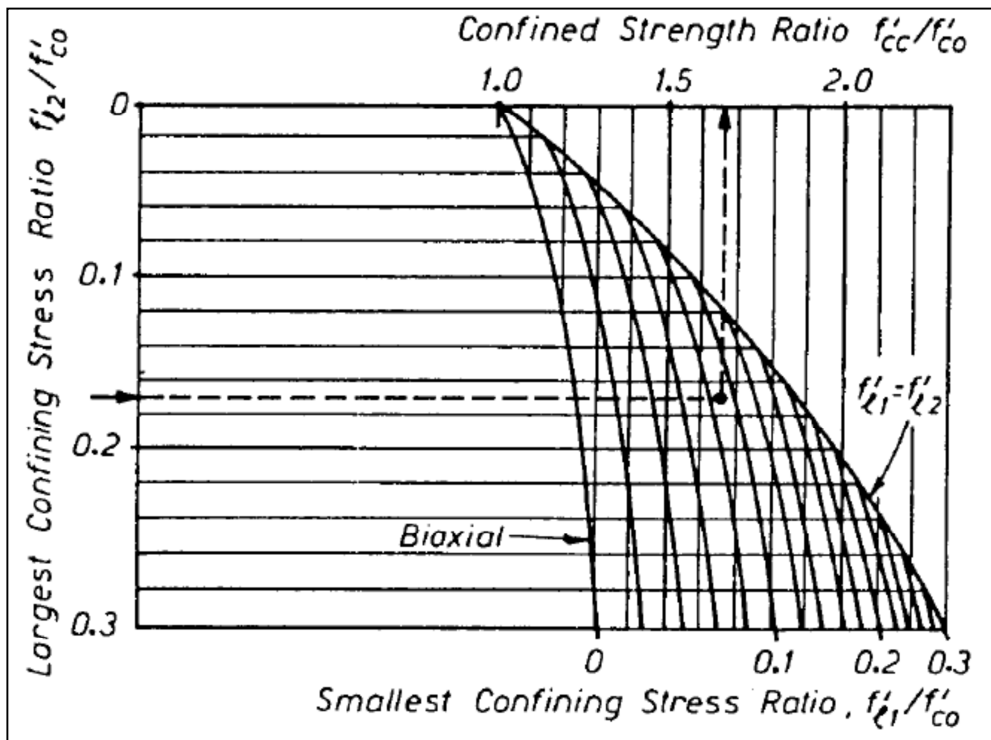


Figure 6.3: Confined strength determination from lateral confining stresses for rectangular sections (Mander *et al.*, 1988, p. 1813)

The strain at peak stress may be obtained from Eq. 6.9 (Mander *et al.*, 1988, p. 1807):

$$\varepsilon_{cc} = 0.002 \left[1 + 5 \left(\frac{f'_{cc}}{f'_{co}} - 1 \right) \right] \quad \dots\dots\dots 6.9$$

The ultimate strain of the confined concrete is defined as the point where the confining reinforcement fractures. This point is determined by equating the strain energy capacity of the confining reinforcement at fracture to the energy absorbed by the confined concrete. Paulay & Priestley (1992, p.103) propose the following conservative estimate:

$$\varepsilon_{ccu} = 0.004 + \frac{1.4\rho_s f_y h \varepsilon_{sm}}{f'_{cc}} \quad \dots\dots\dots 6.10$$

where

$$\rho_s = \rho_1 + \rho_2 \quad \dots\dots\dots 6.11$$

where ρ_1 and ρ_2 are defined in Eqs. 6.7 and 6.8, and ε_{sm} is the strain at peak stress of the confining reinforcement.

The stress-strain relationship of confined concrete is defined by Eqs. 6.12 to 6.15.

$$f_c = \frac{f'_{cc} x^r}{r-1+x^r} \quad \dots\dots\dots 6.12$$

where

f_c is the concrete stress,

f'_{cc} is obtained from Figure 6.3, and

$$x = \frac{\varepsilon_c}{\varepsilon_{cc}} \quad \dots\dots\dots 6.13$$

where

ε_c is the concrete strain,

ε_{cc} is the strain at peak stress defined in Eq. 6.9, and

$$r = \frac{E_{cc}}{E_{cc} - E_{sec}} \quad \dots\dots\dots 6.14$$

where

$E_{cc} = 4700\sqrt{f'_{cc}}$ is the modulus of elasticity of the confined concrete (Paulay & Priestley, 1992, p.96), and

$$E_{sec} = \frac{f'_{cc}}{\epsilon_{cc}} \quad \dots\dots\dots 6.15$$

6.2.2 Reinforcing steel

According to SIA 262 (2004) reinforcing steel used for seismic application should have a minimum strain at peak stress ϵ_{sm} of 7.5 % and a strain-hardening ratio f_u/f_y of between 1.15 and 1.35 (See Figure 6.4). SANS 920 (2005) specifies a minimum elongation of 14 %, presumably referring to the ultimate fracture strain ϵ_{su} , and also a minimum strain-hardening ratio of 1.15.

The purpose for the limit on ϵ_{sm} is to ensure that premature fracture of reinforcement does not occur. Dazio *et al.* (2009) showed that walls built using steel with $\epsilon_{sm} > 7.5\%$ performed very well under cyclic loading tests. The hardening ratio should be greater than 1.15 to ensure sufficient spread of inelastic deformations over the wall height in the plastic zone (refer to Chapter 8.3). A wall built using steel with a low hardening ratio would form a horizontal crack at the base. Since very little hardening takes place, all inelastic deformations would be concentrated at this crack, reducing the ductility capacity of the wall (Dazio *et al.*, 2009). A hardening ratio of greater than 1.35 on the other hand might cause the plastic zone to spread to higher parts of the wall not specifically designed for inelastic deformation.

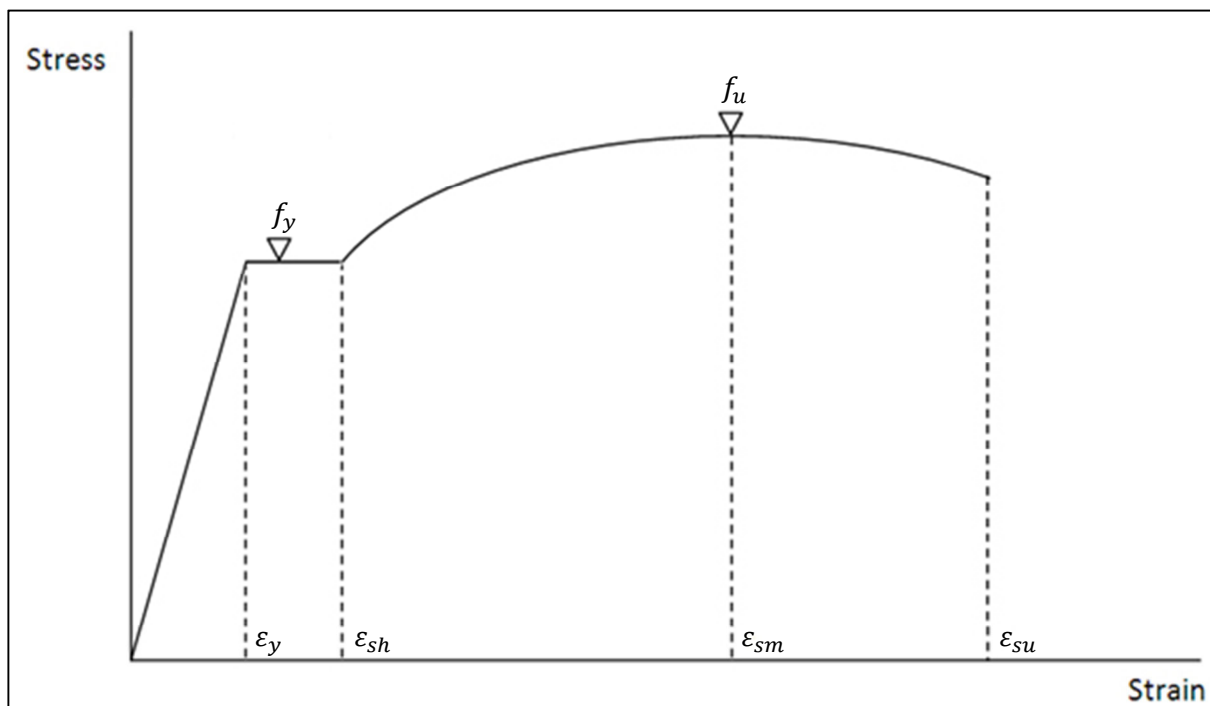


Figure 6.4: Stress-strain relationship for reinforcing steel

For the purpose of this study it was necessary to determine if South African steel conforms to the above mentioned requirements. Within the scope of this study only a small number of tests were carried out on Y10 and Y16 bars. Three of the Y10 bars and the Y16 bars came from the same batch. A fourth Y10 bar was taken from a second batch. The results of the tests are summarized in Table 6.2 and may be seen in Figure 6.5. The last column in Table 6.2 lists the mean material properties assumed for the material model used for moment-curvature analyses.

Table 6.2: Reinforcement experimental results

| Bar diameter | 10 mm | | | | 16 mm | | | | Chosen material model |
|---|-------|------|------|------|-------|------|------|------|-----------------------|
| Batch no. | 1 | | 2 | 1 | | | | | |
| Yield stress f_y [MPa] | 540 | 556 | 550 | 520 | 494 | 498 | 496 | 498 | 495 |
| Peak stress f_u [MPa] | 630 | 643 | 643 | 719 | 658 | 659 | 659 | 659 | 569 |
| Hardening ratio f_u/f_y | 1.17 | 1.16 | 1.17 | 1.38 | 1.33 | 1.32 | 1.33 | 1.32 | 1.15 |
| Strain at peak stress ϵ_{sm} [%] | 8.4 | 8.4 | 9.3 | 12.6 | 11.6 | 12.3 | 12.2 | 12.6 | 7.5 |
| Ultimate strain ϵ_{su} [%] | 9.0 | 9.0 | 9.9 | 15.9 | 17.8 | 18.1 | 17.9 | 15.3 | 7.5 |

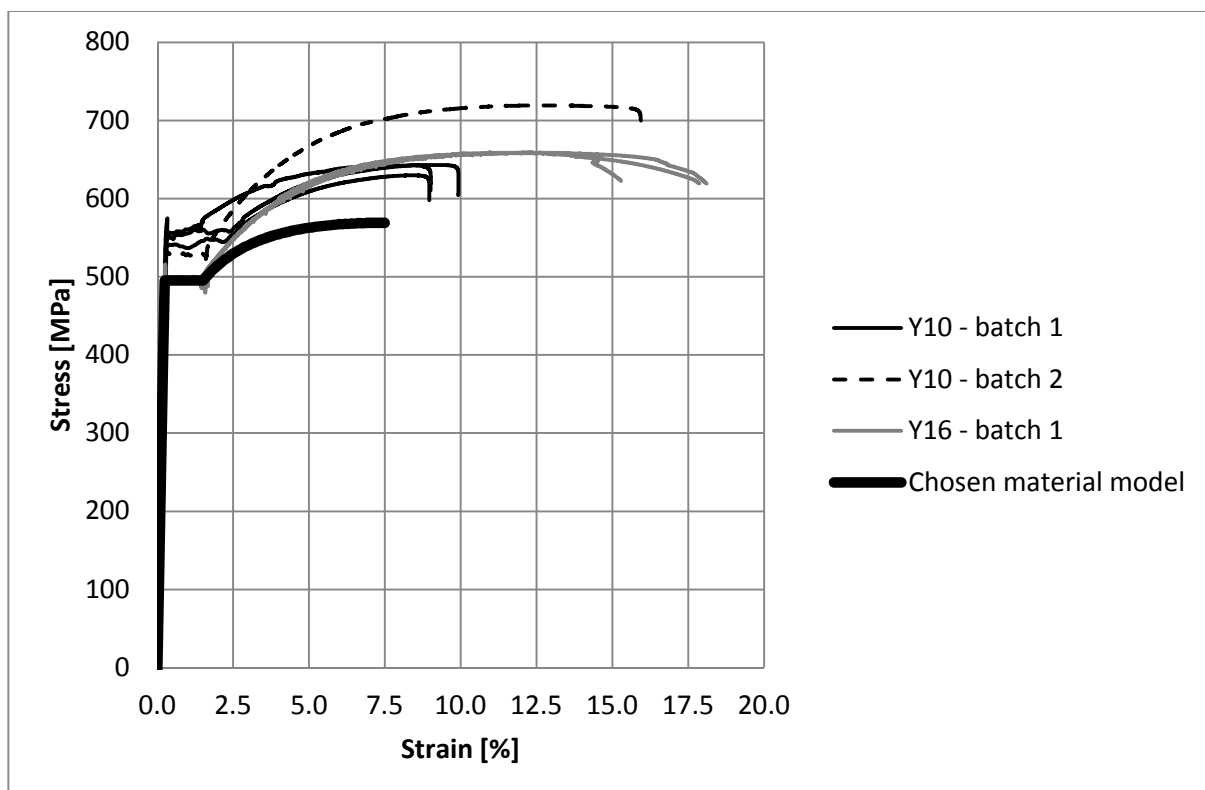


Figure 6.5: Experimental stress-strain curves of reinforcing steel

It has already been stated that the mean yield strength is 495 MPa (Refer to Table 6.1). Judging from the experimental results it would seem safe (and conservative) to assume a

hardening ratio of 1.15, resulting in a peak stress of 569 MPa. All test specimens have a strain at peak stress of more than 7.5%, and thus this would seem to be a conservative, yet large enough value to assume for the material model. The downward sloping tail of the stress-strain curve is unreliable and could thus be ignored. Thus $\varepsilon_{sm} = \varepsilon_{su} = 7.5\%$. The modulus of elasticity is 200 GPa, resulting in a yield strain of 0.2475%. The strain at which strain hardening starts was chosen as 1.5%.

The stress-strain relationship equations used for the steel material model are taken from Priestley *et al.* (2007, p.140):

$$\text{Elastic:} \quad f_s = E_s \varepsilon_s \quad \varepsilon_s \leq \varepsilon_y \quad \dots\dots\dots 6.16$$

$$\text{Yield plateau:} \quad f_s = f_y \quad \varepsilon_y < \varepsilon_s \leq \varepsilon_{sh} \quad \dots\dots\dots 6.17$$

$$\text{Strain hardening:} \quad f_s = f_u - (f_u - f_y) \left(\frac{\varepsilon_{su} - \varepsilon_s}{\varepsilon_{su} - \varepsilon_{sh}} \right)^2 \quad \varepsilon_{sh} < \varepsilon_s \leq \varepsilon_{su} \quad \dots\dots\dots 6.18$$

This chapter has defined the material properties of the concrete and steel used in the design and analysis of the eight walls of this study. It was seen that characteristic material strengths should be used for design, while mean material strengths should be used in analysis so as to predict the most likely response of a structure. It was stated that concrete cube strength is used in design, while concrete cylinder strength is used in moment-curvature analysis. The stress-strain curves for concrete and steel material models were defined. These will be implemented in moment-curvature analysis, which is the topic of the next chapter.

7. Moment-curvature analysis

This chapter summarises the calculation steps which are followed in the MATLAB code developed for this study. Although various moment-curvature analysis programs are readily available, they are not necessarily sufficient for the analysis of structural wall cross-sections. Cumbia (Montejo & Kowalski, 2007) which was developed for the analysis of columns and beams does not allow the definition of unconfined concrete in the web region of the wall. Another program which was considered is Response-2000 (Bentz & Collins, 2009). While this is a very good program, obtaining the output required for the bilinear approximation is a rather tedious process. For these reasons it was decided to develop a custom MATLAB code for this study.

The material models derived in Chapter 6 are implemented to obtain moment-curvature relationships. The derivation of a bilinear approximation to the moment-curvature curve is also discussed. The moment-curvature results of the eight walls of this study are presented, and based on these results a number of factors which would not influence the outcome of this study are identified.

7.1 Section discretization

The discretization of the cross section is illustrated in Figure 7.1. The cross section is divided into a number of concrete layers. Each layer is assigned either a confined or an unconfined concrete material model. The appropriate reinforcement area is subtracted at the correct coordinates. Reinforcement bars, to which the steel material model is assigned, are added to the concrete layers.

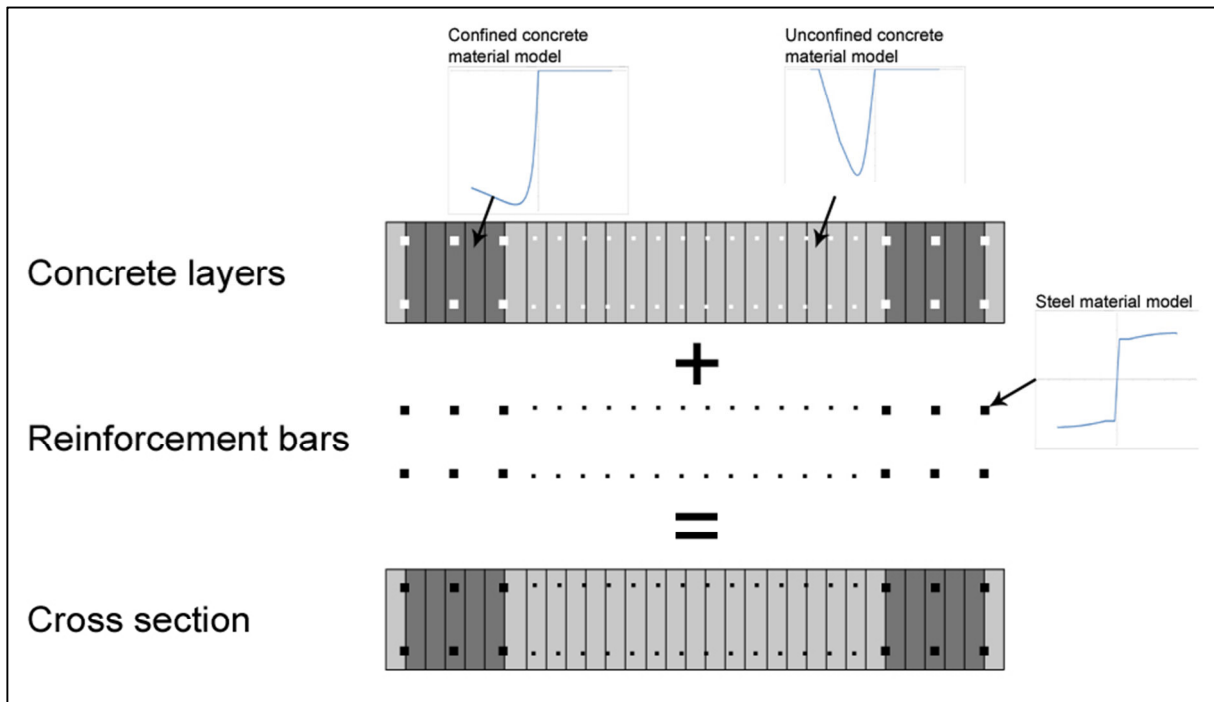


Figure 7.1: Discretization of section

7.2 Calculation steps

The calculation process starts at zero moment and curvature. Moment is calculated as a function of curvature, which is a discrete variable ($\phi = 0, \Delta\phi, 2\Delta\phi, \dots$). The curvature increment, $\Delta\phi$, is supplied by the user as an input variable. The (compressive) axial load must be resisted by the concrete layers and reinforcement bars. The following steps are followed:

1. Calculate the strain across the section which corresponds to the current curvature value and neutral axis position.
2. For each concrete layer and reinforcement bar obtain from the material model the stress corresponding to the strain in that layer or bar.
3. Calculate the force in each concrete layer and steel bar by multiplying the stress with the area of the layer or bar.
4. Compare the axial load value to the total force in the concrete layers and reinforcement bars.
 - a. If equilibrium is satisfied,
 - i. calculate the bending moment. For the first time this step is reached the calculated bending moment should be zero, since the curvature is zero.
 - ii. Increase the curvature by $\Delta\phi$.
 - iii. Return to step 1.

- b. If not,
 - i. reposition the curvature profile by a predetermined amount in an attempt to obtain equilibrium and
 - ii. return to step 1. (Iteration through steps 1 to 4 will be necessary. Continue until force equilibrium is satisfied).

By repeating these steps a set of curvature versus moment values are obtained. The calculations are stopped when either the outermost reinforcement bar or the outermost confined concrete layer reaches its ultimate strain. Figure 7.2 shows a screenshot of the program output for the single storey wall W013 with an axial load of 675 kN.

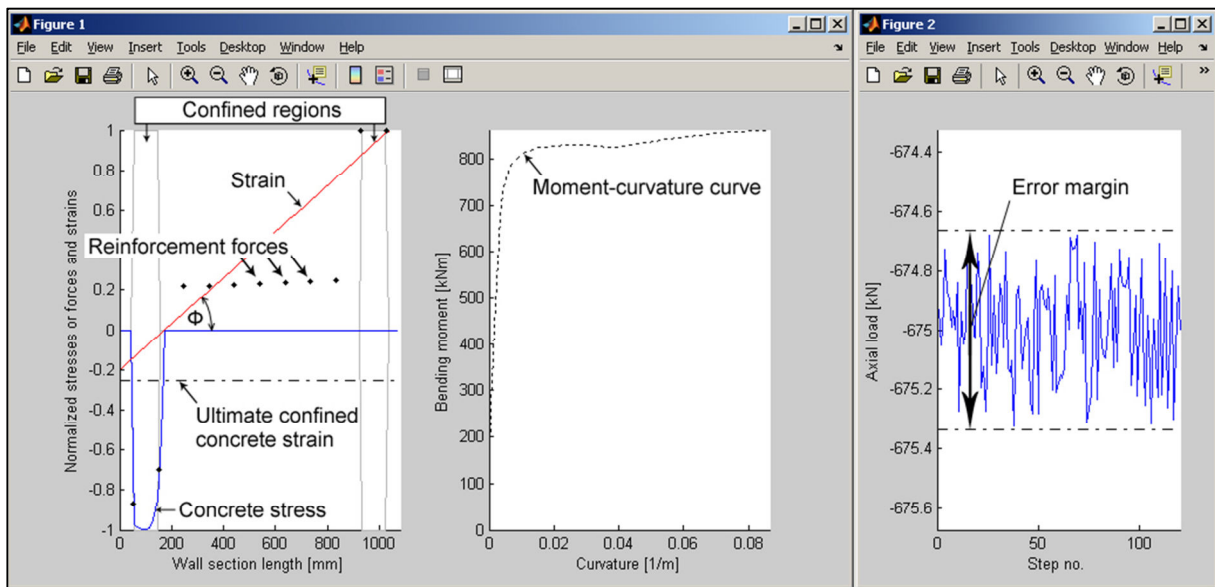


Figure 7.2: MATLAB moment-curvature program screenshot

7.3 Bilinear approximation to the moment-curvature curve

In order to use the moment-curvature results it is necessary to fit a bilinear approximation to the moment-curvature curve. This is done in the following way (Priestley *et al.*, 2007, p.144):

- The point where the outermost reinforcement bar yields in tension defines the “First yield” point with coordinates (ϕ'_y, M'_y) (See Figure 7.3).
- The first instance that the strain in the outermost concrete layer is greater than 0.004 (spalling of cover concrete) or the strain in the outermost reinforcement bar is greater than 0.015 (start of strain hardening) defines the nominal moment M_n .
- The nominal yield curvature is found by extrapolation of the first yield point:

$$\phi_y = \phi'_y \frac{M_n}{M'_y} \dots\dots\dots 7.1$$

- The ultimate point is defined as the point where either the outermost reinforcement bar or the outermost confined concrete layer reaches its ultimate strain.
- The bilinear approximation is found by connecting a line from the origin through the nominal yield point to the ultimate point as shown in Figure 7.3.

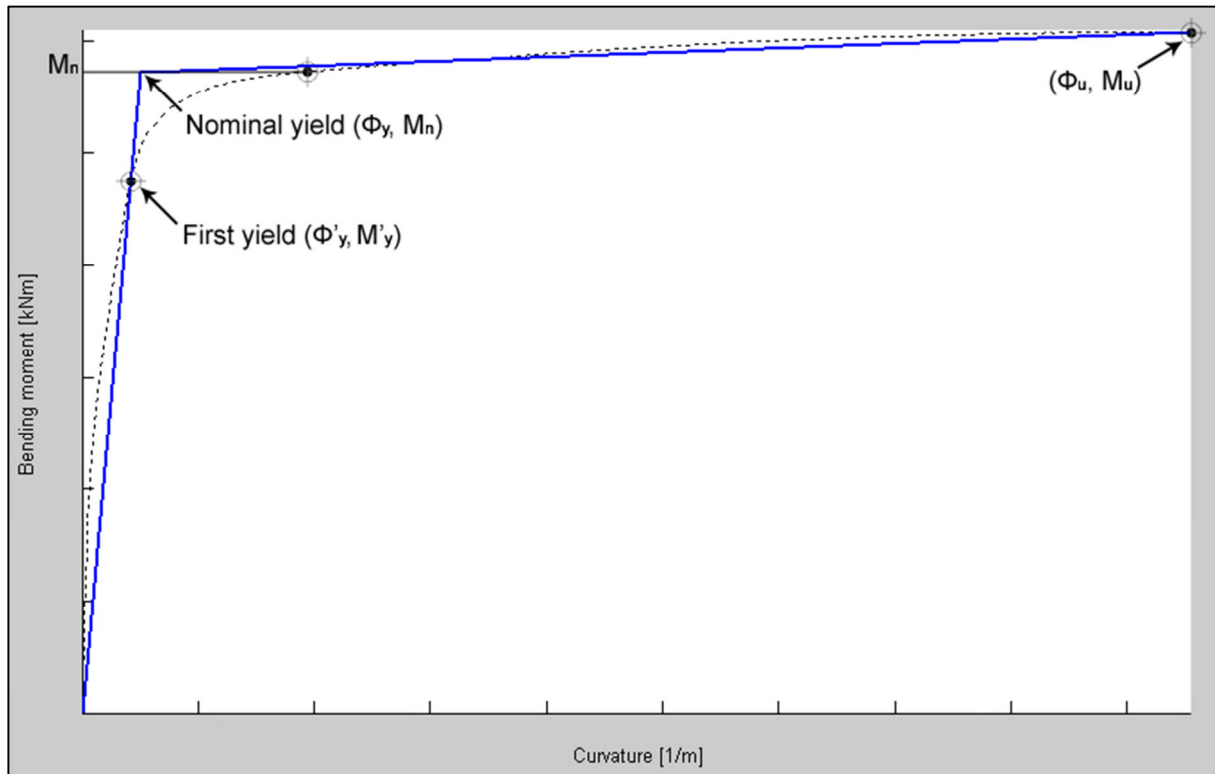


Figure 7.3: Bilinear approximation to moment curvature curve

7.4 Moment-curvature results

The moment-curvature results of the eight walls of this study, introduced in Chapter 4.5, are presented here. Figure 7.4 shows the bilinear approximations of the moment-curvature curves. In Chapter 8.4.1 design equations will be introduced, by which the bending moment capacity of a section can be estimated. These calculated capacities are also shown in Figure 7.4 to the right of each bilinear curve. It can be seen that good correlation exists between moment-curvature curves and the design equation results.

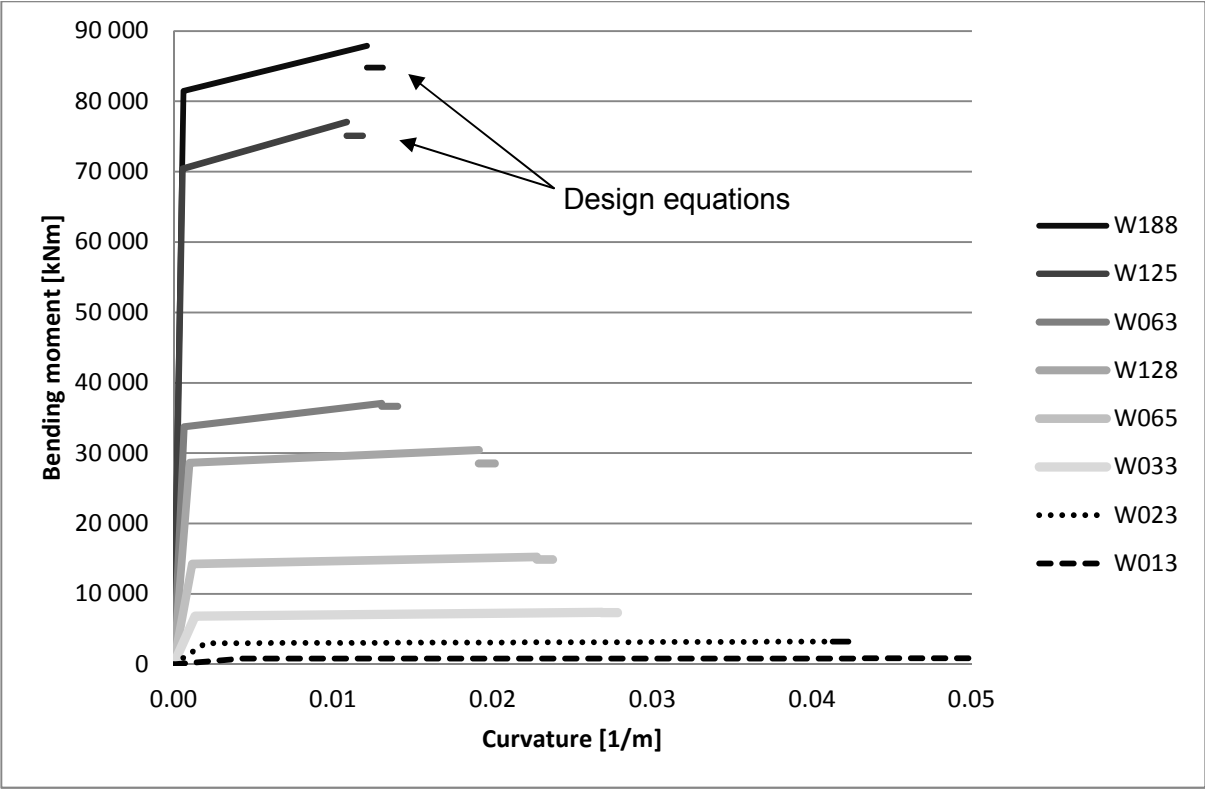


Figure 7.4: Bilinear moment-curvature results

It was stated in Chapter 2.1.7 that “the yield curvature is essentially independent of strength, for a given section...”(Priestley *et al.*, 2007, p. 9). Priestley *et al.* (2007, p. 158) have found that the yield curvature may be represented by:

$$\phi_y = \frac{2\varepsilon_y}{l_w} \dots\dots\dots 7.2$$

where $\varepsilon_y = 0.00225$ is the yield strain of the longitudinal reinforcement, and l_w is the length of the wall section

Figure 7.5 shows the values of the yield curvature obtained for the eight walls of this study. It can be seen that the results correspond to Eq. 7.2.

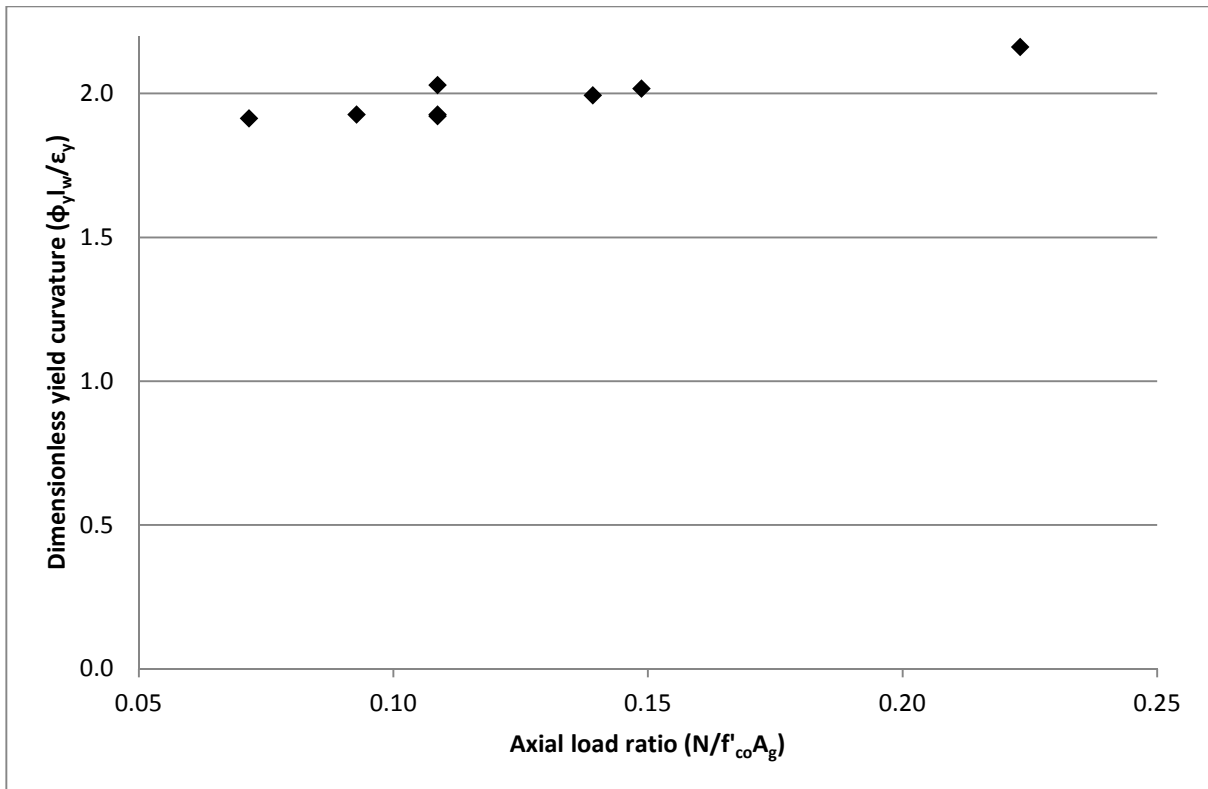


Figure 7.5: Dimensionless yield curvature as a function of axial load ratio

The interrelation of strength and stiffness is shown in Figure 7.6 and Figure 7.7. Figure 7.6 shows the bilinear moment curvature curves of wall W063 with varying reinforcement ratio. Figure 7.7 shows the bilinear moment-curvature curves of wall W063 with varying axial load. In both figures it can clearly be seen that the yield curvature is relatively independent of strength and that strength and stiffness are interrelated.

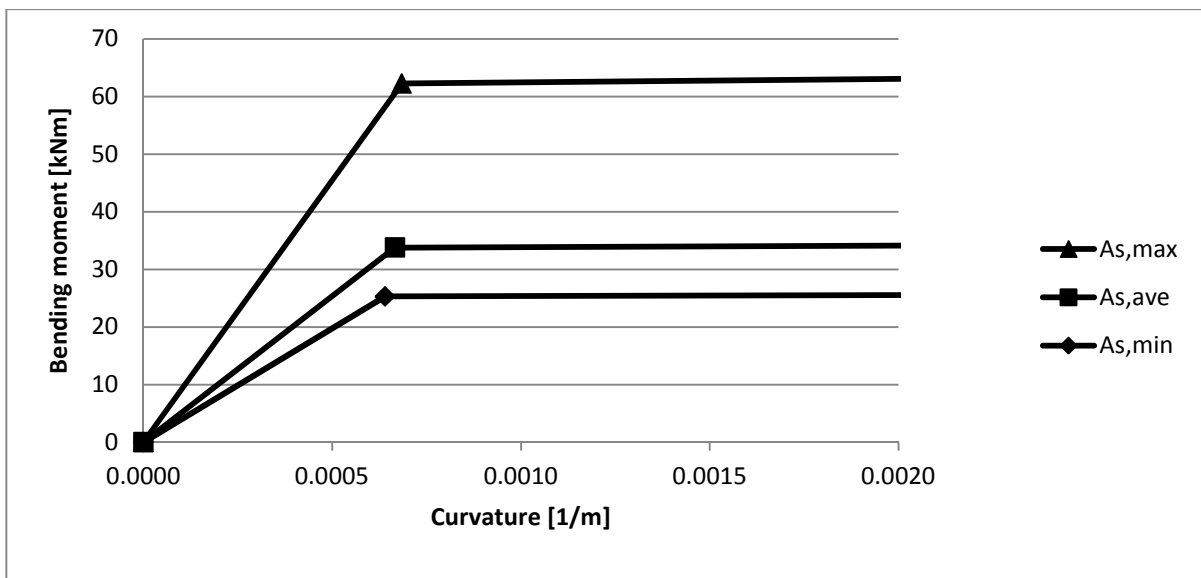


Figure 7.6: Influence of reinforcement content on strength and stiffness

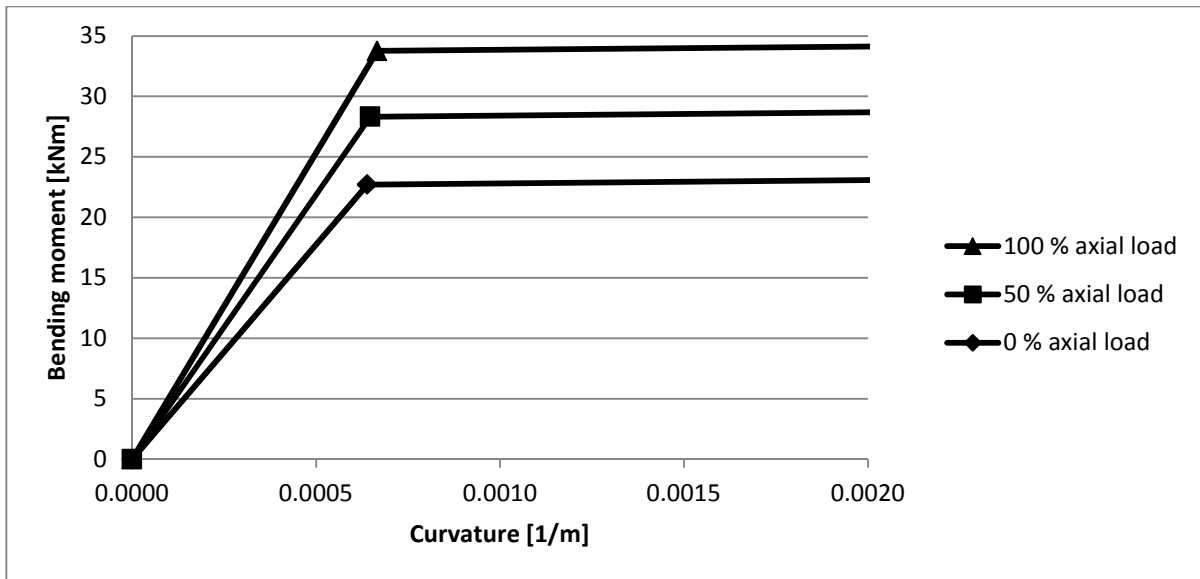


Figure 7.7: Influence of axial load on strength and stiffness

7.5 Parameters which would not influence the outcome of this study

Bearing in mind the aforementioned interrelation of strength and stiffness, it is of interest to identify parameters which would affect the outcome of this study. Ductility capacity is related to a fixed drift limit, and is therefore constant. Ductility demand, on the other hand, is related to the period of the structure (T) and the force reduction factor (R), as described by the R-μ-T relationship of Eq. 2.15. Since the behaviour factor is constant, and therefore also the force reduction factor, only parameters that could influence the fundamental period need to be investigated. The following parameters may at first glance appear to influence the fundamental period:

- The reinforcement content of the wall section
- The axial load on the section
- The width of the wall section (b_w)
- Material strengths

All four of these parameters would influence the stiffness, and therefore also the strength, of the cross section. With reference to step 3.1 and 3.2 of the methodology, the floor masses (m_1 and m_2) are directly related to the moment capacity of the cross section (M'_n). Since all the above mentioned parameters would influence the stiffness and strength in equal proportions, they would also influence the stiffness and mass in equal proportions. The fundamental period is related to the stiffness and mass of a system according to the familiar equation:

$$T = 2\pi\sqrt{m^*/k^*} \dots\dots\dots 7.3$$

Thus it can be seen in Eq. 7.3 that any parameter which influences the stiffness and mass in equal proportions would not affect the fundamental period, and thus also not the ductility demand. The four above mentioned parameters are therefore not included in the scope of this study. Parameters that would influence the fundamental period are included in the scope of this study and were discussed in Chapter 4.

Thus, in this chapter we have seen an algorithm that could be used for moment-curvature analysis. The derivation of the bilinear moment-curvature approximation was introduced. This bilinear moment-curvature results are used in the design of the walls, as described in step 3.1.4 and 3.2.4 of the methodology (Chapter 5). It is also used in the assessment of the walls as described in step 4.2 of the methodology, and in defining the characteristics of the finite element members used in ITHA (see Chapter 10). Finally we saw how the interrelation of strength and stiffness proved that some parameters would not influence the outcome of this study.

8. Design

In this chapter all aspects of the design of structural walls required for this study are discussed. Firstly, the calculation of bending moment demand is discussed. The second section deals with capacity design, where a specific part of a structure is designed for inelastic action. The final part of this chapter discusses bending moment capacity. Design equations are derived for the calculation of bending moment capacity.

8.1 Equivalent static lateral force

According to SANS 10160-4 (2009, p. 23) buildings which are not significantly affected by higher modes of vibration may be designed according to the equivalent static lateral force procedure. Such buildings have the following characteristics (SANS 10160-4, 2009, p. 23):

- a) *The fundamental period of vibration $T_1 < 4T_c$ or $T_1 < 2$ seconds (refer to Table 2.1 for T_c and to Eq. 4.1 for T_1);*
- b) *All lateral load resisting systems (cores, walls, frames) run without interruption from their base to the top of the building, or if setbacks at different heights are present, to the top of the relevant zone of the building;*
- c) *Both lateral stiffness and the mass of the individual storeys remain constant or reduce gradually, without abrupt changes, from the base to the top;*
- d) *The sum of setbacks at any storey is less than 30% of the plan dimension at the first storey and less than 10% of the previous plan dimension and*
- e) *The plan layout of the building regarding the stiffness of the lateral force resisting elements, and the distribution of mass are approximately symmetric with respect to the two orthogonal directions and without significant discontinuities throughout the height of the building.*

All of the structural walls of this study, defined in Chapter 4, comply with these five requirements. According to SANS 10160-4 (2009, p. 24) the equivalent static lateral force is obtained from Eq. 8.1:

$$V_b = m_{tot} S_d(T) \quad \dots\dots\dots 8.1$$

where m_{tot} is the total mass of the structure, which is equal to the sum of the individual floor masses. For design purposes it is sufficiently accurate to ignore the weight of the structural wall itself.

$S_d(T)$ is the design pseudo acceleration defined in Eqs. 2.16 to 2.19.

Using the total mass of the structure in the calculation of the equivalent static lateral force is a contradiction of the assumption that higher modes do not significantly affect the structures mentioned above. If higher modes had no effect on the structure whatsoever, the equivalent static lateral force could be calculated according to:

$$V_b = m^* S_d(T) \quad \dots\dots\dots 8.2$$

where m^* is the effective first modal mass. See Chapter 9.2.1.

The total structural mass is used in Eq. 8.1 to account in some way for higher mode effects, since higher modes will always have some effect on any MDOF structure. This measure is however conservative, leading to additional strength. This additional strength becomes evident in the design results (see Figure 11.1 to Figure 11.4).

Figure 8.1 shows the ratio of the effective first modal mass (m^*) to the total mass (m_{tot}) as a function of the number of degrees of freedom for a MDOF cantilever beam. Bachmann, Dazio, Bruchez, Mittaz, Peruzzi & Tissières (2002, p. 132) obtained similar results. In Chapter 12 it will be seen that SANS 10160-4 (2009) assumes an average mass ratio of 0.7.

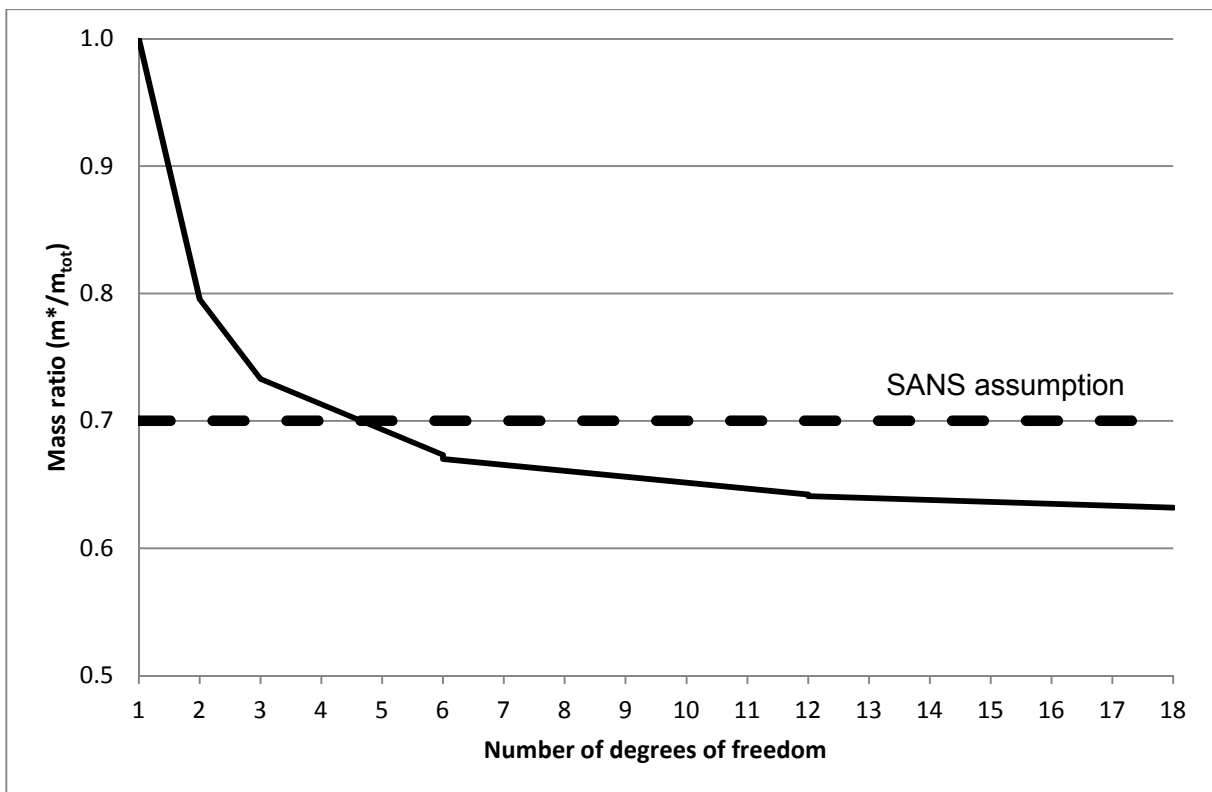


Figure 8.1: Mass ratio as a function of the number of degrees of freedom

8.2 Bending moment demand

To calculate the bending moment demand over the height of the wall it is necessary to distribute the total base shear along the height of the wall. According to SANS 10160-4 (2009, p. 25) the lateral seismic force F_j acting on a storey at level j should be calculated from the following equation:

$$F_j = \frac{W_j \times h_j}{\sum_{i=1}^n W_i \times h_i} \times V_b \quad \dots\dots\dots 8.3$$

where W_j, W_i is the weight assigned to level j and i respectively
 h_j, h_i is the height above the base to level j and i respectively
 i is the storey number
 n is the total number of storeys

It may be seen that for equal floor weights Eq. 8.3 results in a force distribution which varies linearly with height. The resulting bending moment demand is shown in Figure 8.3. The design bending moment, labelled “Design requirement”, takes higher mode effects and tension shift (see description below) into account. The higher mode effects are taken into account by changing the curved moment profile to a linear profile (Paulay & Priestley, 1992, p. 394).

Tension shift is discussed in detail in Paulay & Priestley (1992, pp. 155-156) and Park & Paulay (1975, pp. 304-307). It is briefly explained here with the aid of Figure 8.2.

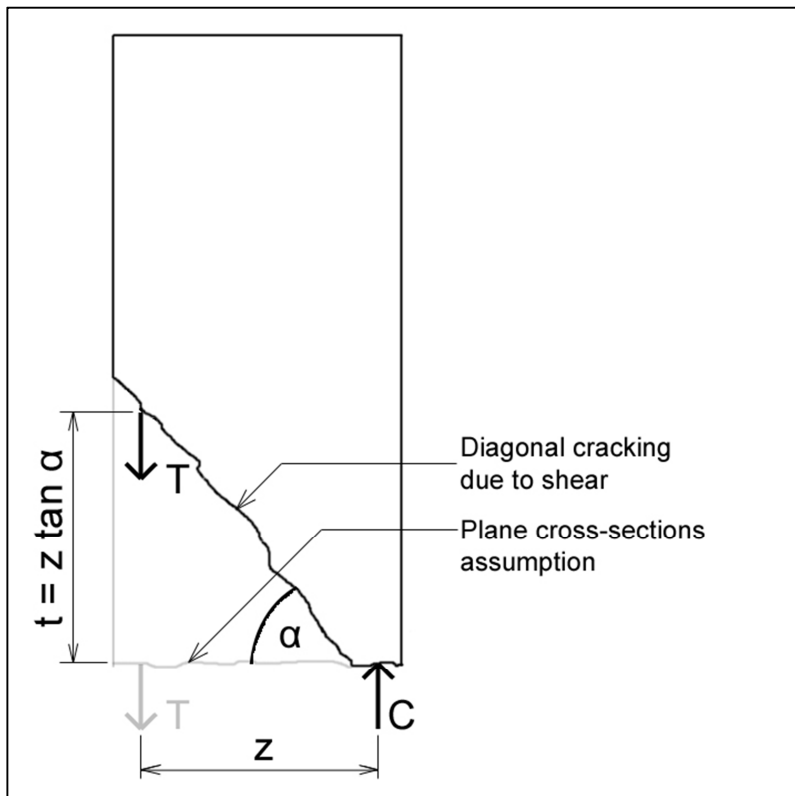


Figure 8.2: Tension shift

According to the assumption that plane cross-sections remain plane and normal to the neutral axis, the cracks which form in the wall should be horizontal as shown in Figure 8.2. Due to shear force the cracks are however inclined at an angle α and thus the tension force in the reinforcing steel occurs at a level $t = z \tan \alpha$ higher than predicted by the plane cross-sections assumption. Conservatively it may be assumed that $z = l_w$ and $\alpha = 45^\circ$, which results in $t = l_w$. Thus tension shift may be taken into account by lifting the linear moment profile by the wall section length (l_w) (Paulay & Priestley, 1992, p. 395) (see Figure 8.3).

The bending moment capacity of a wall with constant reinforcement content over the height of the wall is also shown in Figure 8.3. It can be seen that the capacity reduces as the axial load reduces. In tall walls the reinforcement content may gradually decrease with height so that the “capacity” matches the “design requirement” over the height of the wall.

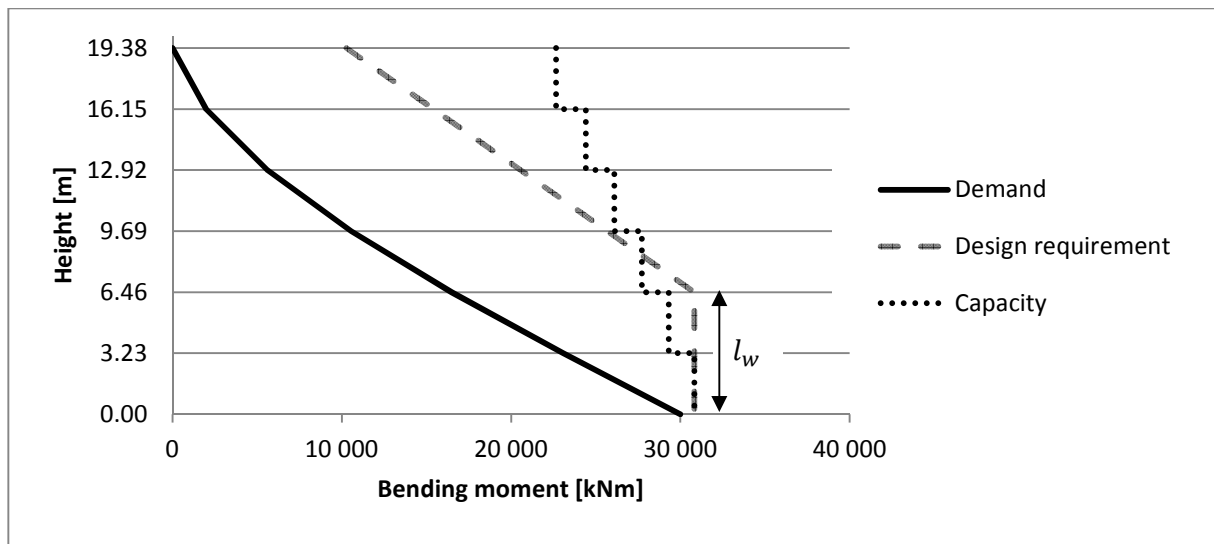


Figure 8.3: Bending moment demand and capacity

8.3 Capacity design

Once the bending moment demand is known it is necessary to capacity design the structural wall. In capacity design of structures specific structural members are chosen and detailed for energy dissipation. Critical regions of these members, called plastic hinges, are detailed for inelastic flexural action (Paulay & Priestley, 1992, pp. 39-39).

In structural wall buildings the only available members for capacity design are the structural walls themselves. The critical region of a structural wall is located at the base of the wall. The minimum plastic region length (h_{pl}) should comply with the following requirements (SANS 10160-4, 2009, p. 36):

1. $h_{pl} > l_w$
2. $h_{pl} > \frac{h_w}{6}$
3. If $h_s > 2l_w/3$ and $h_s > h_w/9$ are both complied with, then $h_{pl} = h_s$ may be assumed (see Figure 8.4)

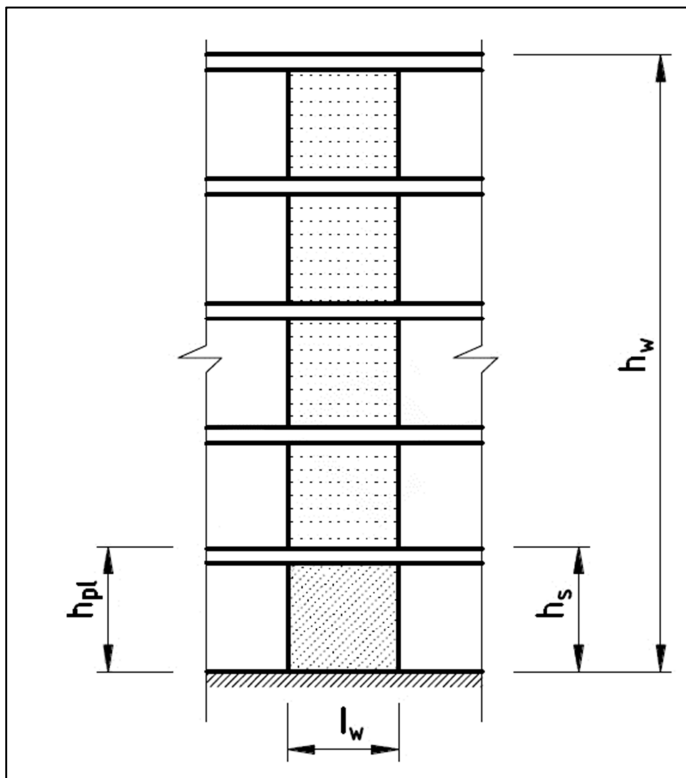


Figure 8.4: Height of plastic region (SANS 10160-4, 2009, p. 38)

The bending moment capacity is usually supplied by concentrating reinforcement in so-called boundary elements of the wall section (see Figure 8.5). In the plastic region confinement reinforcement should however be provided around the boundary elements to fulfil the following functions (Dazio & Beyer, 2009, p. 7-24):

1. Stabilize the longitudinal reinforcement
2. Confine the concrete in the boundary elements
3. Transfer shear

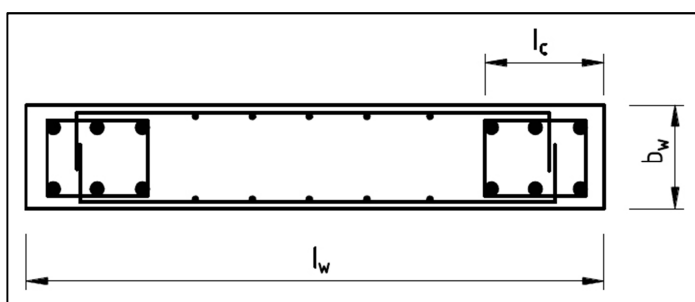


Figure 8.5: Reinforcement layout of structural wall section (SANS 10160-4, 2009, p. 38)

To fulfil these three functions the confining reinforcement should comply with the following requirements (SANS 10160-4, 2009, p. 37):

1. $A_{shi} > 0.077s_h h_i \frac{f_{cu}}{f_{yh}}$ 8.4
2. $s_h < 100 + \frac{350-h_x}{3}$ 8.5
3. $s_h < h_x/4$ 8.6
4. $s_h < 6 \times \text{longitudinal bar diameter}$ 8.7
5. $100 < s_h < 150 \text{ mm}$ 8.8

where A_{shi} and h_i are defined in Figure 6.2 (repeated here as Figure 8.6 for convenience) for $i = 1$ and 2.

s_h is the vertical spacing of the confining reinforcement

f_{cu} is the concrete characteristic cube strength

f_{yh} is the characteristic yield strength of the confining reinforcement

h_x is the maximum horizontal spacing of the legs of the confining reinforcement.

In the case of Figure 8.6 this would be the maximum of h_1 and $h_2/3$.

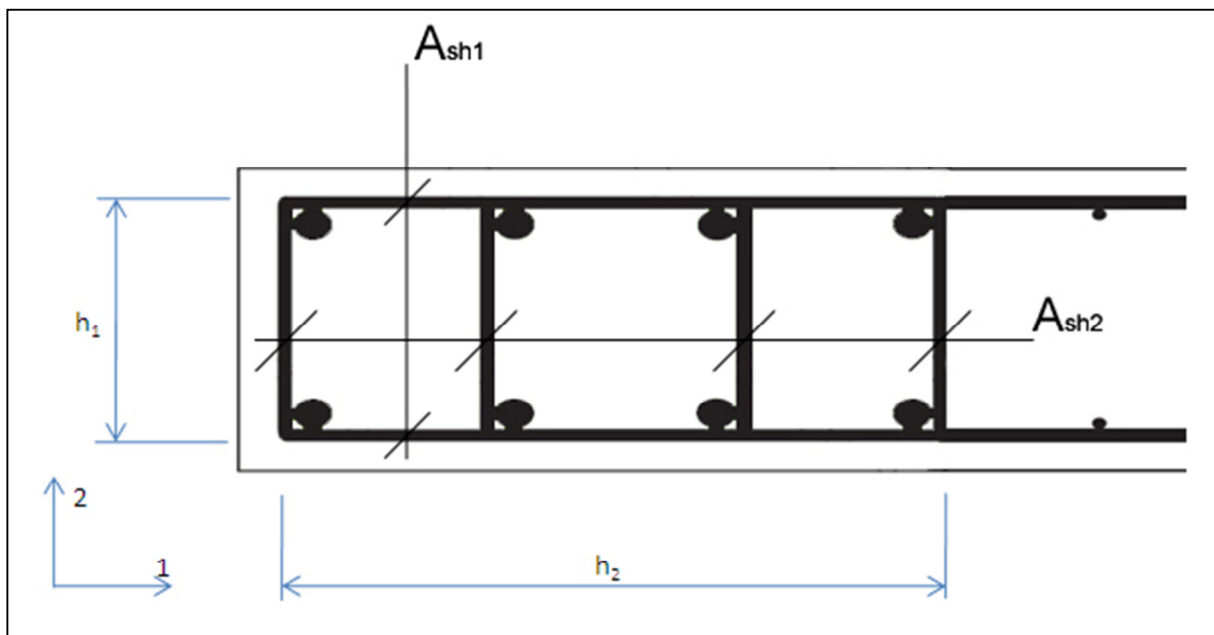


Figure 8.6: Confinement in a wall boundary element

The size of the boundary element is determined by the parameter l_c in Figure 8.5. According to SANS 10160-4 (2009, p. 37) “the boundary element should extend horizontally from the extreme compression fibre a distance l_c of not less than the larger of $x_n - 0.1l_w$ and $x_n/2$ ”, where x_n is the depth of the neutral axis. For the design of the walls of this study the neutral axis depth (x_n) was calculated using design equations (developed in 8.4.1).

In order to prevent wall instability due to out-of-plane buckling in the plastic hinge region of the wall, the wall section should be wide enough. Reference is here made to the dimension

defined as b_w (see Figure 4.2). The critical section width (b_c) may be determined from Figure 8.7, assuming a value for the ductility demand μ . A good assumption is $\mu = q$.

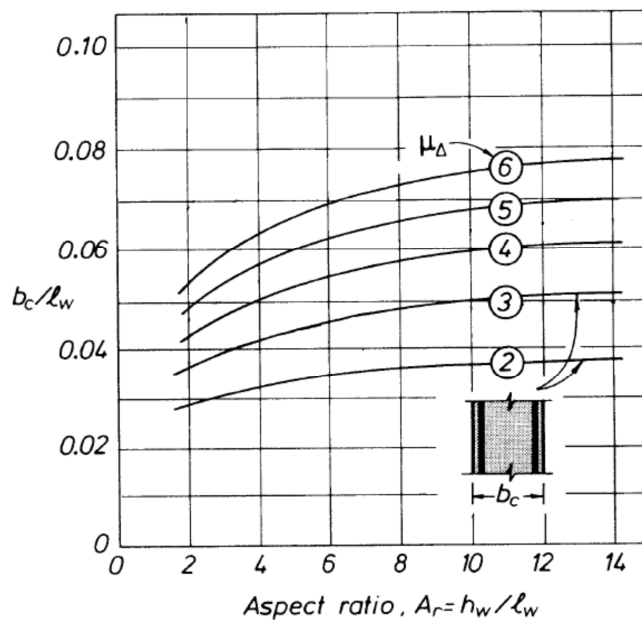


Figure 8.7: Critical wall thickness ductility relationship (Paulay & Priestley, 1992, p.403)

8.4 Bending moment capacity

8.4.1 Design equations

The moment capacity of a wall cross section may be determined using an equivalent stress block method such as the one set out by Bachmann *et al.* (2002, p.137). In Figure 8.8 it is adapted to conform to the assumptions of the stress block method of SANS 10100-1 (2000):

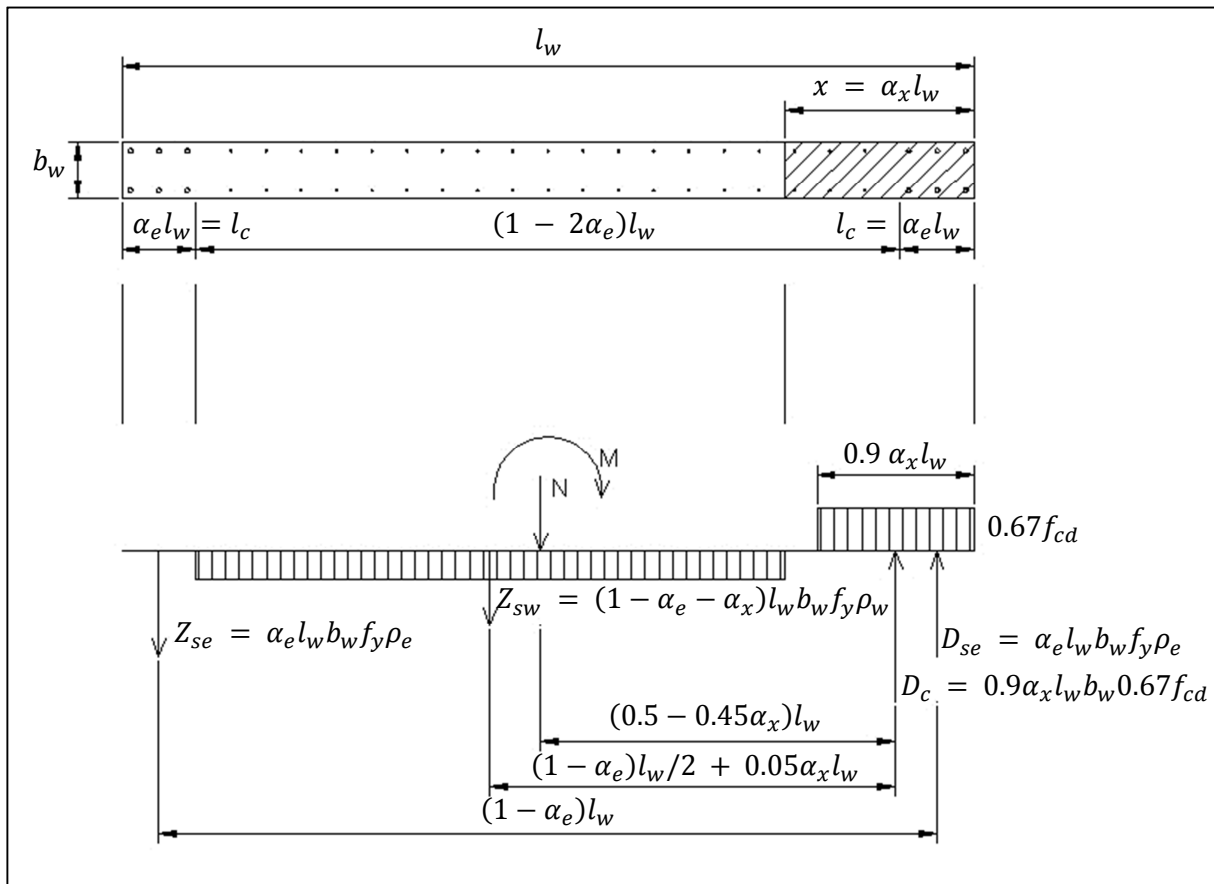


Figure 8.8: Equivalent stress block

In this method the following assumptions are made:

- The steel is elastic-perfectly plastic.
- The reinforcement in the boundary regions yields in both tension and compression.
- The reinforcement in the web yields only in tension for all positive strain values.
- The concrete compressive stress is modelled using the compression block of SANS 10100 (2000).
- It was shown in Figure 7.4 that the design equations compare well with moment-curvature analysis results. Therefore it is sufficiently accurate to ignore the effect of confinement on concrete properties.

Definitions

- N Internal axial load
- M Internal bending moment
- f_{cd} Design compressive cube strength
- f_y Design steel yield strength
- l_w Length of wall section

- $l_c = \alpha_e l_w$ is equal to l_c of Figure 8.5 plus concrete cover, so that the distance from the end of the section to $l_c/2$ coincides with the center of the boundary element (see Figure 8.9).
- b_w Width of wall section
- x Distance from the outer compressive concrete fibre to the neutral axis
- s Horizontal spacing of the web reinforcement
- A_{st} Total reinforcement area
- A_{sw} Web reinforcement area per pair of bars
- A_{se} Boundary element reinforcement area
- Total reinforcement content:
 - $\rho_t = \frac{A_{st}}{b_w l_w}$ 8.9
 - $\omega_t = \rho_t \frac{f_y}{f_{cd}}$ 8.10
- Web reinforcement content:
 - $\rho_w = \frac{A_{sw}}{b_w s}$ 8.11
 - $\omega_w = \rho_w \frac{f_y}{f_{cd}}$ 8.12
- Boundary element reinforcement content:
 - $\rho_e = \frac{A_{se}}{\alpha_e b_w l_w}$ 8.13
 - $\omega_e = \rho_e \frac{f_y}{f_{cd}}$ 8.14
- Axial load ratio: $n = \frac{N}{l_w b_w f_{cd}}$ 8.15
- Bending moment ratio: $m = \frac{M}{l_w^2 b_w f_{cd}}$ 8.16

The two unknowns to be solved are the depth of the neutral axis and the moment capacity. These are obtained from force equilibrium and moment equilibrium of the section.

Force equilibrium of the section forces:

$$0.9\alpha_x l_w b_w \times 0.67f_{cd} = N + (1 - \alpha_e - \alpha_x)l_w b_w f_y \rho_w \quad \text{.....8.17}$$

In Eq. 8.17 α_x can be found by utilizing Eqs. 8.9 to 8.16. Thus, the neutral axis depth ratio α_x is defined by Eq. 8.18:

$$\Rightarrow \alpha_x = \frac{n+(1-\alpha_e)\omega_w}{0.603+\omega_w} \dots\dots\dots 8.18$$

Moment equilibrium of the section forces around the centre of the concrete compression block:

$$M = (1 - \alpha_e)l_w \times \alpha_e l_w b_w f_y \rho_e + (0.5 - 0.45\alpha_x)l_w N + \left[\frac{(1-\alpha_e)l_w}{2} + 0.05\alpha_x l_w \right] \times (1 - \alpha_e - \alpha_x)l_w b_w f_y \rho_w \dots\dots\dots 8.19$$

Eq. 8.19 can be rewritten to find an equation for *m*:

$$m = \left(\frac{1-\alpha_e}{2} \right) \omega_t + (0.5 - 0.45\alpha_x)n + \left[\frac{\alpha_e - \alpha_e^2}{2} + 0.45(\alpha_e - 1)\alpha_x - 0.05\alpha_x^2 \right] \omega_w \dots\dots\dots 8.20$$

With the reinforcement content and wall dimensions as input, the moment capacity of the section can be calculated.

8.4.2 Design example

To illustrate the implementation of the above equations a design example is provided. This is in fact the design of the base of wall W033 as defined in Chapter 4. Figure 8.9 shows the end of the cross section of the wall and the layout of the reinforcement.

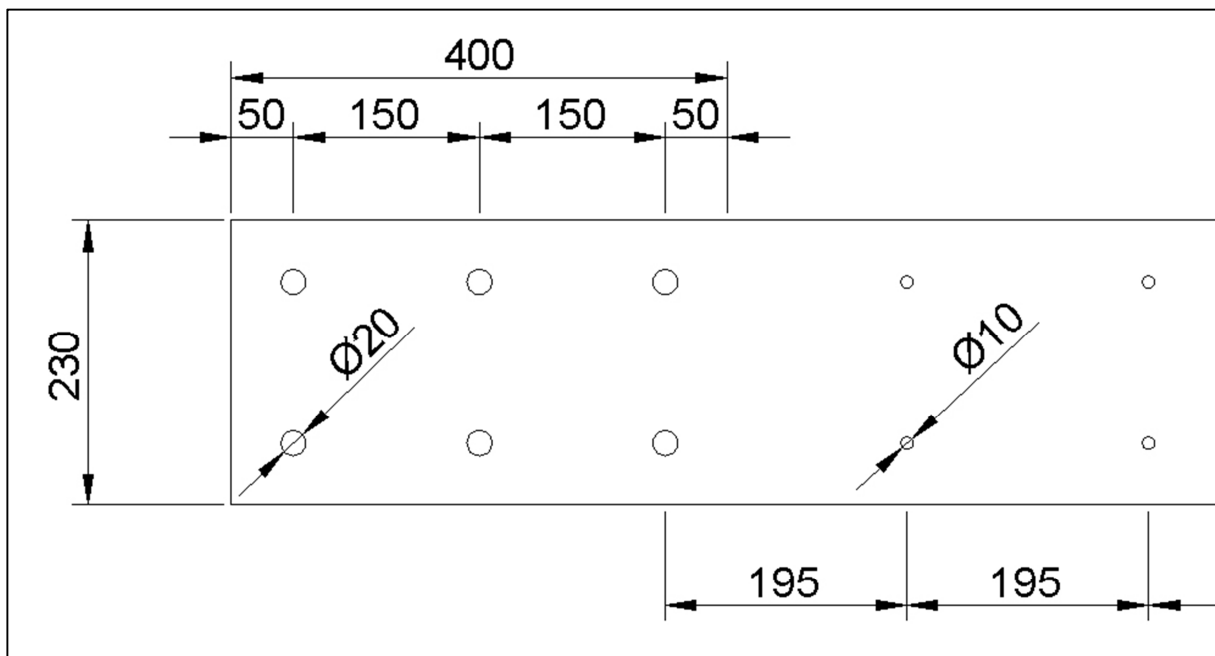


Figure 8.9: Design example

The following are the wall dimensions:

Wall section width $b_w = 230 \text{ mm}$

Wall section length $l_w = 3240 \text{ mm}$

Boundary element length $l_c = 400 \text{ mm}$

The following defines the reinforcement content:

Reinforcement spacing in boundary element $s_e = 150 \text{ mm}$

Reinforcement spacing in web region $s_w = 195 \text{ mm}$

Reinforcement diameter in boundary element $\phi_e = 20 \text{ mm}$

Reinforcement diameter in web region $\phi_w = 10 \text{ mm}$

Axial load at the base of the wall $N = 2\,025 \text{ kN}$

Boundary element length ratio $\alpha_e = \frac{l_c}{l_w} = \frac{400}{3240} = 0.123$

Boundary element reinforcement area $A_{se} = 6 \times \frac{\pi \times 20^2}{4} = 1\,885 \text{ mm}^2$

Web reinforcement area per pair of bars $A_{sw} = 2 \times \frac{\pi \times 10^2}{4} = 157 \text{ mm}^2$

Boundary element reinforcement ratio $\rho_e = \frac{A_{se}}{\alpha_e b_w l_w} = \frac{1\,885}{0.123 \times 230 \times 3\,240} = 0.0205 \text{ (2.05\%)}$

$$\omega_e = \rho_e \frac{f_y}{f_{cd}} = 0.0205 \frac{450}{30} = 0.307$$

Web reinforcement ratio $\rho_w = \frac{A_{sw}}{b_w s} = \frac{157}{230 \times 195} = 0.0035 \text{ (0.35\%)}$

$$\omega_w = \rho_w \frac{f_y}{f_{cd}} = 0.0035 \frac{450}{30} = 0.052$$

Total reinforcement ratio

$$\begin{aligned} \rho_t &= 2\alpha_e \rho_e + (1 - 2\alpha_e) \rho_w \\ &= 0.246 \times 0.0205 + 0.754 \times 0.0035 \\ &= 0.00769 \text{ (0.769\%)} \end{aligned}$$

$$\omega_t = \rho_t \frac{f_y}{f_{cd}} = 0.00769 \frac{450}{30} = 0.115$$

Axial load ratio

$$n = \frac{N}{l_w b_w f_{cd}} = \frac{2\,025 \times 10^3}{3240 \times 230 \times 30} = 0.091$$

Neutral axis depth ratio

$$\begin{aligned} \alpha_x &= \frac{n + (1 - \alpha_e) \omega_w}{0.603 + \omega_w} \\ &= \frac{0.091 + (1 - 0.123) 0.052}{0.603 + 0.052} \\ &= 0.208 \end{aligned}$$

Bending moment ratio

$$\begin{aligned} m &= \left(\frac{1 - \alpha_e}{2} \right) \omega_t + (0.5 - 0.45 \alpha_x) n + \left[\frac{\alpha_e - \alpha_e^2}{2} + 0.45(\alpha_e - 1) \alpha_x - 0.05 \alpha_x^2 \right] \omega_w \\ &= \left(\frac{1 - 0.123}{2} \right) 0.115 + (0.5 - 0.45(0.208)) 0.091 \\ &\quad + \left[\frac{0.123 - 0.123^2}{2} + 0.45(0.123 - 1) 0.208 - 0.05(0.208)^2 \right] 0.052 \\ &= 0.086 \end{aligned}$$

The bending moment capacity of the section can then be obtained by inverting Eq. 8.16:

$$M = m l_w^2 b_w f_{cd} = 0.086 \times 3240^2 \times 230 \times 30 = 6\,213 \text{ kNm}$$

Good correlation between these design equations and moment-curvature analysis results was observed in Figure 7.4.

8.5 Longitudinal reinforcement content

It was stated in step 1 of the methodology (Chapter 5) that an amount of reinforcement, somewhere between maximum and minimum allowable limits, is provided for each structural wall cross section. The allowable limits of reinforcement content are obtained from a recommendation by Dazio & Beyer (2009, p. 7-12):

- $0.3\% < \rho_w < 0.5\%$
- $\rho_e < 4\%$
- $0.3\% < \rho_t < 1\%$

The design equations of 8.4.1 were implemented in a spreadsheet, and with all the capacity design requirements of 8.3 taken into account, the reinforcement for each wall cross section was chosen so as to comply with the three abovementioned reinforcement limits.

9. Ductility capacity and demand

The purpose of this chapter is to describe ductility capacity in terms of a code defined interstorey drift limit and to derive ductility demand from a set of ITHA results. For this purpose it is necessary to discuss the calculation of force-displacement responses of SDOF and MDOF walls from moment-curvature results.

9.1 Force-displacement response of a SDOF wall from moment-curvature analysis

The purpose of this section is to describe the derivation of the force-displacement response of a SDOF wall from the moment-curvature results of the wall cross section. This discussion is extended to MDOF walls in the next section.

As shown in Figure 9.1, the primary purpose is to write equations for the yield- and ultimate displacements, Δ_y and Δ_u , in terms of the yield- and ultimate curvatures, ϕ_y and ϕ_u .

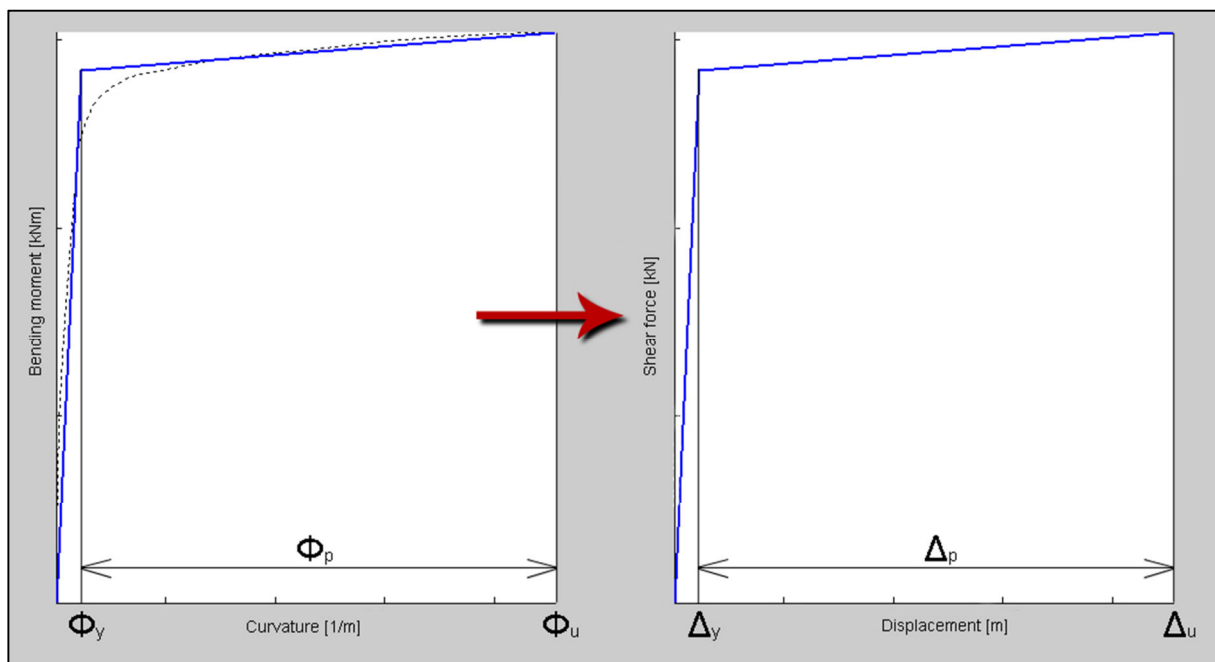


Figure 9.1: Conversion from moment-curvature to force-displacement

A method for determining the force-displacement relationship of a SDOF structural wall from a moment-curvature relationship is illustrated in Figure 9.2.

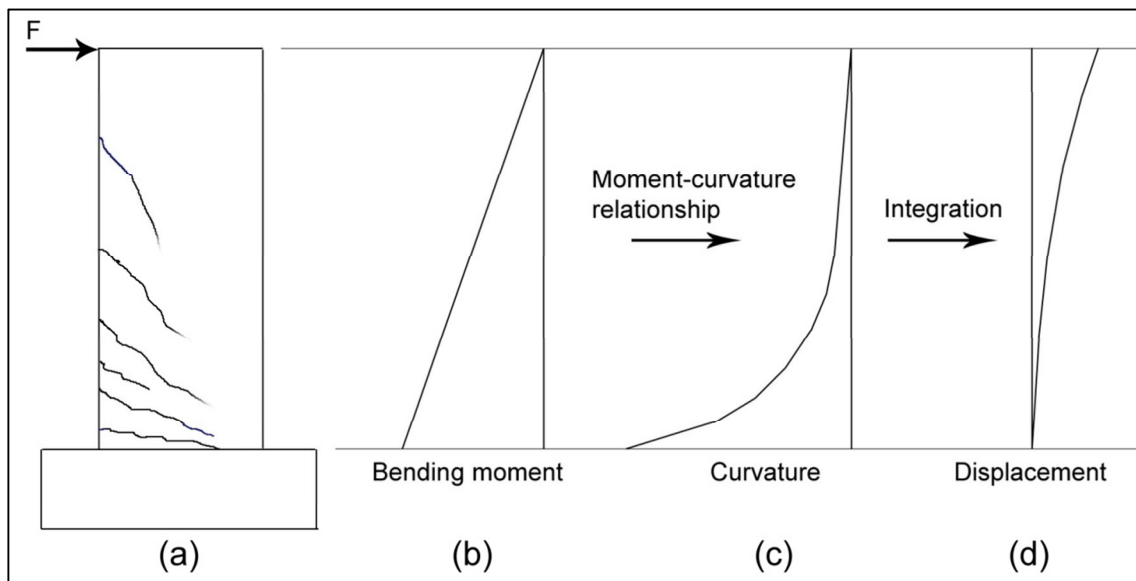


Figure 9.2: Calculating the displacement profile from applied forces

The bending moment distribution can be obtained from the applied force. In this case it is a linear distribution. For each bending moment value, the corresponding curvature value can be read from the moment-curvature curve, to produce the curvature distribution. The curvature distribution can then be integrated twice to produce the displacement profile.

This process unfortunately does not produce force-displacement responses which correspond to experimental results. According to Priestley *et al.* (2007, p.148) some reasons for this are:

- The effect of tension shift, discussed in Chapter 8.2, is ignored.
- The effect of shear deformation is ignored.
- Strain penetration into the foundation is ignored. The curvature profile in Figure 9.2(c) implies an immediate curvature reduction to zero immediately below the base of the wall. The strain in the tension reinforcement would however only reduce to zero below a depth equal to the full development length of the reinforcement. On the other side of the wall section the concrete strain would also not drop to zero immediately.

The solution to these problems is to use a simplified approach where the curvature profile is approximated as shown in Figure 9.3.

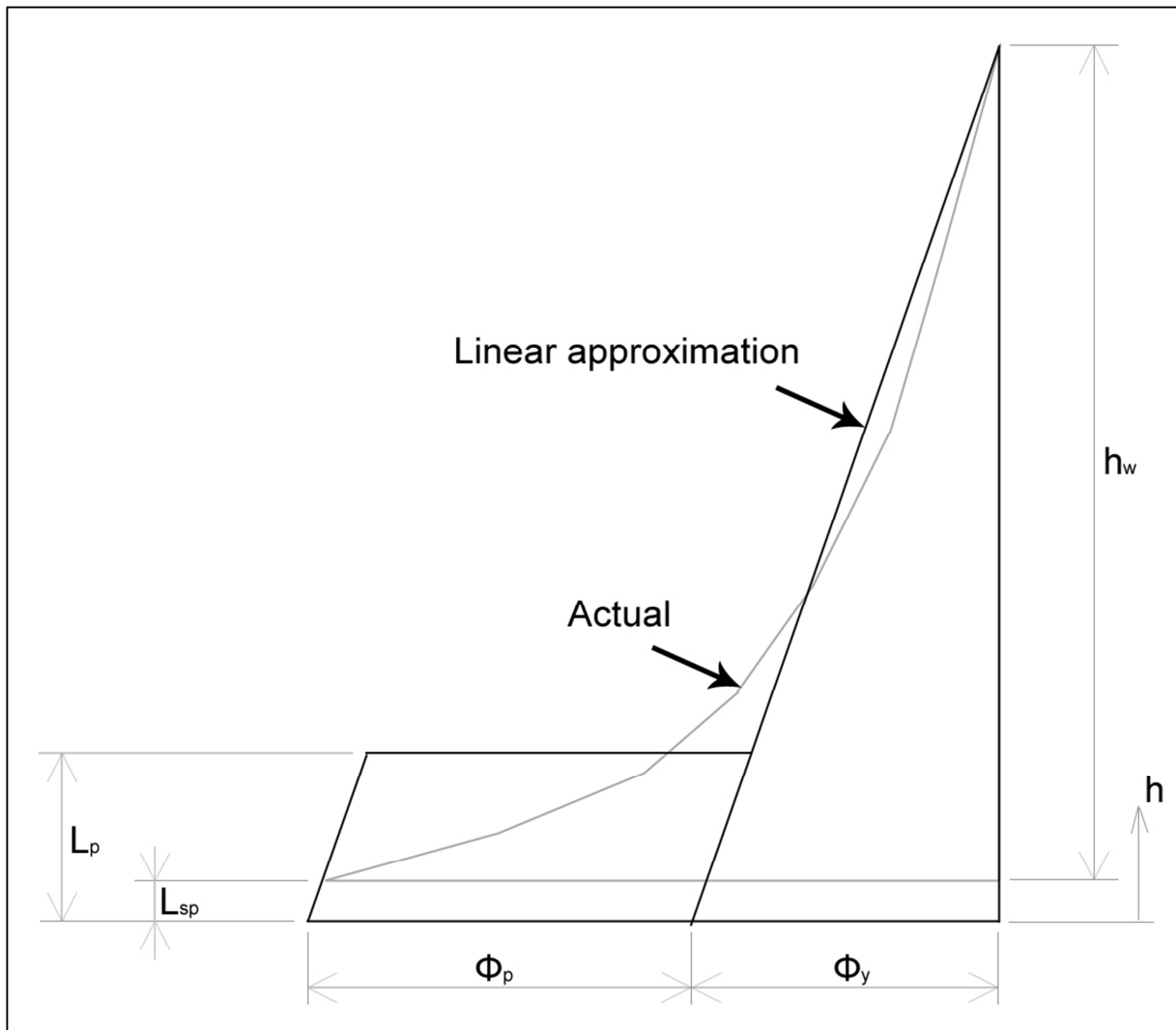


Figure 9.3: Plastic hinge method

This method, known as the plastic hinge method, assumes that a plastic hinge exists at the base of the wall over which the plastic curvature ϕ_p is constant. The length of the plastic hinge L_p includes the depth of strain penetration L_{sp} , as shown in Figure 9.3. Furthermore, the linear approximation of the yield curvature compensates for the increase in displacement due to tension shift, and at least partially for shear displacement (Priestley *et al.*, 2007, p.148).

According to Priestley *et al.* (2007, pp.148-149) the following equations may be used:

$$L_{sp} = 0.022f_y d_{bl} \tag{9.1}$$

where f_y and d_{bl} are the yield strength (in MPa) and diameter of the longitudinal reinforcement in the boundary elements of the wall.

$$L_p = kh_w + L_{sp} \geq 2L_{sp} \quad \dots\dots\dots 9.2$$

where

$$k = 0.2 \left(\frac{f_u}{f_y} - 1 \right) \leq 0.08 \quad \dots\dots\dots 9.3$$

As indicated in Eq. 9.2, the plastic hinge should be longer than at least twice the strain penetration depth. It can also be seen that the variable k takes account of the strain hardening ratio of the reinforcing steel (Refer to Chapter 6.2.2).

To obtain the yield displacement Δ_y the yield curvature could be integrated twice. The linear yield curvature profile may be expressed as follows:

$$\phi_y(h) = \phi_y \left(1 - \frac{h}{h_w + L_{sp}} \right) \quad [1/m] \quad \dots\dots 9.4$$

Integrating the curvature with respect to the height results in an equation for the drift profile:

$$\theta_y(h) = \phi_y \left(h - \frac{h^2}{2(h_w + L_{sp})} \right) + c_1 \quad [\text{rad}] \quad \dots\dots 9.5$$

Integration of the drift over the height produces an equation for the displacement profile:

$$\Delta_y(h) = \phi_y \left(\frac{h^2}{2} - \frac{h^3}{6(h_w + L_{sp})} \right) + c_1 h + c_2 \quad [m] \quad \dots\dots 9.6$$

Both integration constants, c_1 and c_2 , are zero since $\theta(0) = 0$ and $\Delta(0) = 0$.

For a SDOF wall the yield displacement Δ_y is the displacement at $h = h_w + L_{sp}$:

$$\Delta_y = \Delta_y(h_w + L_{sp}) = \phi_y \frac{(h_w + L_{sp})^2}{3} \quad \dots\dots\dots 9.7$$

The plastic displacement Δ_p is derived in the same way, except that the integration is greatly simplified. Integration of the plastic curvature over L_p produces the plastic drift $\theta_p = \phi_p L_p$.

The plastic displacement at the top of the wall is then simply $\Delta_p = \theta_p h_w$. \dots\dots\dots 9.8

The ultimate displacement Δ_u is the sum of the yield displacement and plastic displacement.

$$\Delta_u = \Delta_y + \Delta_p = \phi_y \frac{(h_w + L_{sp})^2}{3} + \phi_p L_p h_w = \phi_y \frac{(h_w + L_{sp})^2}{3} + (\phi_u - \phi_y) L_p h_w \quad \dots\dots\dots 9.9$$

Eq. 9.8 implies that the centre of the plastic hinge is at the base of the wall. This is only exact when $L_p = 2L_{sp}$, but is an acceptable approximation in all cases (Priestley *et al.*, 2007, p.150).

9.2 Force-displacement response of a MDOF wall from moment-curvature analysis

We now extend the discussion from SDOF to MDOF walls. The purpose is to find an equation for the ductility capacity in terms of an allowable drift limit, and to calculate the ductility demand from inelastic time history analysis (ITHA) results.

9.2.1 Conversion from MDOF to SDOF

As shown in Figure 9.4, the displacement of a MDOF wall can be measured by an equivalent SDOF wall (Chopra, 2007, pp. 522-532). This equivalent SDOF wall must have the same dynamic characteristics as the first mode of the MDOF wall. In addition, the height of the wall is chosen such that the base moment of the SDOF wall due to the concentrated force F^* is equal to the base moment of the MDOF wall due to the distributed force (Priestley *et al.*, 2007, p.316). This height h^* is referred to as the effective height.

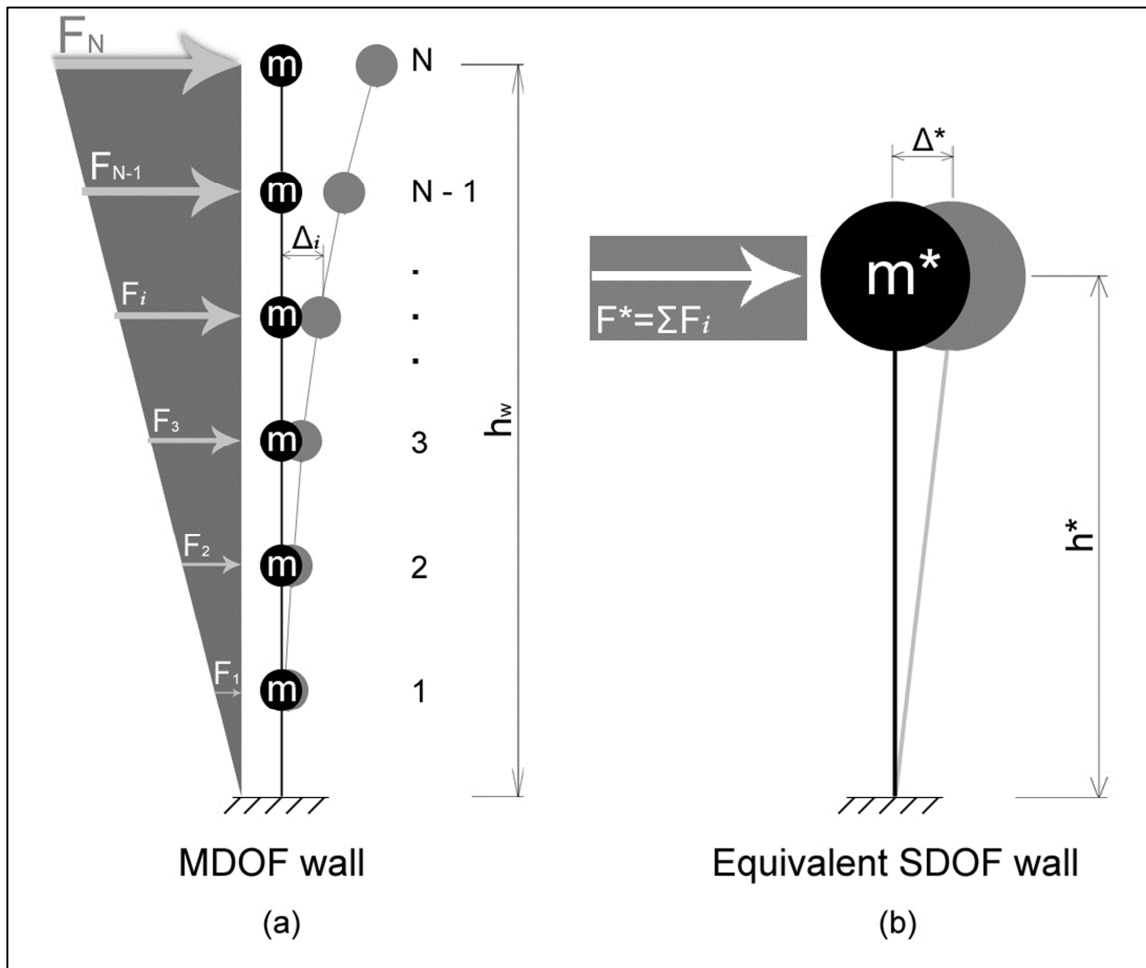


Figure 9.4: Equivalent SDOF wall

Given a displaced shape of the MDOF wall, described by a set of values Δ_i , it is of interest for the discussion to follow to calculate the equivalent SDOF displacement Δ^* . The equation for the SDOF displacement in terms of the MDOF displacement (Eq. 9.19) was derived by Kowalski (2010). It is repeated here:

Assumptions

- Let c_i be a shape function that, when multiplied by Δ^* , results in the MDOF displacement pattern, Δ_i .
- Assume accelerations are controlled by the same shape function:

○ $\Delta_i = c_i \Delta^*$ 9.10

○ $a_i = c_i a^*$ 9.11

Derivation

Apply force equilibrium between the MDOF wall and the equivalent SDOF wall:

$$\begin{aligned}
 F^* &= \sum F_i = \sum m_i a_i = \sum m_i c_i a^* \\
 &= a^* \sum m_i c_i \quad \dots\dots\dots 9.12
 \end{aligned}$$

Since $F^* = a^* m^*$, from Eq. 9.12 the SDOF mass must be:

$$m^* = \sum m_i c_i = \frac{\sum m_i \Delta_i}{\Delta^*} \quad \dots\dots\dots 9.13$$

The force function on the MDOF wall is:

$$F_i = m_i a_i = m_i c_i a^* \quad \dots\dots\dots 9.14$$

Solve Eq. 9.12 for a^* and substitute into Eq. 9.14:

$$F_i = \frac{m_i c_i F^*}{\sum m_i c_i} = F^* \frac{m_i c_i}{\sum m_i c_i} \quad \dots\dots\dots 9.15$$

Solve Eq. 9.10 for c_i and substitute into Eq. 9.15:

$$F_i = F^* \frac{m_i \Delta_i / \Delta^*}{\sum m_i \Delta_i / \Delta^*} = F^* \frac{m_i \Delta_i}{\sum m_i \Delta_i} \quad \dots\dots\dots 9.16$$

Define Δ^* by requiring equivalence in work between SDOF and MDOF walls:

$$F^* \Delta^* = \sum F_i \Delta_i \quad \dots\dots\dots 9.17$$

$$\Delta^* = \sum F_i \Delta_i / F^* \quad \dots\dots\dots 9.18$$

Substitute Eq. 9.16 into Eq. 9.18:

$$\Delta^* = \frac{\sum F^* \frac{m_i \Delta_i}{\sum m_i \Delta_i} \Delta_i}{F^*} = \frac{\sum m_i \Delta_i^2}{\sum m_i \Delta_i} \quad \dots\dots\dots 9.19$$

The equation for the effective height may be derived by bearing in mind that the base moment of the SDOF wall should be equal to the base moment of the MDOF wall.

The base moment of the MDOF and SDOF walls is:

$$M = \sum F_i h_i \quad \dots\dots\dots 9.20$$

Substitute Eq. 9.16 into Eq. 9.20:

$$M = \sum F^* \frac{m_i \Delta_i}{\sum m_i \Delta_i} h_i = \frac{F^*}{\sum m_i \Delta_i} \sum m_i \Delta_i h_i \quad \dots\dots\dots 9.21$$

The base shear force of the MDOF and SDOF walls is:

$$V_b = \sum F^* \frac{m_i \Delta_i}{\sum m_i \Delta_i} = \frac{F^*}{\sum m_i \Delta_i} \sum m_i \Delta_i \quad \dots\dots\dots 9.22$$

Thus, the effective height is:

$$h^* = \frac{M}{V_b} = \frac{\sum m_i \Delta_i h_i}{\sum m_i \Delta_i} \quad \dots\dots\dots 9.23$$

where Δ_i , for the calculation of h^* , is the i^{th} value of the first mode shape.

9.2.2 Validity of linear curvature profile

In the previous section we approximated the yield curvature by a linear profile (see Figure 9.3). For a MDOF wall one would expect such an approximation to be invalid, since the bending moment distribution corresponds to distributed lateral forces (Figure 9.4(a)), and thus the yield curvature profile would be curved, not linear.

This curved curvature profile, labelled “**Design forces**”, obtained from an inverted triangular force distribution is shown in Figure 9.5. Another profile which is shown is similar except that in the upper half of the wall the section may be uncracked, resulting in much lower curvatures in this region. This is labelled “**Uncracked**”. The “**Linear**” curvature profile is also shown. Priestley *et al.* (2007, pp.317-319) calculated the displacement at an effective height of $0.7h_w$ for these three curvature profiles and found that the displacement corresponding to the linear profile is 14.9% and 16.8% higher than the displacement corresponding to the “Design forces” and “Uncracked” curvature profiles respectively.

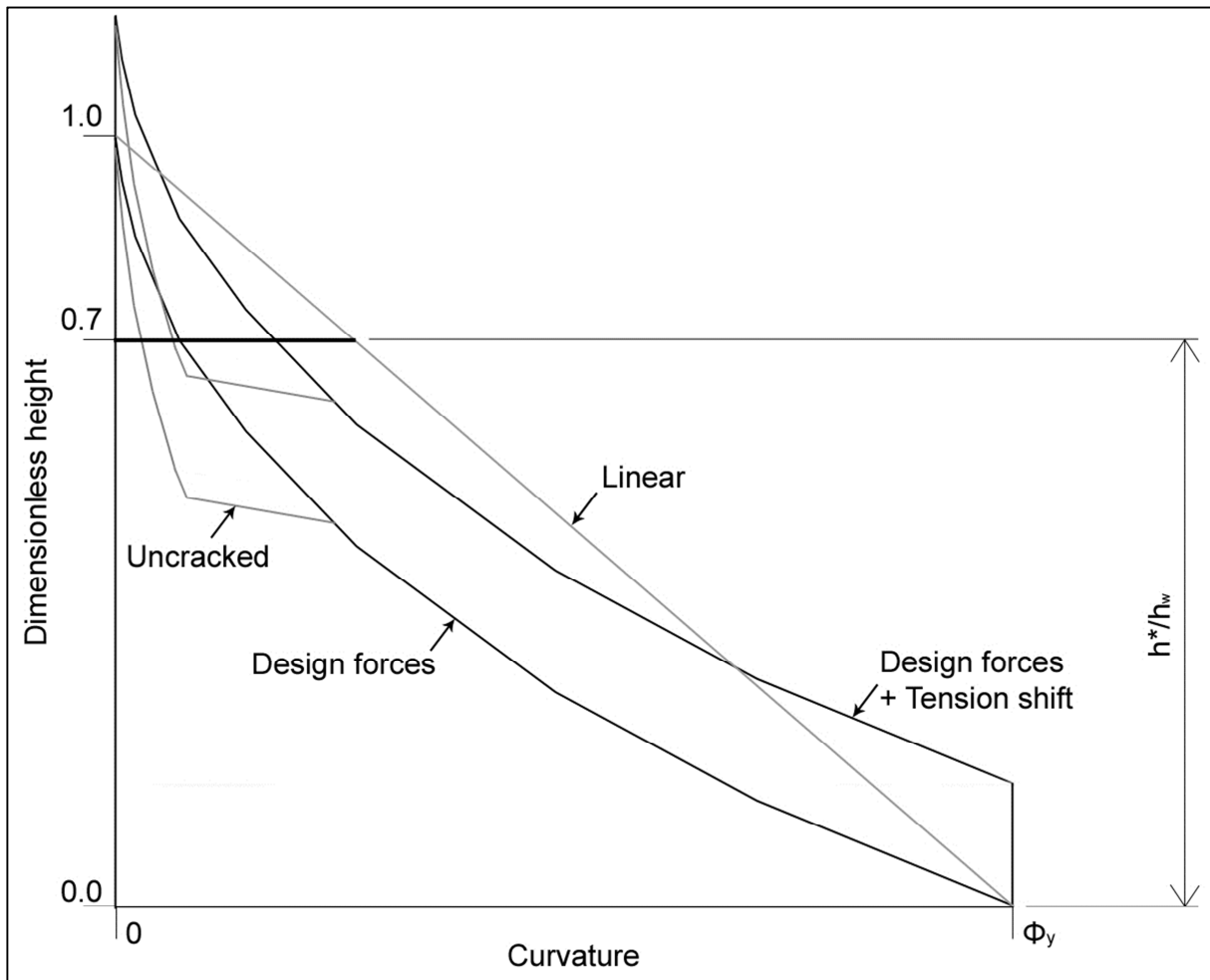


Figure 9.5: MDOF wall curvatures at yield

Tension shift may however be taken into consideration by lifting the curvature profile by a distance equal to $l_w/2$. This profile is also shown in Figure 9.5. When tension shift was taken into account, the displacement corresponding to the linear profile was found to be only 2.7% lower than the displacement corresponding to the curved profile, and almost equal to that of the uncracked section. “It is thus seen that for typical conditions the linear curvature profile provides a reasonable prediction of the yield displacement at the effective height” (Priestley *et al.*, 2007, p.319).

For MDOF walls the strain penetration length is usually very small in comparison to the height of the wall and may thus be neglected. Similar to Eqs. 9.4 to 9.6, the equations for curvature, drift, and displacement may be derived by integration. Here the equations are written in index notation with the index i indicating the degree of freedom ($i = 0, 1, 2, \dots, N$).

The equation for the linear curvature profile is:

$$\phi_{yi} = \phi_y \left(1 - \frac{h_i}{h_w}\right) \quad \dots\dots\dots 9.24$$

Integration of Eq. 9.24 produces an equation for the yield drift profile:

$$\theta_{yi} = \phi_y \left(h_i - \frac{h_i^2}{2h_w}\right) \quad \dots\dots\dots 9.25$$

Integration of Eq. 9.25 produces an equation for the yield displacement profile:

$$\Delta_{yi} = \frac{\phi_y h_i^2}{2} \left(1 - \frac{h_i}{3h_w}\right) \quad \dots\dots\dots 9.26$$

9.3 Defining ductility capacity in terms of a code drift limit

9.3.1 Plastic hinge method

The yield displacement can be obtained from Eq. 9.19 by setting $\Delta_i = \Delta_{yi}$:

$$\Delta_y = \frac{\sum m_i \Delta_{yi}^2}{\sum m_i \Delta_{yi}} \quad \dots\dots\dots 9.27$$

where Δ_{yi} is obtained from Eq. 9.26. The effective height can be calculated from Eq. 9.23:

$$h^* = \frac{\sum h_i m_i \Delta_i}{\sum m_i \Delta_i} \quad \dots\dots\dots 9.28$$

where Δ_i is the i^{th} value of the first mode shape vector.

The maximum yield drift can be calculated from Eq. 9.25:

$$\theta_{yN} = \phi_y \left(h_w - \frac{h_w^2}{2h_w}\right) = \frac{\phi_y h_w}{2} \quad \dots\dots\dots 9.29$$

Since this would be the maximum yield drift for all values of i , the allowable plastic rotation is the difference between the code drift limit θ_c and θ_{yN} . Having obtained the allowable plastic rotation, the plastic displacement at the effective height is

$$\Delta_p = (\theta_c - \theta_{yN})h^* \quad \dots\dots\dots 9.30$$

The ductility capacity in terms of the code drift limit is then $\mu_c = \frac{\Delta_y + \Delta_p}{\Delta_y} \quad \dots\dots\dots 9.31$

9.3.2 Approximate equation

Priestley *et al.* (2007, pp. 325-326) derived a convenient equation which relates ductility to code drift limit. The following simplifying assumptions are made:

From a series of moment-curvature analyses the yield curvature of rectangular reinforced concrete structural walls has been found to be represented by Eq. 9.32 (Priestley *et al.*, 2007, p. 158):

$$\phi_y = \frac{2\varepsilon_y}{l_w} \quad \dots\dots\dots 9.32$$

Thus, from Eq. 9.29 the maximum yield drift is:

$$\theta_{yN} = \frac{\phi_y h_w}{2} = \frac{\varepsilon_y h_w}{l_w} = \varepsilon_y A_r \quad \dots\dots\dots 9.33$$

where A_r is the aspect ratio of the wall. From Eq. 9.26 the yield displacement profile can be described by:

$$\Delta_{yi} = \frac{\phi_y h_i^2}{2} \left(1 - \frac{h_i}{3h_w}\right) = \frac{\varepsilon_y h_i^2}{l_w} \left(1 - \frac{h_i}{3h_w}\right) = \varepsilon_y A_r h_w \left(\frac{h_i}{h_w}\right)^2 \left(1 - \frac{h_i}{3h_w}\right) \quad \dots\dots\dots 9.34$$

The equivalent yield displacement can be obtained by substituting Eq. 9.34 in Eq. 9.27 and assuming equal floor masses:

$$\Delta_y = \frac{\sum m_i \Delta_{yi}^2}{\sum m_i \Delta_{yi}} \approx 0.45 \varepsilon_y A_r h_w \quad \dots\dots\dots 9.35$$

The effective height at yield, from Eq. 9.23, is $h^* \approx 0.77h_w$. Thus, by substituting Eq. 9.33 in Eq. 9.30, the plastic displacement is:

$$\Delta_p = 0.77h_w(\theta_c - \varepsilon_y A_r) \quad \dots\dots\dots 9.36$$

Hence, from Eq. 9.31, the ductility capacity is:

$$\mu_c = \frac{\Delta_y + \Delta_p}{\Delta_y} = \frac{0.45\varepsilon_y A_r h_w + 0.77h_w(\theta_c - \varepsilon_y A_r)}{0.45\varepsilon_y A_r h_w} = 1 + 1.71 \frac{\theta_c - \varepsilon_y A_r}{\varepsilon_y A_r} \quad \dots\dots\dots 9.37$$

Both the plastic hinge method and Eq. 9.37 can be used to calculate the ductility capacity in terms of the code drift limits prescribed by SANS 10160-4 (2009, p. 27) (see Figure 11.5 to Figure 11.8).

9.4 Calculating ductility demand from inelastic time history analysis (ITHA) results

As stated in step 6.2 of the methodology (Chapter 5), ITHA is used to validate the ductility demand obtained from the equal displacement and equal energy principles. For each wall, ITHA is performed for a number of ground motion records (refer to Chapter 10.5). For each ground motion record the peak displacement of each degree of freedom (DOF) is recorded.

The equivalent displacement of the average of the peak displacements can be obtained from Eq. 9.38:

$$\Delta_{\text{eq}} = \frac{\sum m_i \Delta_i^2}{\sum m_i \Delta_i} \quad \dots\dots\dots 9.38$$

where Δ_i is the average of the peak displacement values of the i^{th} DOF. The yield displacement is known from Eq. 9.27, and thus the ductility demand can be calculated using Eq. 9.39:

$$\mu_d = \frac{\Delta_{\text{eq}}}{\Delta_y} \quad \dots\dots\dots 9.39$$

Thus we have seen in this chapter that inter storey drift limits can be expressed in terms of ductility. This is done in step 5 of the methodology (Chapter 5) according to both the plastic hinge method (9.3.1) and the approximate equation (9.3.2).

It was also shown that ductility demand can be calculated from a set of ITHA. This corresponds to step 6.2 of the methodology. All aspects of ITHA are discussed in Chapter 10.

10. Inelastic time history analysis

ITHA is used in step 6.2 of the methodology (Chapter 5) to validate ductility demand predicted by means of the equal displacement and equal energy principles (Chapter 2.1.6). The calculation of ductility from a set of ITHA results was discussed in Chapter 9.4.

All aspects of ITHA, including member properties, hysteresis rules, and damping is discussed in this chapter. Background information regarding the modelling of a plastic hinge is also provided (10.3). In 10.5 the selection and manipulation of ground motion records are discussed. Finally, in 10.7, the validity of the equal displacement principle is investigated.

10.1 Degree of sophistication in element modelling

The two primary finite elements used to model beam-column structural members are line and fibre elements (Priestley *et al.*, 2007, p. 193). Line elements are beam-column elements with the ability to form plastic hinges at the ends of the member. With a suitable moment-curvature hysteresis rule assigned to the plastic hinges, the structural response can be predicted with remarkable accuracy (Priestley *et al.*, 2007, p. 193). The moment-curvature envelope which is assigned to the plastic hinges is obtained from moment-curvature analysis. Line elements have the advantage of not requiring much computation time.

Fibre elements are beam-column elements of which the cross section is divided into a number of fibres. Each fibre is assigned the material hysteresis rule of either concrete or steel. Thus, no prior moment-curvature analysis is required and no assumption regarding the appropriate moment-curvature hysteresis rule is required (Priestley *et al.*, 2007, p. 195). Fibre elements are however less computationally efficient.

Since this study required a large number of inelastic time history analyses, and since line elements predict structural response with adequate accuracy (Priestley *et al.*, 2007, p. 193), it was decided to use line elements. For this purpose the free 2D student version of Ruaumoko (Carr, 2007) was used.

10.2 Beam properties

The two types of line elements available in Ruaumoko are the elastic beam and the Giberson beam. The first storey was modelled with a Giberson beam element which contains a rotational spring at each end of the member. The top spring is disabled (by defining a high yield moment), while the bottom spring represents the plastic hinge which forms at the base

of the wall. An equation which relates the stiffness of this spring to the hysteresis rule is developed in 10.3 (Eq. 10.2).

The upper part of the wall is required to remain elastic. Thus all higher storeys were modelled with elastic beam elements. An illustration of a typical finite element model of one of the walls of the study is shown in Figure 10.1. Lumped floor masses were used in accordance with the assumptions of Chapter 3.1.4.

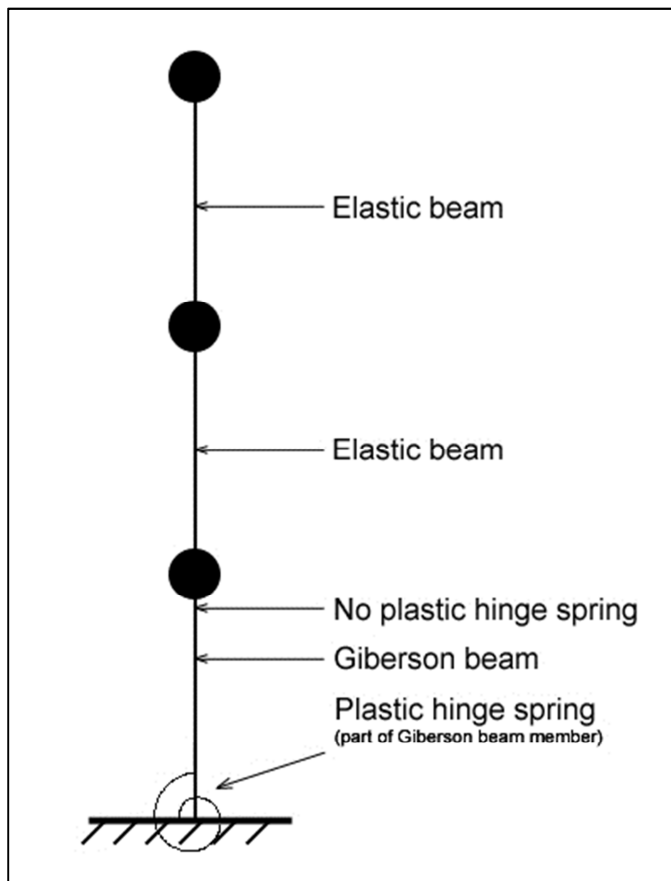


Figure 10.1: Typical finite element model of a structural wall

10.2.1 Elastic properties

The input required for the elastic beam is summarized in Table 10.1:

Table 10.1: Elastic beam properties

| Elastic section properties | | |
|----------------------------|-----------------------------|---------------------------------|
| Symbol | Name | Equation or value |
| E_c | Young's Modulus of concrete | 27 GPa |
| G | Shear modulus of concrete | $E/2(1 + \nu)$ ($\nu = 0.2$) |
| A | Cross-sectional area | $b_w \times l_w$ |
| A_s | Shear area | $5A/6$ |
| I_{eff} | Sectional moment of inertia | $M_n/E\phi_y$ (see Figure 10.2) |

As indicated in Table 10.1, the cracked sectional moment of inertia is obtained from the pre-yield branch of the bilinear moment-curvature relationship. Only one moment-curvature analysis was done, namely for the base of the wall (Dazio & Beyer, 2009). The stiffness obtained from this analysis was applied over the full height of the wall. The properties obtained from the moment curvature analysis are illustrated in Figure 10.2.

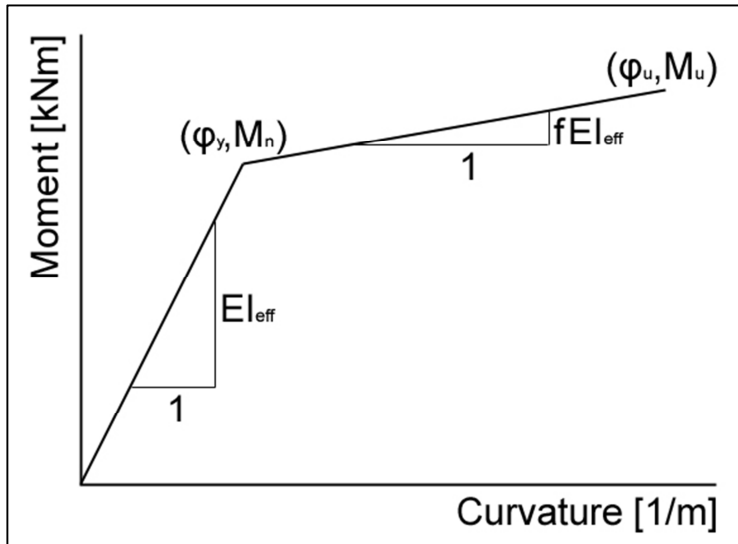


Figure 10.2: Moment-curvature properties

10.2.2 Inelastic properties

In addition to the elastic section properties the Giberson beam requires the input listed in Table 10.2:

Table 10.2: Giberson beam properties

| Bilinear factors and hinge properties | | |
|---------------------------------------|------------------------------|--|
| Symbol | Name | Equation or value |
| f | Bilinear factor | See Figure 10.2 |
| L_p | Plastic hinge length (end 1) | Defined in Chapter 9.1. (Eq. 9.2) |
| | Plastic hinge length (end 2) | Any value. A zero length is interpreted as a length of 1.0. The hinge is disabled under <i>Yield moment (end 2)</i> below. |
| Beam yield conditions | | |
| Symbol | Name | Equation or value |
| M_n | Yield moment (end 1) | See Figure 10.2 |
| | Yield moment (end 2) | Choose a very large value so that yield does not occur. |

10.2.3 Hysteresis rule

The envelope of the response of the plastic hinge is determined by the bilinear moment-curvature relationship, but the hysteretic behaviour of the hinge is determined by a hysteresis rule. The Modified Takeda Rule shown in Figure 10.3 is appropriate for reinforced concrete and reinforced masonry structures (Priestley *et al.*, 2007, p. 201). It may be seen that the shape of the hysteresis response depends on the value of β . For members without axial

load, such as reinforced concrete beams a β value of 0.6 is generally considered to be appropriate, while a β value of zero applies to members with high axial load, such as columns, bridge piers, and structural walls (Priestley *et al.*, 2007, pp. 201-202).

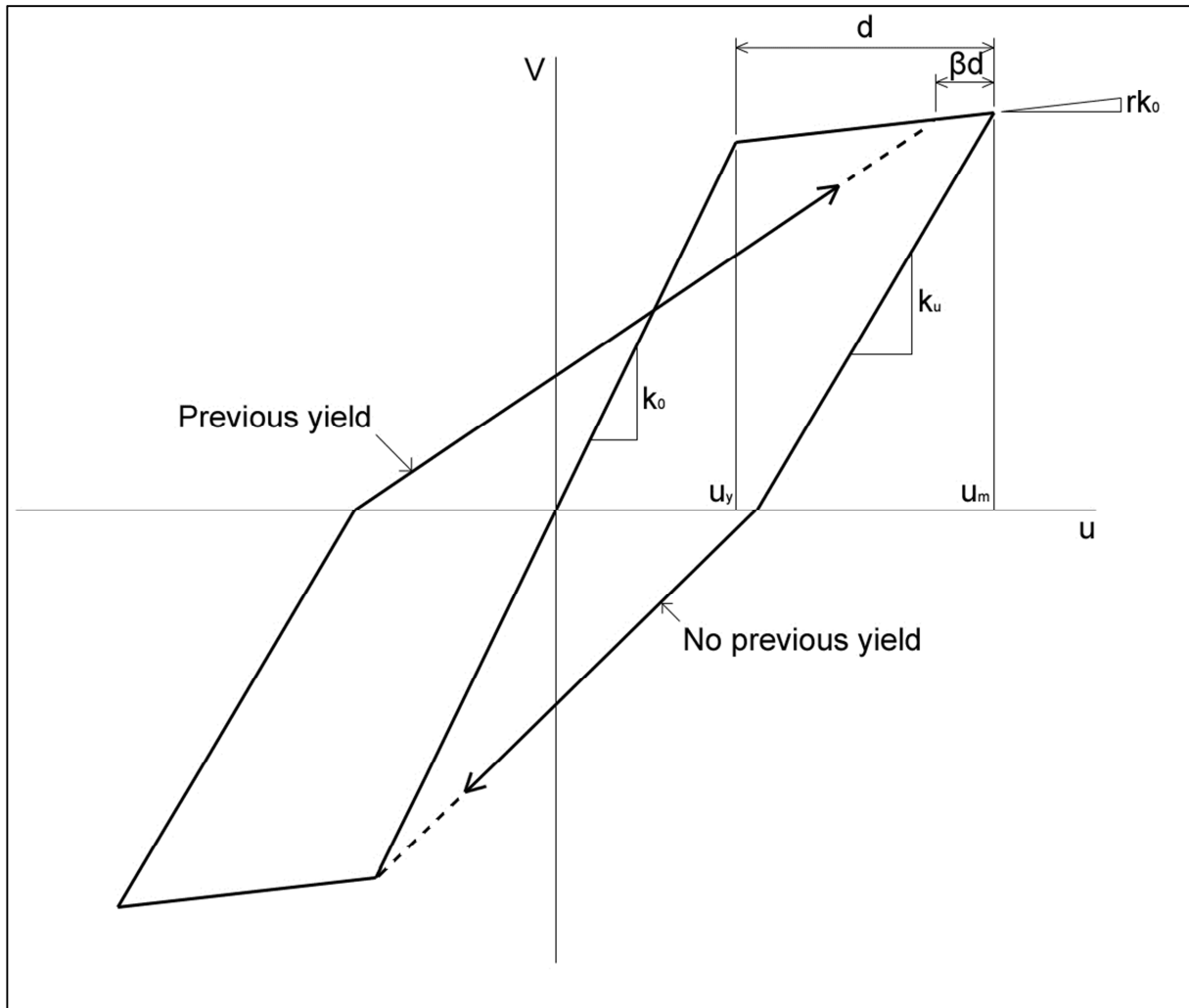


Figure 10.3: Modified Takeda Hysteresis rule (Priestley *et al.*, 2007, p. 202)

The unloading stiffness k_u is a function of the elastic stiffness k_0 and the ductility at the onset of unloading ($\mu = u_m/u_y$) (Priestley *et al.*, 2007, p. 201):

$$k_u = k_0 \mu^{-\alpha} \quad \dots\dots\dots 10.1$$

where $\alpha = 0.5$ is appropriate for reinforced concrete structural walls (Priestley *et al.*, 2007, p. 201). Table 10.1 to Table 10.3 thus contain all input required for the Giberson beam.

Table 10.3: Hysteresis rule properties

| Hysteresis rule | | |
|-----------------|----------------------------|-------------------|
| Symbol | Name | Equation or value |
| α | Unloading stiffness factor | 0.5 |
| β | Reloading stiffness factor | 0.0 |

10.3 Representation of the plastic hinge in the finite element model

It was stated in Chapter 9.1 that we assume that all inelastic deformation is concentrated at the base of the wall over a length L_p , called the plastic hinge length. We assume that the plastic curvature within the plastic hinge is constant. This plastic hinge is modelled in the finite element model with a rotational spring of appropriate stiffness connected to a beam with elastic section properties. This combination is contained within the Giberson beam and therefore does not need to be modelled explicitly. This section therefore serves only to inform the interested reader about the inner working of the Giberson beam. The following paragraphs present the derivation of the equation relating the spring stiffness k_s to the plastic hinge length L_p and bilinear factor f (Figure 10.2).

Figure 10.4 shows the finite element model near the base of the wall and the corresponding plastic hinge assumption. The stiffness of the spring is such that the rotation of the spring together with the deflection of the beam (with stiffness EI_{eff}) produces the same rotation θ as the deflection of the beam alone (with stiffness $f \times EI_{eff}$).

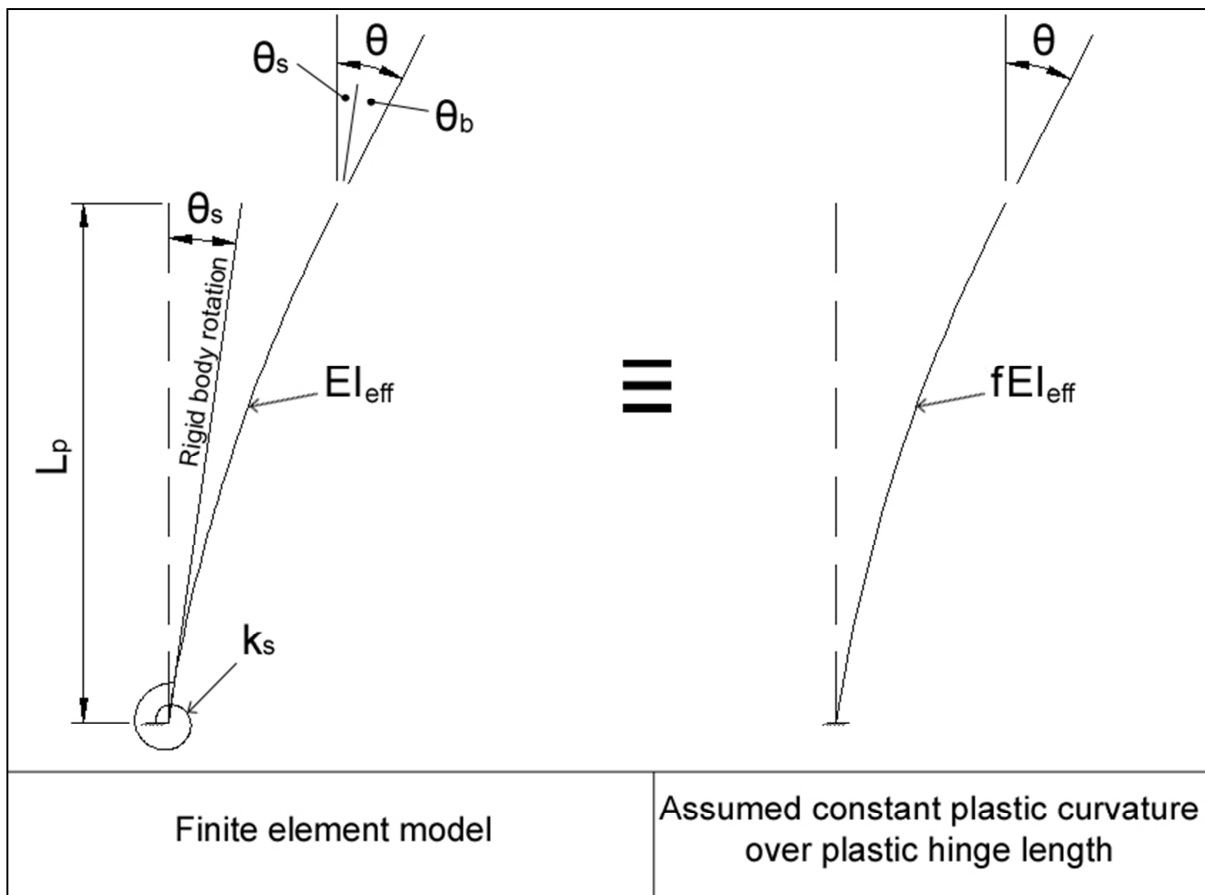


Figure 10.4: Plastic hinge spring

Assuming a constant bending moment M over the plastic hinge length, the total rotation θ may be equated for both cases as:

Finite element model

$$\begin{aligned} \theta &= \theta_s + \theta_b \\ &= \frac{M}{k_s} + \frac{ML_p}{EI_{eff}} \end{aligned}$$

Plastic hinge assumption

$$\begin{aligned} \theta &= \phi_p L_p \\ &= \frac{ML_p}{fEI_{eff}} \end{aligned}$$

$$\begin{aligned} \therefore \frac{M(EI_{eff} + k_s L_p)}{k_s EI_{eff}} &= \frac{ML_p}{fEI_{eff}} \\ \frac{EI_{eff} + k_s L_p}{k_s} &= \frac{L_p}{f} \\ fEI_{eff} + f k_s L_p &= k_s L_p \end{aligned}$$

$$\therefore k_s = \frac{EI_{eff}}{L_p} \left(\frac{f}{1-f} \right) \quad \dots\dots\dots 10.2$$

(The same equation appears in the Theory Manual of Ruaumoko (Carr, 2007)). Thus, for any point on the hysteresis curve (Figure 10.3) the appropriate stiffness of the rotational spring can be found by substituting the current value of the bilinear factor f into Eq. 10.2. It may be seen that for the elastic part of the hysteresis rule $f = 1$, and thus the spring stiffness is infinitely large according to Eq. 10.2. This is the expected result since the spring rotation θ_s should be zero when the wall is still elastic.

10.4 Time step integration parameters

For the ITHA Newmark’s average acceleration time-stepping method was used (Chopra, 2007, p. 175). The ground motion records used in this study had been recorded in a time interval of 0.005 seconds. The same time-step was used in the time-stepping method.

10.5 Ground motions

10.5.1 Number of records

According to Priestley *et al.* (2007, p. 210) it is sufficient to use the result of the average response of a minimum of seven ground motion records. Initially twenty ground motion records were used in this study to enable possible probabilistic future studies. It was soon realized however that twenty ground motions were very time consuming. It was subsequently found that the result obtained from seven ground motions did not differ much from the result obtained from twenty ground motions, and thus the number of ground motions were reduced to seven.

10.5.2 Selection of records

According to Priestley *et al.* (2007, p. 211) three basic means exist of obtaining spectrum-compatible accelerograms:

- *Amplitude scaling of acceleration records from real earthquakes to provide a “best fit” to the design spectrum over the period range of interest.*
- *Generating artificial spectrum-compatible records using special purpose programs.*
- *Manipulating existing “real” records to match the design spectrum over the full range of periods.*

Records obtained through amplitude scaling of existing records are likely to have large scatter between records. A large number of records might therefore be necessary to obtain a reliable result. It is also important to carefully select the period range over which the scaling is done so as to include longer periods at which the structure would respond inelastically (Priestley *et al.*, 2007, p. 211).

Artificial accelerograms can be generated to match the design spectrum over the full period range. Thus a lesser number of records are required to obtain a reliable average response (Priestley *et al.*, 2007, p. 211).

Obtaining artificial records by manipulating real records has recently become more common. It has the advantage over purely artificial records that it preserves the essential character of the original real records (Priestley *et al.*, 2007, p. 211).

Thus it was decided to obtain real records with characteristics similar to that of ground types 1 and 4, and to manipulate these records to match the SANS 10160-4 (2009) elastic spectra. For this purpose the free student version of Oasys Sigrath (Oasys Limited, 2010a) was used.

According to the Sigrath manual (Oasys Limited, 2010b) the manipulation of a real ground motion is done as follows: The user specifies the starting time history, target spectrum, and damping. Sigrath calculates the response spectrum and the Fast Fourier Transform of the starting time history. The response spectrum is then compared to the target spectrum and the spectral values are adjusted up or down in proportion to the difference in the target and actual response spectra. An inverse Fast Fourier Transform is then used to generate a new time history. This procedure is repeated until the difference between the target and actual spectra is less than a user-specified tolerance.

The primary variable which differentiates ground types is $v_{s,30}$, which is defined as “the average value of propagation of S-waves in the upper 30 m of the soil profile at shear strains of 10^{-5} or less” (SANS 10160-4, 2009, p. 10). Ground type 1 is defined by $v_{s,30} > 800$ m/s and ground type 4 by $v_{s,30} < 180$ m/s. Ground motion records were also selected based on PGA. The design PGA for the Cape Town region is 0.15 g. Thus, ground motions with a PGA between 0.1 g and 0.2 g were chosen so that the minimum amount of scaling would be required. The selected ground motions are listed in Table 10.4. Each earthquake has two orthogonal components. The seven ground motions were thus obtained from both components of the first three earthquakes and one component of the fourth. The records were obtained from the PEER NGA Database (2007).

Table 10.4: Selected ground motions

| Ground type 1 | | | | |
|---------------|--------------------------------------|-----------|---------|------------------|
| Record | Earthquake | Magnitude | PGA [g] | $v_{s,30}$ [m/s] |
| NGA0023 | San Francisco 1957-03-22 19:44 | 5.28 | 0.107 | 874 |
| NGA0098 | Hollister-03 1974-11-28 23:01 | 5.14 | 0.117 | 1428 |
| NGA0146 | Coyote Lake 1979-08-06 17:05 | 5.74 | 0.120 | 1428 |
| NGA0680 | Whittier Narrows-01 1987-10-01 14:42 | 5.99 | 0.102 | 969 |
| Ground type 4 | | | | |
| Record | Earthquake | Magnitude | PGA [g] | $v_{s,30}$ [m/s] |
| NGA0201 | Imperial Valley-07 1979-10-15 23:19 | 5.01 | 0.141 | 163 |
| NGA0780 | Loma Prieta 1989-10-18 00:05 | 6.93 | 0.121 | 170 |
| NGA0808 | Loma Prieta 1989-10-18 00:05 | 6.93 | 0.132 | 155 |
| NGA1866 | Yountville 2000-09-03 | 5.00 | 0.150 | 155 |

These fourteen records were manipulated to match the SANS 10160-4 (2009) spectra. The tolerance on the convergence error was specified as a root mean square of 10 percent. Damping was specified as 5% of critical in accordance with the 5% damped code spectra. The pseudo acceleration spectra of the manipulated records are plotted with the elastic SANS 10160-4 (2009) spectra in Figure 10.5.

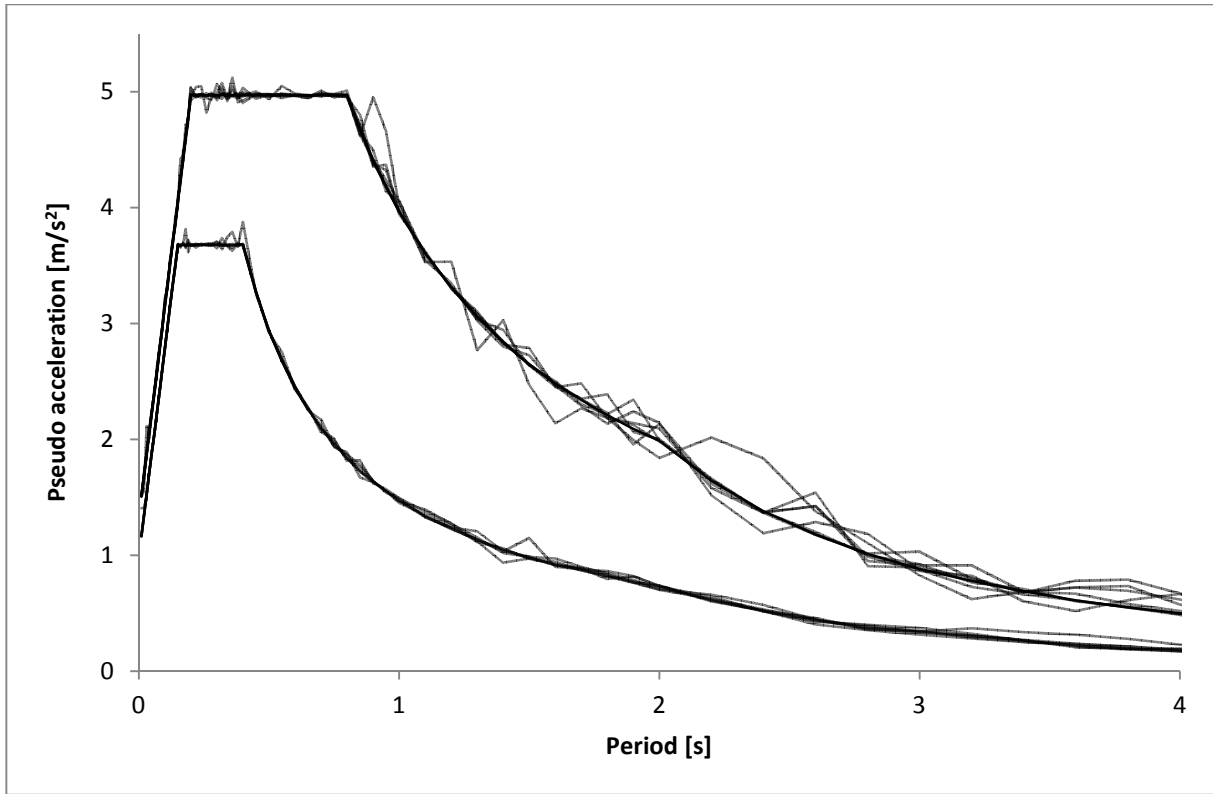


Figure 10.5: Artificial ground motion spectra

10.6 Damping

In elastic and inelastic time history analyses a certain level of viscous damping is defined, expressed as a ratio of critical damping (typically 5%). Hysteresis rules assume linear elastic response below the yield moment. This is not absolutely correct, since some hysteretic action takes place within this range. Viscous damping thus represents the energy dissipated in the elastic range by the hysteretic action of structural components. Viscous damping also represents energy dissipated by the hysteretic response of non-structural components and the relative movement between structural and non-structural components (Priestley *et al.*, 2007, p. 204).

Additional energy is dissipated in the inelastic range through the hysteretic action of plastic hinges. This energy dissipation is accounted for by the hysteresis rule defined in 10.2.3.

A commonly used viscous damping model is Raleigh damping, which defines damping as a combination of stiffness proportional and mass proportional damping (Chopra, 2007, pp. 455-458):

$$[C] = a_0[M] + a_1[K] \tag{10.3}$$

where $a_0 = 2\zeta_i\omega_i$ 10.4

$$a_1 = 2\zeta_j/\omega_j \quad \dots\dots\dots 10.5$$

[C] is the system damping matrix

[M] is the system mass matrix

[K] is the system stiffness matrix

and ζ_i, ζ_j are the damping ratios of mode i and j

ω_i, ω_j are the circular natural frequencies of mode i and j

Mode i and j are typically chosen so that the damping ratio for all the significant modes are approximately equal to the desired damping ratio $\zeta = \zeta_i = \zeta_j$. For a five degree of freedom system for instance this damping ratio could be specified for the first and fourth mode. Mode 2 and 3 would thus have a slightly lower damping ratio, while mode 5 will have a higher damping ratio (Chopra, 2007, pp. 457-458). This is illustrated in Figure 10.6 for $\zeta_i = \zeta_j = 0.05$:

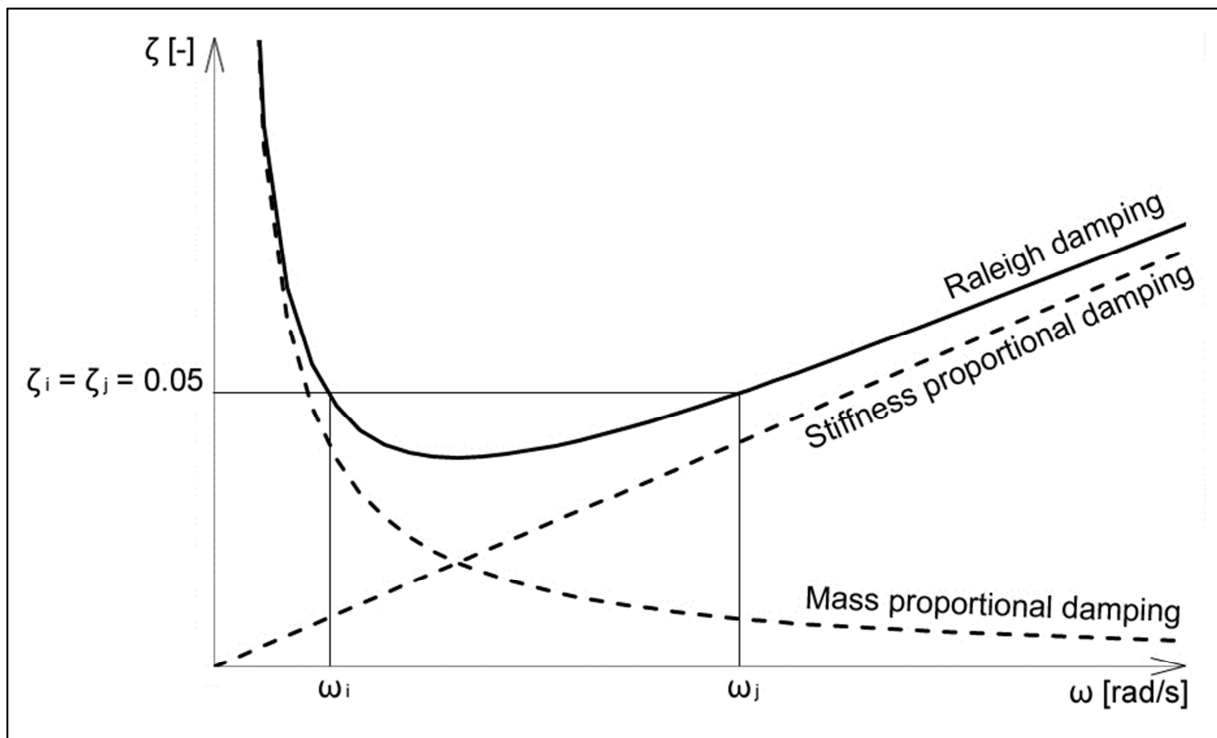


Figure 10.6: Raleigh damping

Since viscous damping represents energy dissipation in the elastic range of response, and all inelastic energy dissipation is accounted for by the plastic hinge hysteresis, it would make sense that the viscous damping should be zero in the post-yield range, except when the structure unloads or reloads elastically (Priestley *et al.*, 2007, p. 204). One way to accomplish this is to base the viscous damping on the tangent stiffness matrix. Since the stiffness reduces greatly in the post-yield range, the damping would reduce by the same ratio. For this reason Priestley *et al.* (2007, p. 207) state that the most appropriate damping

model for structural response is tangent-stiffness proportional damping. Refer to Priestley *et al.* (2007, pp. 203-210) for a detailed discussion on the subject.

Stiffness proportional damping should however not be confused with Raleigh damping with a stiffness proportional component, since most of the viscous damping in the critical first mode would be mass proportional, which is constant with inelastic action (Priestley *et al.*, 2007, pp. 208-210). This can clearly be seen in Figure 10.6 where ω_i is the first modal circular frequency.

Thus it was decided to use a tangent-stiffness proportional damping ratio of 0.05 for the first mode. When applying stiffness proportional damping, one should also be careful that the damping of highest mode is less than 100% (Carr, 2007). Thus, the damping in the highest mode was limited to 100%, resulting in some cases in a damping of less than 5% in the first mode.

10.7 The validity of the equal displacement principle

Damping models based on initial-stiffness have been used extensively in the past. The equal displacement and equal energy principles were based on ITHA conducted with these damping models. In recent years the use of initial-stiffness damping has been questioned, and instead, the use of tangent-stiffness proportional damping has been proposed by Priestley *et al.* (2007), Petrini, Maggi, Priestley & Calvi (2008), and Priestley & Grant (2005).

Priestley & Grant (2005) performed time history analyses on elastic and inelastic SDOF systems for various hysteresis rules, force reduction factors, post-yield stiffness ratios, and fundamental periods, using five synthetic time histories and one real ground motion record. The synthetic ground motions were matched to the ATC-32 spectrum for ground type C. The average of the peak displacements obtained from inelastic analyses was compared to that of the elastic analyses. The displacement ratio ($\Delta/\Delta_{elastic}$) of peak inelastic displacement to peak elastic displacement is shown on the vertical axes of Figure 10.7. The fundamental periods of the SDOF systems are shown on the horizontal axes. In Figure 10.7 (a) the post yield stiffness was 0.2% of the initial stiffness, and in Figure 10.7 (b) the post yield stiffness was 5% of the initial stiffness.

For the equal displacement principle to be valid, the displacement ratio ($\Delta/\Delta_{elastic}$) should be equal to unity. Since the displacement ratio is significantly larger than one, it can clearly be seen in Figure 10.7 that the equal displacement principle is generally unconservative if

damping is assumed to be tangent-stiffness proportional. It can also be seen that the post-yield stiffness does not influence the results significantly, since the difference between Figure 10.7 (a) and (b) is small.

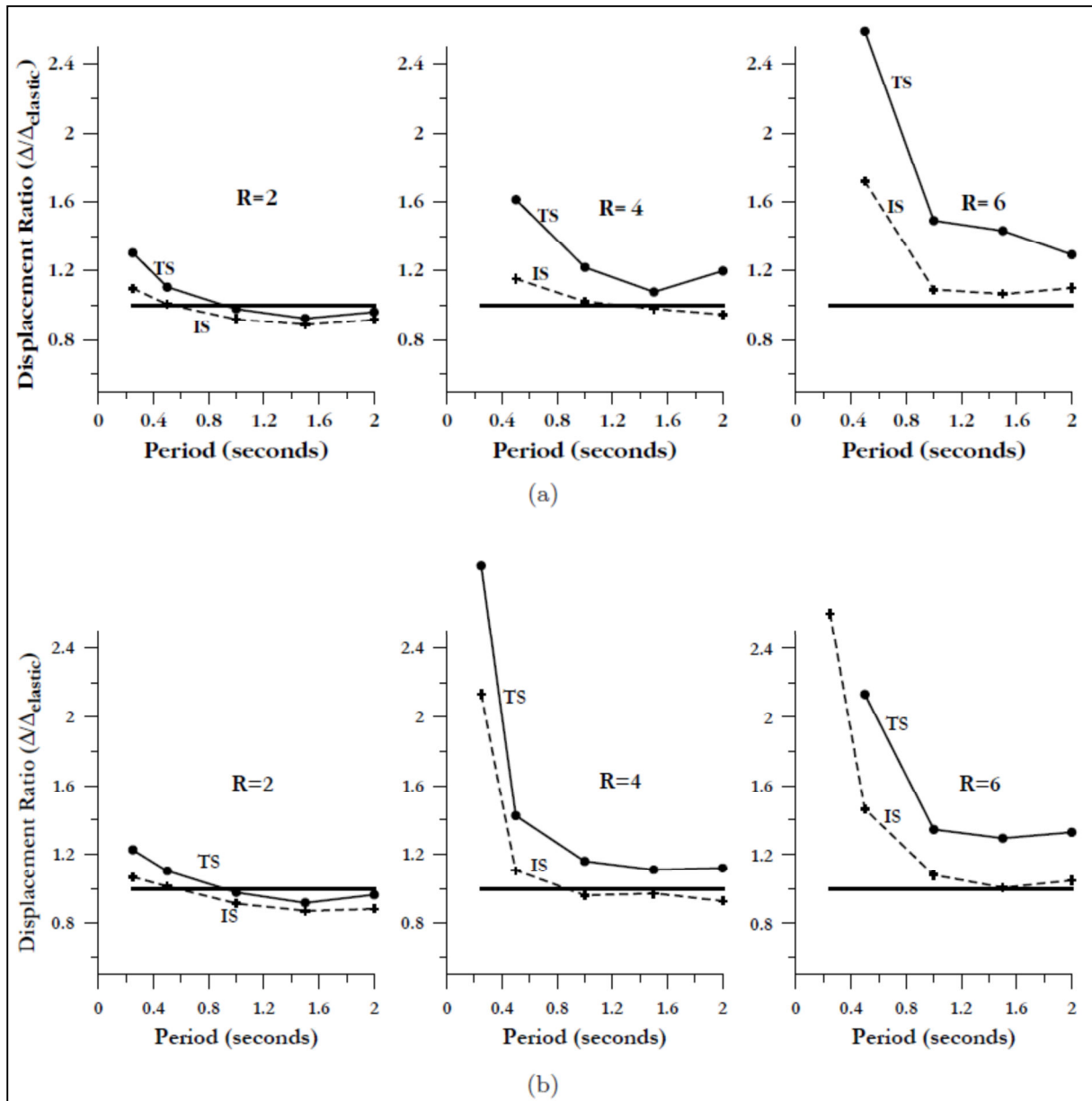


Figure 10.7: Average ratio of peak inelastic displacement to elastic displacement for modified Takeda hysteresis. (TS = tangent-stiffness proportional damping, IS = initial stiffness proportional damping, R = force reduction factor) (Priestley & Grant, 2005, p. 242)

In order to validate the ITHA of this study a similar investigation was performed using the seven manipulated records of ground type 1 shown in Figure 10.5. This was done for force reduction factors of 2 and 4 and a post yield stiffness of 5% (in kN/m). The results are compared in Figure 10.8 to that of Priestley & Grant (2005).

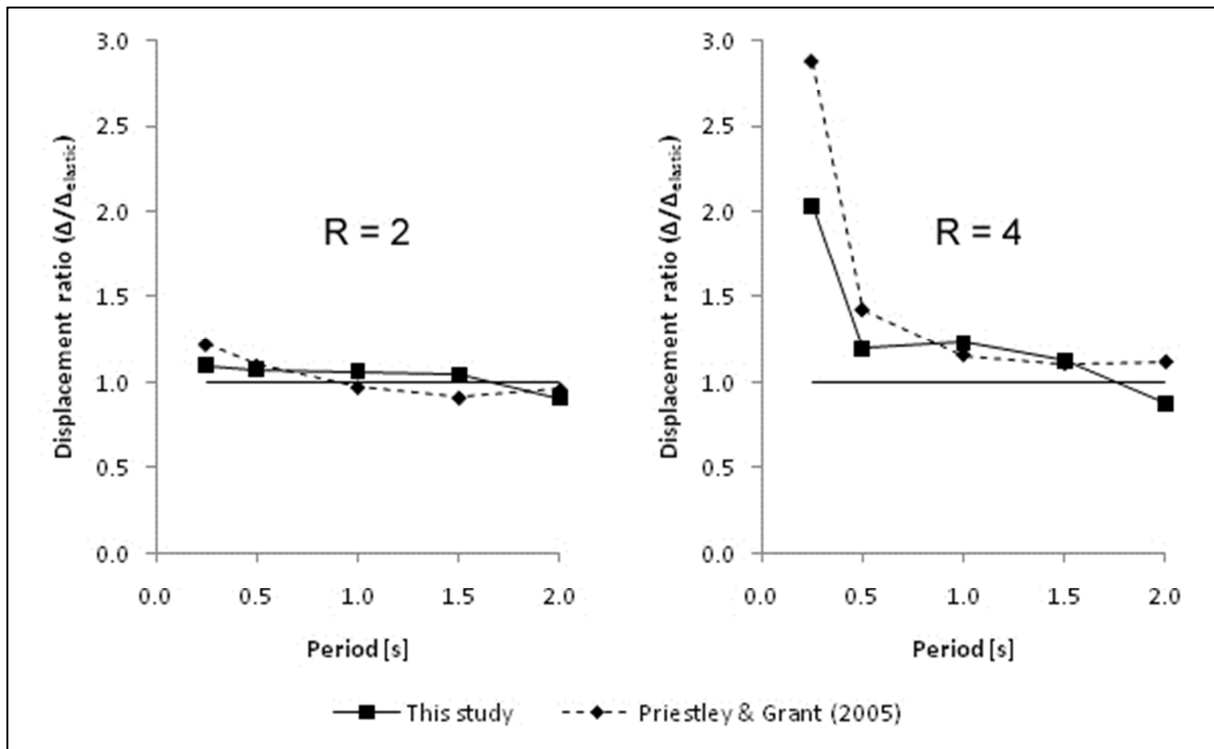


Figure 10.8: Comparison of displacement ratios

It can be seen that the results compare fairly well. The greatest discrepancy lies within the short period range. In Chapter 11 it will be shown that the structural walls of this study respond at fundamental periods of more than approximately 0.7 seconds (see Figures 11.1 to 11.8), for which the discrepancy is small. Moreover, as a final validation for the ITHA of this study the artificial time histories used by Priestley & Grant (2005) were obtained from Grant (2010). These time histories delivered results equal to that of Priestley & Grant (2005).

This chapter has discussed all major aspects of ITHA. It was shown that a very important parameter is the type of damping assumed in ITHA. It was argued that tangent-stiffness proportional viscous damping should be used for ITHA, since inelastic energy dissipation is accounted for by the plastic hinge hysteresis, and thus viscous damping should reduce in proportion to the stiffness in the post-yield range. It was also shown that the equal displacement principle is relatively unconservative if damping is assumed to be tangent-stiffness proportional.

In Chapter 11 the results of this study are discussed. The results of the ITHA, converted to ductility demand according to Chapter 9.4, are compared to that of the equal displacement and equal energy principles in Chapter 11.2.

11. Results

In this chapter the behaviour of the eight walls of this study (refer to Chapter 4) are assessed. This chapter is divided into two sections: Firstly the design results are discussed with the aid of pseudo acceleration spectra which relate the design assumptions of the walls, capacity of the walls, and demand on the walls. The second section compares the ductility demand to ductility capacity. Ductility demand is obtained from the equal displacement and equal energy principles and ITHA. Ductility capacity is based on inter storey drift limits, as described in Chapter 9.3.1 and 9.3.2. The chapter concludes with a discussion regarding the value of the behaviour factor.

11.1 Design results (Figure 5.1 (3) of the methodology)

Figure 11.1 to Figure 11.4 show the elastic, capacity, and design spectra of ground types 1 and 4.

- The design acceleration (a) of the eight walls of this study, each with a different fundamental period, are shown on the design spectrum.
- The names of the walls, defined in Chapter 4.5, are included in the figures. It may be seen that for design method 1, the design acceleration values (a_1) is the same for walls of equal height since Eq. 4.1 depends only on the height of the wall (refer to Chapter 4.4.1).
- The capacity of the walls is also shown in Figure 11.1 to Figure 11.4. For the purpose of this discussion, we refer to this as the capacity spectrum¹. The pseudo acceleration capacity was calculated from the yield moment capacity as described in step 4 of the methodology (Chapter 5).

The relationship between the design spectrum and the capacity spectrum is influenced by three factors, namely overstrength, design conservatism, and period shift.

Overstrength

The capacity spectrum is higher than the design spectrum due to overstrength. Overstrength was discussed in Chapter 2.1.7. It was pointed out that the main factors which lead to overstrength are:

- (a) Mean material strengths, which are used to predict the most likely bending moment capacity of a section, are higher than the characteristic material

¹ Not to be confused with the “Capacity Spectrum Method” by Freeman (2004).

strengths, used to predict bending moment capacity during design. Refer to Chapter 6.1 for material strengths.

- (b) The provided reinforcement is always more than the required reinforcement.

Design conservatism

In this study *Design conservatism* is the name given to the assumption made during design that the design force is related to the total mass of the structure. This was discussed in Chapter 8.1. The equivalent static lateral force design is based on the assumption that higher modes do not significantly influence the dynamic response of the structure. However, to account in some way for the effect that higher modes inevitably have on the structure, the design seismic force is based on the total building mass, instead of the effective first modal mass. The effect of *design conservatism* is most clearly seen in Figure 11.2 by the steadily increasing capacity spectrum with increasing period.

Period shift

The term “period shift” here refers to the difference in fundamental period predicted by the code (SANS 10160-4, 2009) in Eq. 4.1 and the “true” period predicted by moment-curvature analysis of the cross section. Period shift only occurs for design method 1 (refer to Chapter 5). The fundamental period calculated according to design method 2 is based on moment-curvature analysis, and thus no period shift can occur.

The relation of the demand spectrum to the capacity spectrum determines the extent to which the walls respond inelastically. As stated in step 4 of the methodology, the force reduction factor (R) is equal to the ratio between acceleration demand (A_1 or A_2) and capacity ($a_{1(real)}^+$ or a_2^+). Thus, if the demand is less than the capacity, the force reduction factor is less than one, and thus no inelastic action is expected. This is illustrated in Figure 11.1 to Figure 11.4 by the dividing line which intersects at the intersection of the demand and capacity spectra.

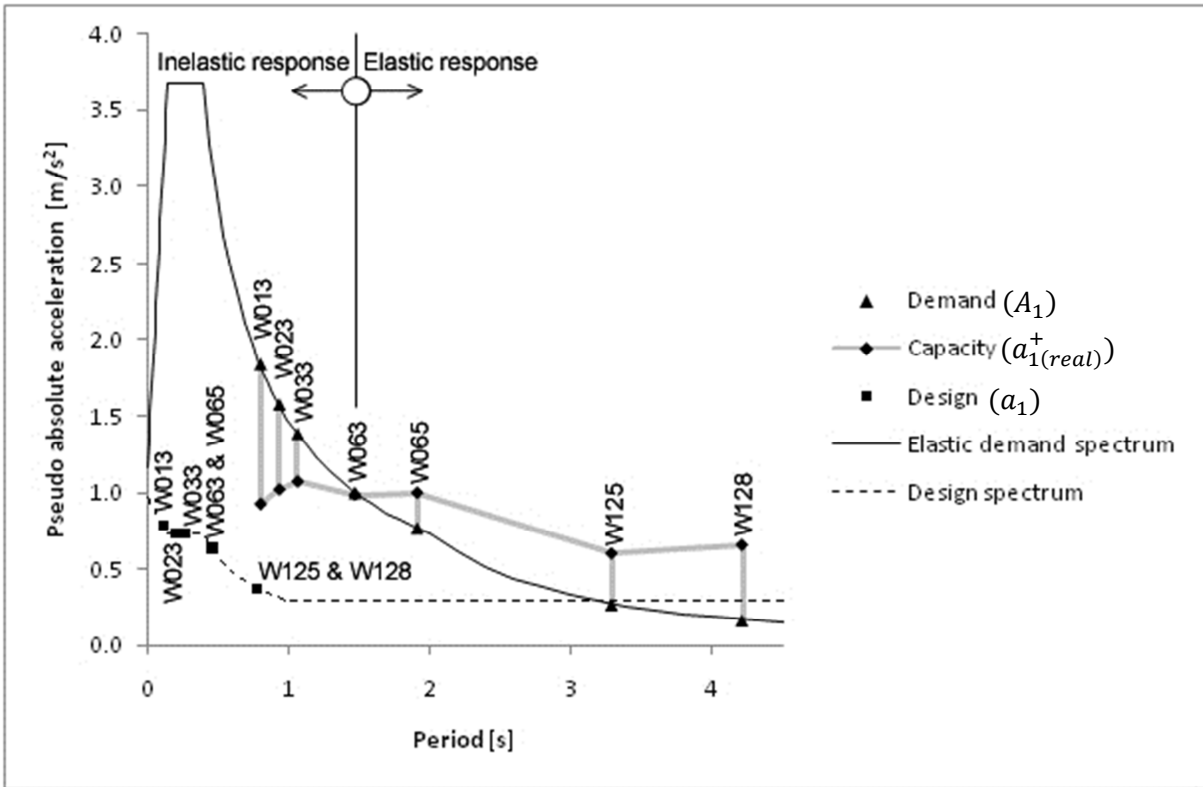


Figure 11.1: Design results for ground type 1, design method 1

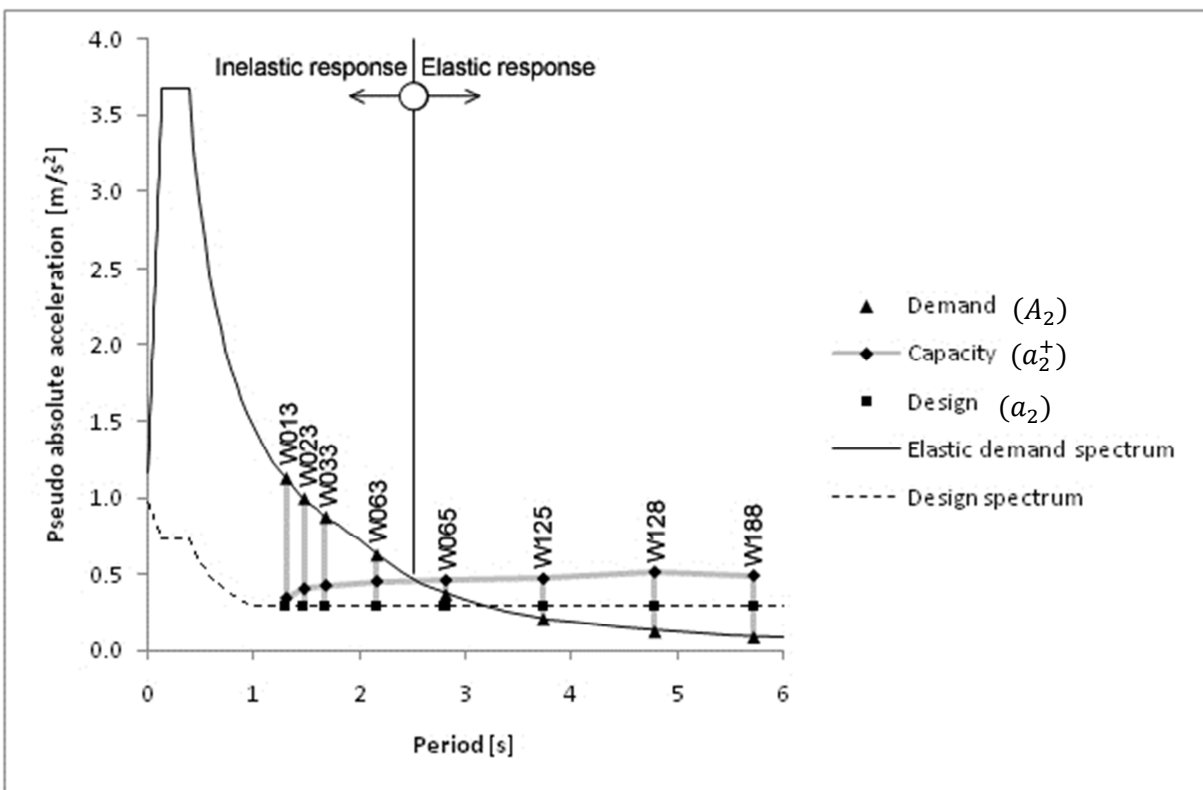


Figure 11.2: Design results for ground type 1, design method 2

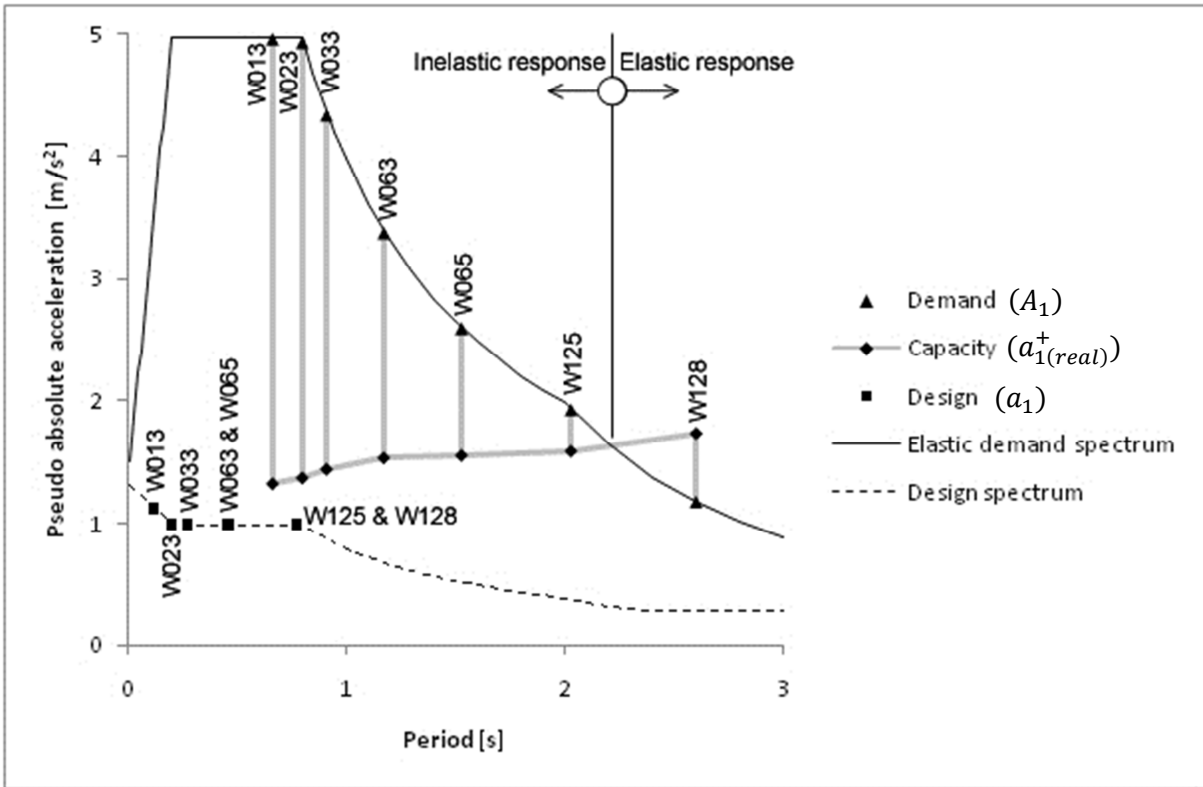


Figure 11.3: Design results for ground type 4, design method 1

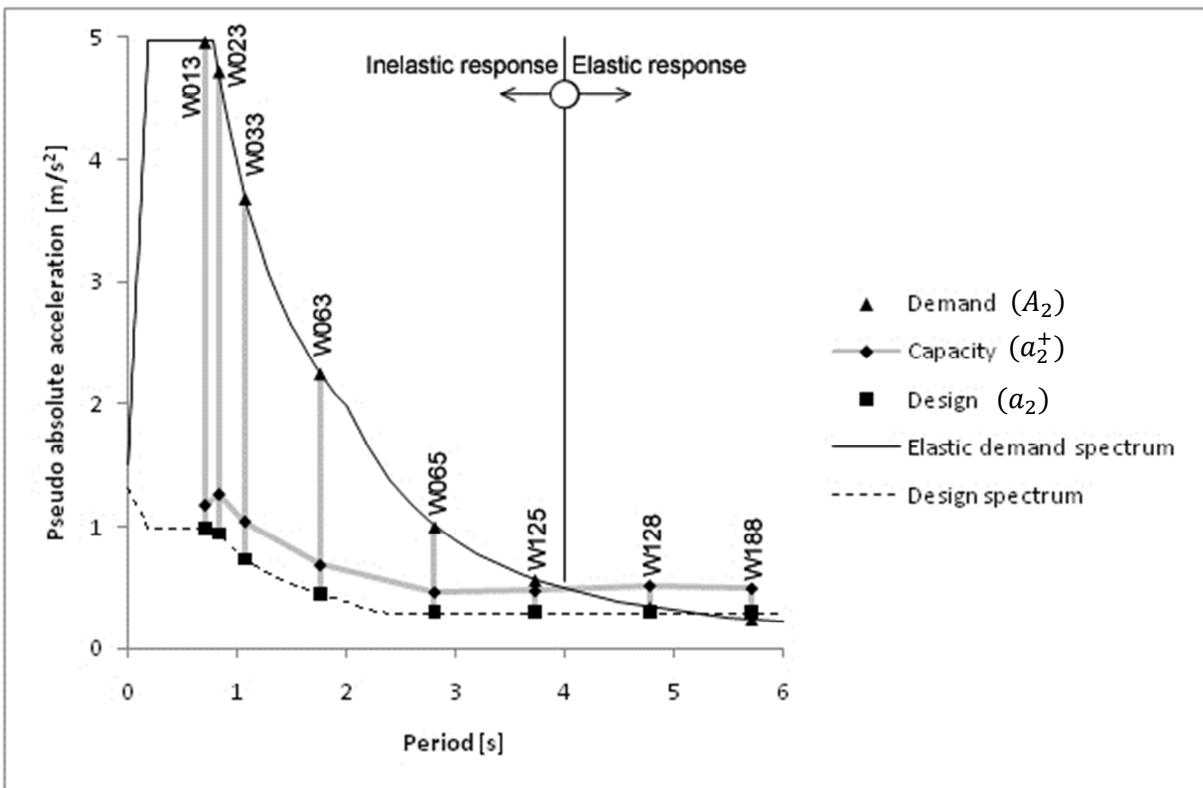


Figure 11.4: Design results for ground type 4, design method 2

11.2 Analysis results (step 4 to 6 of the methodology)

With the force reduction factor (R) known, the ductility demand can be calculated using the R - μ - T relationship (Eq. 2.15). This is however only an estimate and therefore the ductility demand is verified with ITHA. As discussed in Chapter 9.3.1 to 9.3.2 the ductility capacity is based on code drift limits and is calculated according to the plastic hinge method and an approximate equation (Eq. 9.37). Figure 11.5 to Figure 11.8 show the comparison between ductility demand and capacity for ground types 1 and 4, and design methods 1 and 2.

What is evident in Figure 11.5 to Figure 11.8, on the capacity side, is that the plastic hinge method and the approximate equation (Eq. 9.37) predict similar results. The approximate equation is however slightly conservative since it predicts a lower ductility capacity. The effect of the wall aspect ratio (A_r) on the ductility capacity is also evident. It was shown in Eq. 9.37 (repeated here as Eq. 11.1) that the ductility capacity reduces as the aspect ratio increases.

$$\mu_c = 1 + 1.71 \frac{\theta_c - \varepsilon_y A_r}{\varepsilon_y A_r} \quad \dots\dots\dots 11.1$$

It may also be seen that the ductility demand predicted by the R - μ - T relationship corresponds to that of the ITHA. Any difference between the two methods is small in comparison to the difference observed for the ductility capacity.

The only wall which complied with the defined criteria of the equal energy principle is the single storey wall on ground type 4. For this wall its ductility demand exceeds its ductility capacity. This implies that the drift of the single storey wall would exceed the code drift limits, and would thus suffer non-structural damage in excess of the design limit state. This does however only apply to walls with an aspect ratio of three or higher. As stated in Chapter 4.5, this wall was only included in the scope of this study to obtain structural walls with a very short period. The aspect ratio was limited to three, since flexural response was desired of structural walls. In general, structural walls used for single storey construction have aspect ratios of less than three, and would therefore fall outside the scope of this study. The reader is referred to Paulay & Priestley (1992, p. 473) for the design of squat structural walls.

For all of the other walls the ductility demand is less than the ductility capacity. Inter storey drift levels for these walls are thus below code drift limits. It can be seen that the ductility demand reduces as the period increases. This is due to the artificial acceleration plateau of the design spectrum (see Figure 11.1 to Figure 11.4). It can also be seen that method 1

produces “safer” structures than method 2 because of its assumption of a short period, and thus higher acceleration demand. It will however be shown in the next chapter that method 1 severely underestimates structural displacement.

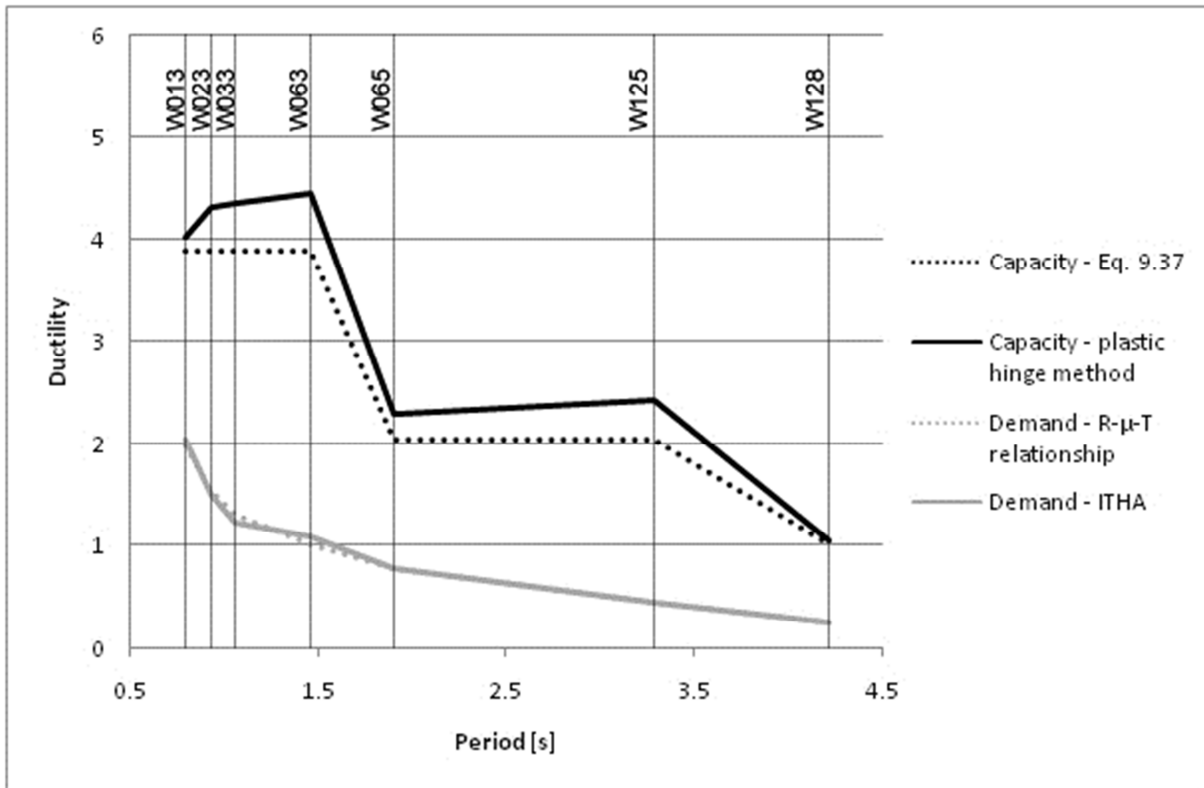


Figure 11.5: Analysis results for ground type 1, design method 1

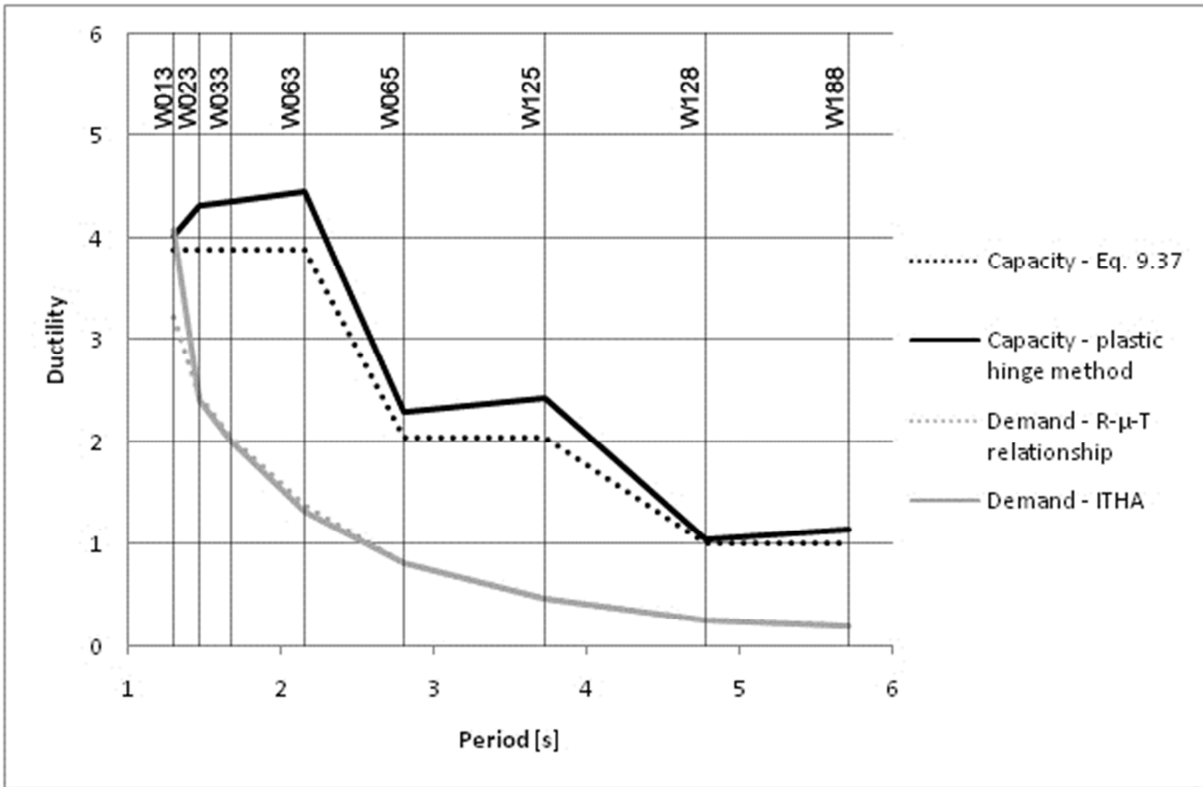


Figure 11.6: Analysis results for ground type 1, design method 2

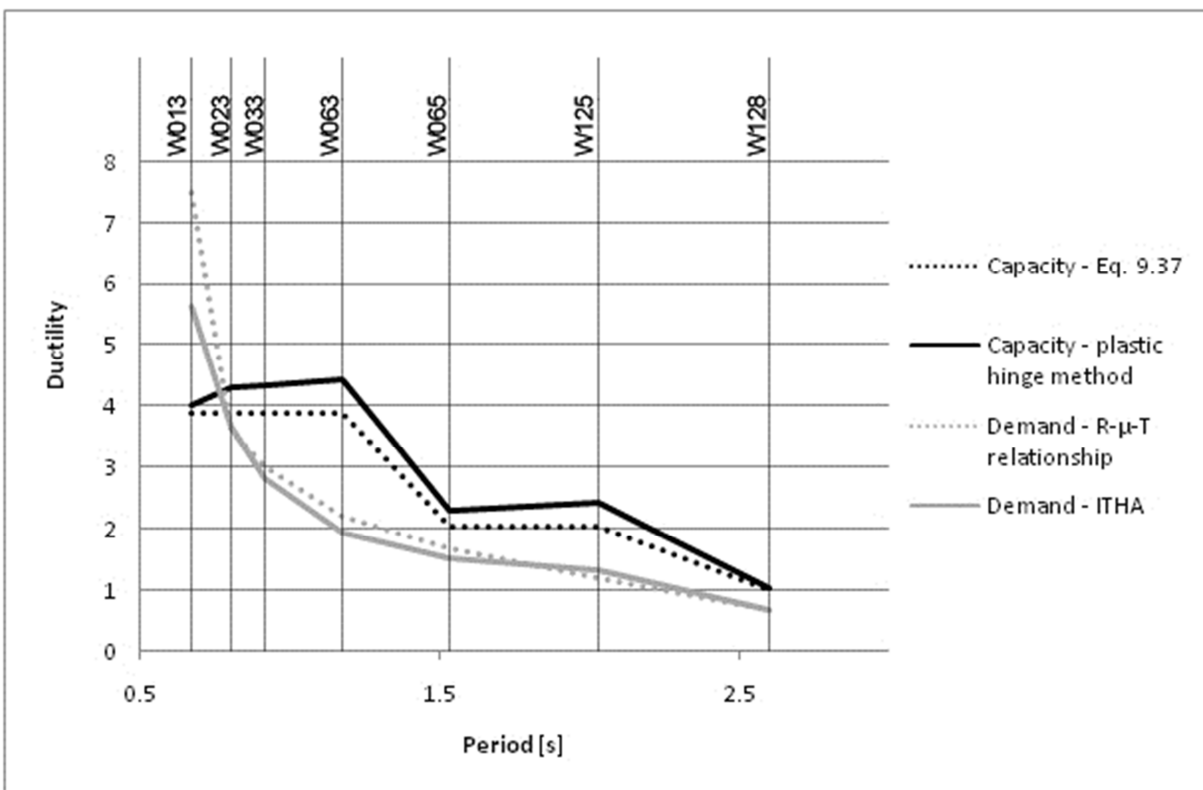


Figure 11.7: Analysis results for ground type 4, design method 1

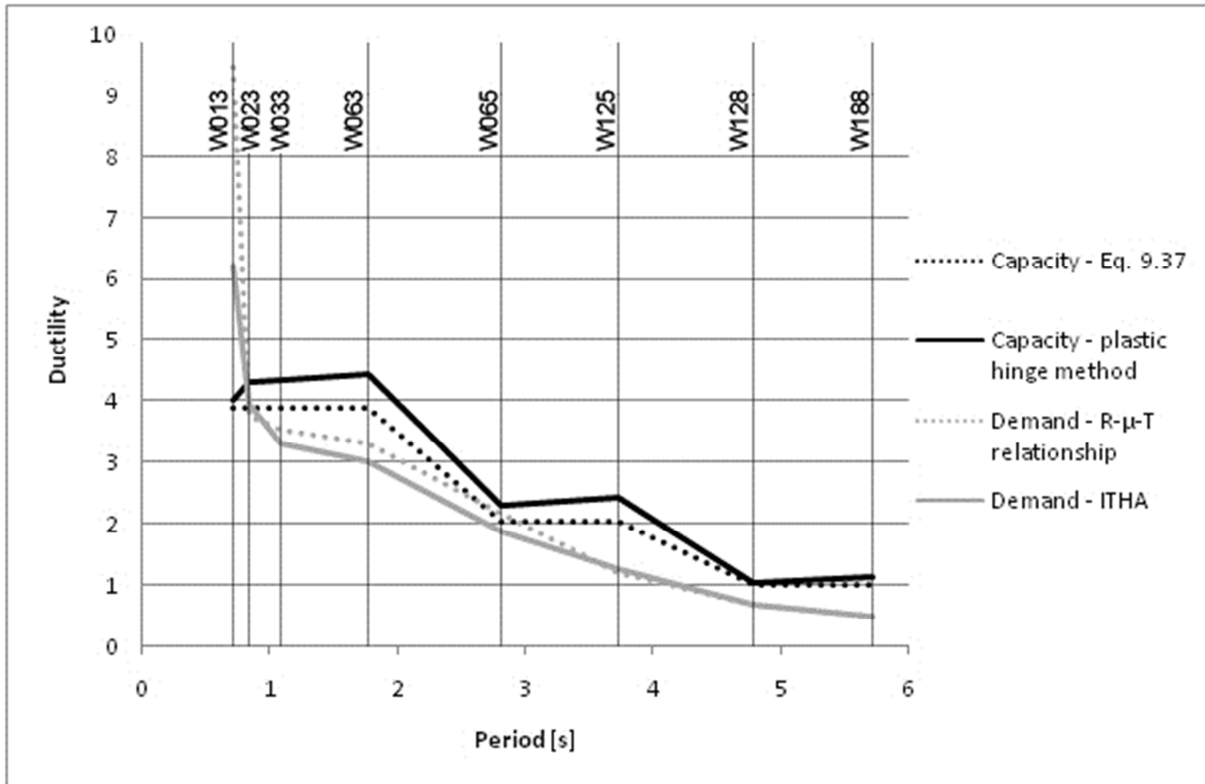


Figure 11.8: Analysis results for ground type 4, design method 2

It may therefore be concluded that the current value of the behaviour factor, defined by SANS 10160-4 (2009) as five, is adequate to ensure that code drift limits are not exceeded, whether design is done according to method 1 or 2. The designer is however still required by the code to calculate structural displacements as the final step in the seismic design process (SANS 10160-4, 2009, p. 27). It will be shown in Chapter 12 that this final step requires careful consideration.

12. Assessment of displacement prediction methods

The purpose of this chapter is to evaluate the accuracy of the displacement prediction method prescribed by SANS 10160-4 (2009) and to point out some pit falls in seismic displacement prediction.

According to SANS 10160-4 (2009, p. 27) the maximum inelastic response displacement, d_s should be calculated using Eq. 12.1:

$$d_s = 0.7qd_e \tag{12.1}$$

where

q is the behavior factor, and

d_e "is the displacements from the static elastic analysis in meters" (SANS 10160-4, 2009, p. 27).

Eq. 12.1 is based on the equal displacement principle (refer to Chapter 2.1.6). Figure 2.4 illustrated the equal displacement principle. It is repeated here as Figure 12.1.

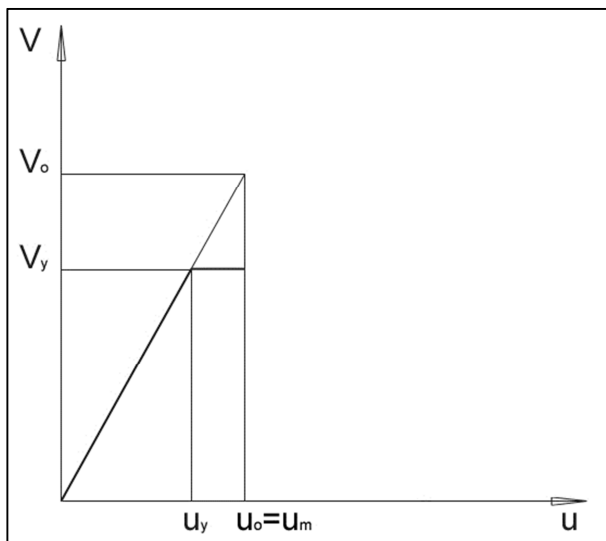


Figure 12.1: Equal displacement principle

Since the equal displacement principle states that the peak displacement of the inelastic system (u_m) is equal to the peak displacement of the elastic system (u_o), it would make sense that Eq. 12.1 should read: $d_s = d_e$. The reasons for the $0.7q$ factor in Eq. 12.1 are the following:

1. In determining the design load the elastic demand was reduced by the behaviour factor q . It is thus necessary to multiply the design load by q to obtain the elastic force demand (V_0).
2. In the calculation of the design load the spectral pseudo acceleration was multiplied by the full mass of the building (m_{tot}) instead of the effective first modal mass (m^*). This was done to account for higher mode effects (refer to Chapter 8.1). The effective first modal mass is approximately 70 % of the total building mass over the full period range (see Figure 8.1). Thus, it is possible that the 0.7 factor serves to reverse the conservatism applied during design.

The code does not make provision for very short period structures to which the equal energy principle applies. In Chapter 11.2 it was seen that the equal energy principle applied only to the single storey wall built on ground type 4.

The displacement of the equivalent elastic system (d_e) is obtained from a static elastic analysis of the structure. Such an analysis of the structure could be as complicated as a 3D finite element analysis of a MDOF structure to as simple as one equation. For the sake of this discussion, the following SDOF equation will be used:

$$d_e = V_d/k^* \tag{12.2}$$

where k^* is the stiffness of the SDOF system, and V_d is the design shear force, and is obtained, in accordance with equivalent static lateral force design (Chapter 8.1), from:

$$V_d = m_{tot}a \tag{12.3}$$

where m_{tot} is the total mass of the structure, and a is the design pseudo acceleration (as a function of period)

It is however unclear on which period the force (V_d) and the stiffness (k^*) should be based. SANS 10160-4 (2009) provides two estimates of the fundamental period. In addition to the height dependent equation (Eq. 4.1) provided by SANS 10160-4 (2009, p. 24) the code also states that the fundamental period may be obtained from an analysis which takes the cracked sectional properties into account. In the absence of a more accurate analysis it may be assumed that the cracked sectional stiffness is equal to half of that of the un-cracked section (SANS 10160-4, 2009, p. 24). The period calculated in this manner may however not be more than 40 % greater than the period calculated according to Eq. 4.1.

Thus, there exist three possible interpretations as to what period the stiffness (k^*) and/or force (V_d) should be based:

1. $T = C_T h_w^{3/4}$ (Eq. 4.1)
2. Period obtained from eigenvalue analysis based on cracked sectional stiffness (assumed = $0.5EI$). The period calculated in this way should, according to the code, be limited to $1.4 C_T h_w^{3/4}$. However, since the code does not provide any other guidance, some designers might base the stiffness (k^*) on this assumption.
3. Period obtained from eigenvalue analysis based on cracked sectional stiffness, where the cracked sectional stiffness is obtained from moment-curvature analysis (see Chapter 7). This period was labelled $T_{1(real)}$ in Figure 5.1 (3).

The stiffness (k^*) is related to the period (T) by the familiar relationship:

$$k^* = \frac{4\pi^2 m^*}{T^2} \dots\dots\dots 12.4$$

The design pseudo acceleration value is required to be greater than $0.2 a_g$ (see Chapter 2.1.7). It should be noted that this requirement is purely artificial and therefore does not have any physical interpretation. When displacement is calculated this artificial plateau should be ignored to avoid overestimation of displacement (Dazio & Beyer, 2009, p. 8-28).

Taking all the above mentioned factors into account, five cases are identified of which only one leads to a reasonable prediction of displacement. These are summarized in Table 12.1:

Table 12.1: Displacement prediction methods considered

| Method | Force (V_0) based on: | Stiffness (k^*) based on: | Comment |
|--------|---|---|---|
| 1 | $T = C_T h_w^{3/4}$ (Eq. 4.1) | $T = C_T h_w^{3/4}$ (Eq. 4.1) | This is the most obvious assumption. |
| 2 | T based on $0.5EI$ | T based on $0.5EI$ | Quick assumption which accommodates cracked sectional stiffness. |
| 3 | $T = T_{1(real)}$ | $T = T_{1(real)}$ | The most correct assumption which leads to the best prediction of displacement. |
| 4 | $T = C_T h_w^{3/4}$ (Eq. 4.1) | $T = T_{1(real)}$ | The designer realizes that the stiffness is based on cracked sectional stiffness, but applies the design forces obtained from Eq. 4.1 to the static elastic analysis. |
| 5 | $T = T_{1(real)}$ with $S_d(T) \geq 0.2a_g$ | $T = T_{1(real)}$ with $S_d(T) \geq 0.2a_g$ | This case illustrates the error made when the artificial acceleration plateau of $0.2a_g$ is applied in displacement prediction. |

Displacement was predicted for seven of the walls of this study using these five methods. The elastic displacement d_e was calculated using Eq. 12.2, and the inelastic displacement d_s was calculated from Eq. 12.1. In Figure 12.2 and Figure 12.3 the results of ductility ($\mu = d_s/\Delta_y$) are compared to the ductility calculated according to the R- μ -T relationship presented in the previous chapter (cp. Figure 11.5).

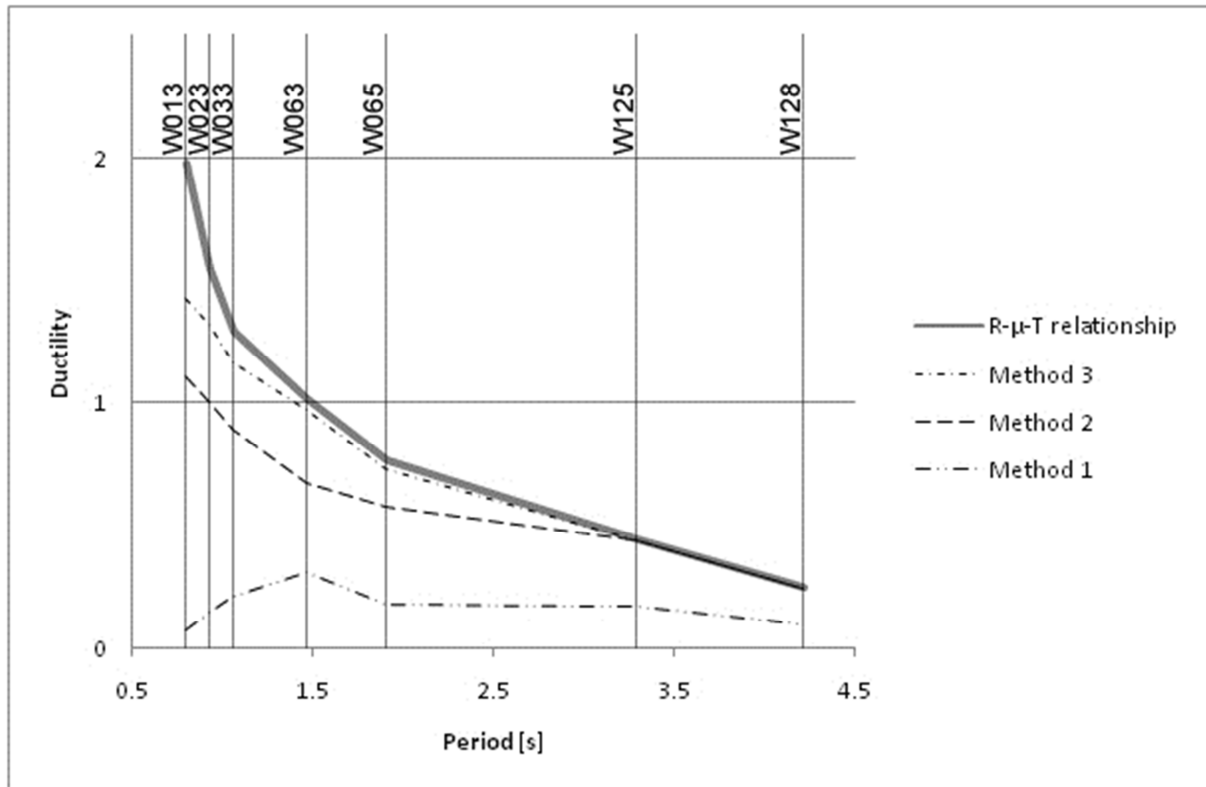


Figure 12.2: Displacement prediction – methods 1 to 4

With displacement calculated according to the R- μ -T relationship taken as reference, it can clearly be seen that method no. 1 leads to a severe underestimation of displacement. This is due to the assumption that the stiffness is based on the un-cracked sectional stiffness (Eq. 4.1).

Method no. 2 leads to a better estimate of displacement, but since the cracked sectional stiffness is usually less than 50 % of the un-cracked sectional stiffness (Priestley *et al.*, 2007, p. 11), there still exists some underestimation.

Method no. 3 leads to the best estimate of displacement, but since the effective first modal mass (m^*) is greater than 70 % of the total building mass (m_{tot}) for short periods, the displacement is underestimated. An accurate estimate of displacement may be obtained if the crude estimate of the effective first modal mass is replaced by the true effective first modal mass, which can easily be obtained from a finite element modal analysis.

The effective sectional stiffness EI_{eff} , used in the calculation of the true fundamental period $T_{1(real)}$, is usually obtained from moment-curvature analysis. There is however an easier method by which EI_{eff} may be obtained:

- At this stage of the design the moment capacity of the section is known. With appropriate assumptions regarding the mean material strengths (refer to Chapter 6) it is possible to calculate the nominal yield moment M_n . This may be accomplished through the design equations of Chapter 8.4.1.
- Eq. 7.2, repeated here as Eq. 12.5, may be used to calculate the yield curvature of a rectangular structural wall section:

$$\phi_y = \frac{2\varepsilon_y}{l_w} \quad \dots\dots\dots 12.5$$

- Thus, the effective sectional stiffness may be obtained from:

$$EI_{eff} = \frac{M_n}{\phi_y} \quad \dots\dots\dots 12.6$$

Thus it is possible to estimate displacement accurately according to method no. 3.

Method no. 4 and 5 show the two most common mistakes that could be made in displacement prediction. The results of these two methods are illustrated in Figure 12.3.

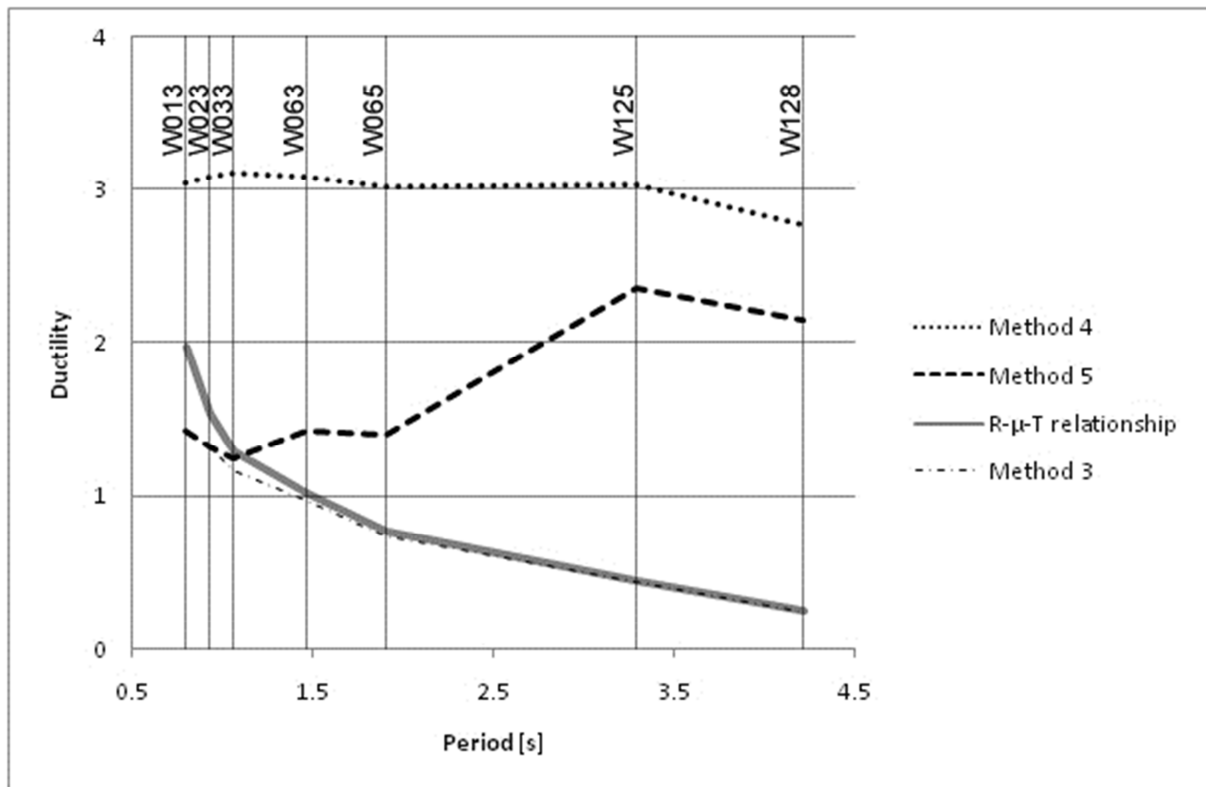


Figure 12.3: Displacement prediction – methods 3 to 5

In method no. 4 the designer based the stiffness on either $0.5EI$ or a moment-curvature analysis, according to the recommendation of the code. However, the designer used the design force, which is based on the period of Eq. 4.1, in the calculation of the elastic displacement d_e .

Method no. 5 illustrates what happens if the artificial plateau of the design pseudo acceleration spectrum is not ignored. The true acceleration spectrum is much lower than the plateau in the longer period range. Thus, an overestimation, such as shown in Figure 12.3, results.

Thus we have seen that it is very important for designers to understand the background of equations such as Eq. 12.1. To apply Eq. 12.1 without consideration of the appropriate force and stiffness to use in elastic displacement analysis, could lead to severe underestimation or overestimation of displacement, depending on the assumptions made. However, displacement can only be predicted accurately if a realistic estimate of the fundamental period is obtained. Even with a realistic estimate of the fundamental period, however, it was shown that displacement is underestimated in the short period range due to an underestimation of the effective first modal mass. It is recommended that the effective first

modal mass be obtained from modal analysis. A simple method for the accurate calculation of the fundamental period was also introduced.

13. Conclusion

The purpose of this study was to assess the value of the behaviour factor currently prescribed by SANS 10160-4 (2009) for the seismic design of reinforced concrete structural walls. The behaviour factor is used in seismic design to reduce the full elastic seismic demand on structures, since well designed structures can dissipate energy through inelastic response. The behaviour factor was evaluated by comparing displacement demand with displacement capacity for eight structural walls.

Displacement demand was calculated by means of the equal displacement and equal energy principles and confirmed by inelastic time history analyses (ITHA). Displacement capacity was based on inter storey drift limits specified by SANS 10160-4 (2009). These drift limits serve to protect building structures against non-structural damage.

Displacement demand was evaluated for two period estimation methods. Firstly, the fundamental period may be calculated from an equation provided by the design code (SANS 10160-4, 2009) which depends on the height of the building. This equation is known to overestimate acceleration demand, and underestimate displacement demand. The second period estimation method involves an iterative procedure where the stiffness of the structure is based on the cracked sectional stiffness obtained from moment-curvature analysis. This method provides a more realistic estimate of the fundamental period of structures, but due to its iterative nature it is seldom applied in design practice.

The conclusion of this study is that the current behaviour factor value of 5, as found in SANS 10160-4 (2009), is adequate to ensure that structural walls comply with code-defined drift limits. This applies to both period estimation methods. For some of the walls in this study the behaviour factor may even be increased. However, since the behaviour factor is relatively large, it is not the intention of the code committee to increase the value of the behaviour factor.

The designer is required by the code (SANS 10160-4, 2009), as the final step in the seismic design process, to calculate displacement demand and evaluate it. If displacement demand exceeds drift limits, redesign is required. Chapter 12 provided background information on the displacement prediction equation prescribed by SANS 10160-4 (2009, p. 27) and identified the mistakes designers can make in displacement prediction. It was shown that it is only possible to accurately predict displacement if the fundamental period is based on the

cracked sectional stiffness. An easy and quick method of obtaining the cracked sectional stiffness was introduced.

This study has focussed on reinforced concrete structural walls with rectangular cross sections. Some topics for further research may include the assessment of the behaviour factor for:

- reinforced concrete structural walls with more complex cross sectional shapes (see Chapter 4.1),
- coupled structural walls (walls coupled by coupling beams or slabs), and
- reinforced concrete moment resisting frames.

14. Bibliography

Applied Technology Council (ATC-33 Project) (1997). NEHRP Guidelines for the Seismic Rehabilitation of Buildings (FEMA Publication 273). [Online]. Available:

<http://www.wbdg.org/ccb/FEMA/ARCHIVES/fema273.pdf> [2010, October 19].

Bachmann, H. (2003). *Basic principles for engineers, architects, building owners, and authorities* [Online]. Available:

<http://www.bafu.admin.ch/publikationen/publikation/00799/index.html?lang=en> [2010, July 15].

Bachmann, H., Dazio, A., Bruchez, P., Mittaz, X., Peruzzi, R. & Tissières, P. (2002).

Erdbebengerechter Entwurf und Kapazitätsbemessung eines Gebäudes mit

Stahlbetontragwänden [Online]. Available: http://www.sgeb.ch/docs/D0171/SIA_D0171.pdf [2010, July 15].

Bentz, E., Collins, M.P. (2009). *Response-2000* [Online]. Available:

<http://www.ecf.utoronto.ca/~bentz/r2k.htm> [2009, May 5].

Carr, A.J. (2007). *Ruaumoko – A program for inelastic dynamic analysis* [CD-ROM]. IUSS Press [2009, October 27].

Ceccotti, A. (2008). New Technologies for Construction of Medium-Rise Buildings in Seismic Regions: The XLAM Case. *Structural Engineering International*, 2(10), 156-165.

Cement & Concrete Institute, *Monitoring concrete strength by the cusum system* [Online].

Available: http://www.cnci.org.za/inf/publications_pdf/cusum.pdf [2010, July 15].

Chopra, A.K. (2007). *Dynamics of Structures – Theory and applications to earthquake engineering*. Upper Saddle River: Pearson Prentice Hall.

Dazio, A. & Beyer, K. (2009). *Short course: Seismic design of building structures*.

Unpublished class notes (Short course: Seismic design of building structures). Stellenbosch: Stellenbosch University.

- Dazio, A., Beyer, K., Bachmann, H. (2009). Quasi-static cyclic tests and plastic hinge analysis of RC structural walls. *Engineering Structures*, 31(7), 1556-1571.
- Dhakal, R.P., Mander, J.B., Mashiko, N. (2006). *Earthquake Records for Multi-Level Seismic Performance Assessment of Structures*. Department of Civil Engineering, University of Canterbury, Christchurch, New Zealand.
- European Standard EN 1998-1. Eurocode 8: Design of Structures for Earthquake Resistance - Part 1: General rules, seismic actions and rules for buildings*. 2004: European Committee for Standardization (CEN)
- Freeman, S.A. (2004). Review of the development of the Capacity Spectrum Method. *ISET Journal of Earthquake Technology*, 41(1), 1-13.
- Grant, D.N. (Damian.Grant@arup.com). (2010, June 29). *Viscous damping in seismic design and analysis*.
- Kowalski, M.J. (2010). *Displacement-based seismic design of bridges*. Unpublished class notes (Displacement-based seismic design of bridges). Pavia: ROSE School.
- Mander, J.B., Priestley, M.J.N., Park, R. (1988). Theoretical stress-strain model for confined concrete. *Journal of Structural Engineering*, 114(8), 1804 – 1826.
- Mirza, S.A. & MacGregor, J.G. (1979). Variability of Mechanical Properties of Reinforcing Bars, *Journal of the Structural Division, Proceedings of the American Society of Civil Engineers*, 105(ST5), 921 – 937.
- Montejo, L.A. & Kowalsky, M.J. (2007). *CUMBIA – Set of codes for the analysis of Reinforced Concrete Members* [CD-ROM]. IUSS Press [2009, October 27].
- Oasys Limited (2010a). *Oasys Sigraph 9.0 build 2* [Online]. Available: <http://www.oasys-software.com/information/universities.shtml> [2010, July 1].
- Oasys Limited (2010b). *Oasys Sigraph Manual* [Online]. Available: http://www.oasys-software.com/products/seismic/sigraph/manuals/sigraph9.0/sigraph9.0_manual.pdf [2010, August 20].

Park, R. & Paulay, T. (1975). *Reinforced Concrete Structures*. New York: John Wiley & Sons, Inc.

Paulay, T. & Priestley, M.J.N. (1992). *Seismic design of reinforced concrete and masonry buildings*. New York: John Wiley & Sons, Inc.

PEER NGA Database (2007). *Pacific Earthquake Engineering Research Center: NGA Database* [Online]. Available: <http://peer.berkeley.edu/nga/index.html> [2010, August 14].

Petrini, L., Maggi, C., Priestley, M.J.N., Calvi, G.M. (2008). Experimental Verification of Viscous Damping Modeling for Inelastic Time History Analyses. *Journal of Earthquake Engineering*, 12(1), 125-145.

Priestley, M.J.N., Calvi, G.M., Kowalski, M.J. (2007). *Displacement-Based Seismic Design of Structures*. Pavia : IUSS Press.

Priestley, M.J.N. & Grant, D.N. (2005). Viscous Damping in Seismic Design and Analysis. *Journal of Earthquake Engineering*, 9(SP2), 229-255.

SANS 10100-1: *The structural use of concrete Part 1: Design*. (2000). Standards South Africa.

SANS 10160-1: *Basis of structural design and actions for buildings and industrial structures Part 1: Basis of structural design*. (2009). Draft: Standards South Africa.

SANS 10160-2: *Basis of structural design and actions for buildings and industrial structures Part 2: Self-weight and imposed loads*. (2009). Draft: Standards South Africa.

SANS 10160-4: *Basis of structural design and actions for buildings and industrial structures Part 4: Seismic actions and general requirements for buildings*. (2009). Draft (October 13): Standards South Africa.

SANS 920: *Steel bars for concrete reinforcement*. (2005). Standards South Africa.

Seismosoft [2010] "SeismoStruct - A computer program for static and dynamic nonlinear analysis of framed structures" [online]. Available from URL: www.seismosoft.com.

SIA 262: Concrete Structures. 2004, Zürich: Swiss Society of Engineers and Architects (SIA), Swiss Standards Organization SN 505 262.

Spathelf, C.A. (2008). *Assessment of the Behaviour Factor for the Seismic Design of Reinforced Concrete Structural Walls according to SANS 10160: Part 4*. MScEng Thesis, Stellenbosch: Stellenbosch University.

Vamvatsikos, D., Cornell, C.A. (2002). Incremental dynamic analysis. *Earthquake Engineering and Structural Dynamics*, 31, 491-514.